Doktoravhandlinger ved NTNU

Rune Hansen

New Techniques for Detection of Ultrasound Contrast Agents

NTNU

NTNU Trondheim
Norges teknisk-naturvitenskapelige universitet

Doktoravhandling 2004:5
Fakultet for informasjonsteknologi, matematikk og elektroteknikk
Institutt for teknisk kybernetikk

New Techniques for Detection of Ultrasound Contrast Agents

Rune Hansen

Submitted to
The Norwegian University of Science and Technology
in partial fulfillment of the requirements
for the degree of
Doctor of Engineering
Doktor Ingeniør

Norwegian University of Science and Technology
Faculty of Information Technology,
Mathematics and Electrical Engineering

December, 2003

Abstract

This thesis analyses medical ultrasound pulse echo detection techniques of contrast bubbles embedded in soft tissue and three new detection techniques are described.

In a medical ultrasound imaging situation, the linearly scattered tissue signal is strong and will typically mask the linearly scattered contrast agent signal. In contrast agent detection techniques, it is therefore usually the strong local nonlinear bubble response which is utilized for image reconstruction.

In a small tissue volume element undergoing compression and expansion due to transmitted ultrasonic waves, there will be nonlinear effects introduced due to deformation of the volume element and intermolecular forces. For typical ultrasound beams, with phase fronts that are not strongly curved, the dominant nonlinear effects are due to the nonlinear intermolecular forces. The local effect of this nonlinearity is low but the nonlinear distortion accumulates in the forward propagation of the wave and can usually not be neglected in medical ultrasound wave propagation of frequencies and amplitudes typically applied.

First, the effect of nonlinear wave propagation on nonlinear contrast bubble scattering is studied. The second harmonic component in the ultrasound transmit field, introduced due to nonlinear intermolecular forces, is shown to potentially reduce the nonlinear second, third, and fourth harmonic components scattered from a contrast bubble. The diminishing effects on the scattered third and fourth harmonic components are especially significant.

In contrast harmonic detection techniques, the noise signal present in a pulse echo imaging system will potentially mask the received harmonic contrast signal. The use of Barker codes, which are a type of pulse compression codes familiar in radar systems and communication theory, is studied and the potential for increasing the Contrast to Noise Ratio of the received scattered third harmonic component is investigated. Generally, an increase of 6 to 9 dB was found both numerically and experimentally applying a four bit Barker code. The Barker code was, however, found to be very sensitive to variations in acoustic properties of the bubble and bubble movement during insonification by the pulse sequence.

The Contrast to Noise Ratio of the received scattered third or fourth harmonic components can also be increased by transmitting a dual frequency band pulse where in particular a fundamental band and its second harmonic component are transmitted, overlapping in the time domain. The received third or fourth harmonic contrast signal and tissue signal amplitudes are then significantly increased relative to when transmitting a conventional fundamental frequency band pulse. The increase in the received third or fourth harmonic tissue signal amplitude can be canceled or reduced by transmitting a second dual frequency band pulse, with inverted polarity on the transmitted second harmonic band, and then combining the two resulting received signals in a general pulse inversion process.

By inverting the polarity of the transmitted second harmonic component, one is able to construct two asymmetric pulses with respect to positive and negative transmit amplitude, thus preventing the resulting contrast agent signal from being significantly reduced in the pulse inversion process.

Finally, a contrast agent detection technique utilizing the total scattered contrast bubble signal is described. Harmonic contrast detection techniques typically impose some important limitations on the range resolution and Contrast to Noise Ratio obtainable in the final ultrasound image. Also, the nonlinear part of the contrast signal scattered in the forward propagation direction adds in phase with the propagating transmit field and may introduce a significant problem when linearly back-scattered from the tissue. In the new detection technique, echoes from a transmitted dual frequency band pulse consisting of a low frequency "pumping" pulse and a high frequency imaging pulse overlapping in the time domain, are stored in the imaging system. A second dual frequency band pulse is transmitted, where the polarity of the transmitted low frequency components are inverted relative to the first transmitted pulse, and the resulting new echoes are linearly combined with the stored echoes. The transmitted low frequency pulse manipulates the acoustic scattering properties of the contrast bubbles at the transmitted high frequency components. The resulting tissue echoes will be canceled in the linear combination of the echoes while the contrast agent echoes, and in particular the linearly scattered high frequency components of these, are preserved and may be used for image reconstruction.

Preface

This thesis is submitted to the Faculty of Information Technology, Mathematics and Electrical Engineering at the Norwegian University of Science and Technology, NTNU, in partial fulfillment of the requirements for the degree of Doktor Ingeniør.

The work has been carried out at the Department of Circulation and Medical Imaging at the Faculty of Medicine where I have been employed and where my supervisor has been Professor Bjørn A. J. Angelsen. Formally, I am affiliated to the Department of Engineering Cybernetics. The thesis describes work done in the period from Spring 2000 to Fall 2003 regarding contrast agent detection techniques in medical ultrasound imaging. The work done is mainly based on theoretical considerations and numerical simulations whereas experimental measurements are carried out only to a small extent.

Financially, the work is supported by the Research Council of Norway.

Acknowledgments

Above all, I would like to thank Professor Bjørn A. J. Angelsen for introducing me to the fascinating fields of medical ultrasound imaging and ultrasound contrast agents, and for his continuous support and guidance during this work. I would also like to thank all my other colleagues at the Division of Medical Imaging and at the GE Vingmed Ultrasound group in Trondheim for an enriching environment both academically and socially. I would like to give a special thank to Tonni F. Johansen at the Division of Medical Imaging for many helpful discussions and for reading the manuscript. Special thanks also to Svein-Erik Måsøy at the Division of Medical Imaging and Trond Varslot at the Department of Mathematical Sciences for numerous fruitful discussions. Finally, I am grateful to Anja-Patrice Auflem, with whom I am sharing my life, for always being so supportive and caring.

Contents

Nomenclature

Latin letters

a	positive amplitude function
a	bubble radius
$\dot{a}$	radius velocity
$\ddot{a}$	radius acceleration
A	bulk modulus
b	damping factor of resonant system
b	positive amplitude function
b	binary Barker sequence
B	Fourier transform of Barker sequence
B	nonlinearity parameter
c	positive amplitude function
c	speed of sound
d	loss factor of resonant system
e	base of natural logarithm
f	frequency
F_r	radiation force
h	causal low-pass filter
H	transfer function
i	imaginary unit, $i = \sqrt{-1}$
I	intensity of wave
k	wave number
m	inertia of resonant system
M	number of individual subpulses in coded sequence
n	noise signal
N	noise parameter
p	transmitted signal
p	acoustic pressure
p_i	incident pressure
P	total pressure
P_0	ambient pressure
$\vec{r}$	orthogonal coordinates for 3-dimensional space
r	length of $\vec{r}$
r	received signal
s	stiffness of resonant system
s	scattered signal
t	time coordinate

u	radial velocity
U	bubble velocity due to radiation force
z	propagation direction for plane wave
Z	acoustical impedance

Greek letters

β	nonlinearity parameter
Θ_{12}	phase angle between 1^{st} and 2^{nd} harmonic component in radius oscillation
κ	compressibility
λ	wave length
μ_v	viscosity
π	ratio of circumference of a circle to its diameter
ρ	density
σ_e	extinction cross section
Σ	summation symbol
τ	time delay
ϕ	phase angle
Φ_{12}	phase angle between 1^{st} and 2^{nd} harmonic component in transmit field
ψ	particle displacement
$\dot{\psi}$	particle velocity
$\ddot{\psi}$	particle acceleration
ω	angular frequency, $\omega = 2\pi f$
Ω	normalized angular frequency

Subscripts and superscripts

$*$	complex conjugate
0	equilibrium or ambient state
0	resonant state
c	contrast agent signal
d	Doppler shift
i	incident field
I	inverse filter
M	matched filter
n	term number n in Power Series expansion
s	isentropic state
t	tissue signal
W	Wiener filter

Abbreviations

CNR	Contrast to Noise Ratio
CTR	Contrast to Tissue Ratio
PI	Pulse Inversion
SNR	Signal to Noise Ratio

Symbols

$\underset{t}{*}$ convolution operation in the time domain

Chapter 1

Introduction

1.1 Medical Ultrasound Imaging

Ultrasound is sound waves with frequency above the audible range which is around 20 kHz. The frequency range used in medical ultrasound imaging is typically from 1 to 10 MHz, giving wave lengths from 1.5 to 0.15 mm in soft tissue, although applications of higher frequencies are interesting when imaging over small regions close to the ultrasound transducer.

Ultrasound transducers are usually made as a plate of piezoelectric material with metallized surfaces acting as electrodes for applying electrical voltage across the thickness direction of the plate. The piezoelectric plate is operated at thickness resonance to maximize the displacement of the plate and the transducer is thus efficient only over a limited frequency range. The thickness vibrations of the transducer produce pressure waves when placed in contact with soft tissue. These pressure waves propagate with the speed of sound in the medium which is compressed and decompressed with a spatial period equal to the spatial wave length along the propagation direction of the wave.

Soft tissue is in the present context considered a heterogeneous continuum made up of components such as muscle, fat, and connective tissue which again, on a smaller scale, are heterogeneous. Acoustic parameters thus have spatial variations, although relatively small, and the variations in mass density and compressibility produce ultrasound scattering from soft tissue [3, Chapter 7].

Due to variations in concentrations of blood cells, blood is also a heterogeneous medium. The heterogeneity is, however, less than for soft tissue and ultrasound scattering from blood is much weaker than from soft tissue [13, Table 4.21-4.22].

Medical ultrasound imaging is performed by placing a transducer in contact with the skin and transmitting ultrasound waves, usually in the form of focused beams, into the region of interest in the body. The transmitted waves are then, due to inhomogeneities in the medium, scattered in various directions and the waves being scattered in the direction of the receiving transducer are picked up as delayed echoes of the transmitted wave. The scattered waves are, due the relatively small variations in mass density and compressibility, low in amplitude relative to the transmitted waves.

Acoustic absorption also reduces the amplitude of the received ultrasound echoes [2, Chapter 4.5]. For each wave length the wave propagates, a small amount of the mechanical energy in the wave is irreversibly converted to heat, and this loss of energy due to absorption is thus proportional to the number of wave lengths traveled. This acoustic absorption mechanism limits the maximum depth for imaging with ultrasound at a certain frequency due to the thermal and electronic noise present in a pulse echo imaging system.

The amplitude of the transmit pressure pulses depends on the frequency applied but may typically be from 0.1 to 2 MPa in medical ultrasound imaging. Depending on the transmit amplitude, the received echoes are distorted relative to the transmitted pulses. This distortion mainly occurs due to the nonlinear nature of tissue elasticity. The relationship between pressure and volume compression is not linear unless very low amplitudes, as in the scattered waves, are considered and the distortion of the wave hence occurs in the transmit field resulting in a forward nonlinear distortion of the transmit pulse. As with the acoustic absorption, the local effect of nonlinearity is low but accumulates as the wave propagates. This nonlinear effect has given rise to the second harmonic imaging technique [6] [7] [38] which today is widely in use in medical diagnostic ultrasound imaging. In this technique, the second harmonic components of the distorted echoes are used to create the ultrasound image.

The spatial variations of acoustic parameters are, as indicated, responsible for the scattering of the incident transmitted waves and are hence the basis for image reconstruction. Inside organs, these spatial variations are usually low, and the scattering can be approximated by a first order scattering often called the Born approximation [3, Chapter 7]. In this approximation, the scattered field is calculated based on the undisturbed homogeneous transmitted field and the heterogeneities. The resulting scattered field is low in amplitude relative to the incident field and propagates as if in a homogeneous medium, *i.e.* without being scattered. Scattering that can be adequately described by this Born approximation gives the best ultrasound images.

In the two or three first centimeters below the skin, the body wall consists of composite muscular tissue and fat. Muscle and fat are the two constituents in soft tissue with the largest differences in acoustic parameters. The Born approximation is thus not valid in the body wall and multiple scattering, or reverberations, are produced. Different parts of the transmitted beam will typically traverse unequal distances of fat and muscle and smooth phase fronts of the transmitted wave are potentially destroyed, giving distorted phase fronts of varying amplitude. This phase front aberration destroys the focus of the transmitted beam and hence reduces the resolution in the image while the reverberations appear as added noise in the image [3, Chapter 11]. Trying to compensate for these phase front aberrations is today a major research area in the field of medical ultrasound imaging [17] [25] [24].

If the transmitted wave is scattered from moving tissue or blood, the Doppler effect can be used to measure the velocity of the moving scatterer [14]. A change in frequency of the received scattered signal can be detected if the scatterer has a velocity in the direction of the ultrasound beam. Since the velocity of the scatterer is much less than the speed of sound, this frequency shift will be small relative to the transmitted frequency and is typically a few kHz, *i.e.* in the audible frequency range. Doppler techniques are today widely in use in diagnostic medical ultrasound.

1.2 Ultrasound Contrast Agents

Ultrasound scattering from blood is, as mentioned, much weaker than ultrasound scattering from soft tissue, and the scattered blood signal can therefore not easily be separated and visualized in a medical ultrasound image. Obtaining information about blood flow in vessels and and blood flow through various organs is from a medical diagnostic point of view very helpful.

Blood flow in larger vessels may be detected using Doppler techniques with highpass filtering to separate the blood signal from the tissue signal. In small vessels, the blood velocity is typically too low for Doppler techniques to be applicable and contrast agents are necessary. As an example, the blood velocity in the capillaries is typically less than 3 mm/s [39]. Also, boarder detection of the heart cavities may be improved applying contrast agents.

The scattering from blood can be significantly increased by adding ultrasound contrast agents, usually made as solutions of small gas bubbles in a liquid, to the blood. From underwater acoustics, it is known that gas bubbles are both powerful and nonlinear scatterers of ultrasound waves. The gas bubbles have high compliance relative to the surrounding water or blood and in medical ultrasound, the gas bubbles are much smaller than the wave lengths of the transmit pulses. Contrary to the weak local tissue nonlinearity, the contrast bubbles show strong nonlinear local responses due to large radius excursions with resulting shear deformation of the surrounding fluid.

The contrast bubbles mainly behave as monopole scatterers and hence scatter energy in all directions, including the forward propagation direction. The contrast signal scattered in the forward direction adds in phase with the propagating transmit pulse and introduces an additional distortion of the transmit pulse in regions that in range direction are beyond a contrast filled area. This additional distortion may then be linearly scattered from soft tissue and interpreted as contrast agent. In contrast imaging of the heart or large vessels, this is typically a problem when the transmit pulse has traveled through the large contrast filled regions. Applying a linear contrast agent detection technique is the only way to avoid or reduce the problem.

Lord Rayleigh [33] studied the behavior of the liquid surrounding a collapsing spherical cavity in 1917 and later in 1933, Minnaert [27] published a model where the bubble was viewed as a harmonic oscillator. In 1949, Plesset [31] included a driving acoustic pressure, by letting the background pressure vary with time, to the equation based on the work by Lord Rayleigh. The resulting Rayleigh-Plesset equation is the foundation for the numerical bubble simulations on which the present thesis is partially based.

The first contrast agents for medical ultrasound were approved by health care authorities in 1991 and the search for good contrast agents and contrast agent detection techniques has been relatively intense during the last 15 to 20 years.

Two signal power ratios have vital importance for the quality of performance of the medical ultrasound contrast agent imaging system. First, the Contrast signal to Tissue signal Ratio (CTR) which gives the ratio of the signal power from the contrast agent in a region to the signal power from the tissue in that region. Second, the Contrast signal to Noise Ratio (CNR) which gives the ratio of the signal power from the contrast agent in a region to the noise power in that region. The CTR describes the ability to differentiate contrast signal and tissue signal in an ultrasound image whereas CNR describes the enhancement of the contrast signal above the noise signal and determines the maximum depth for imaging the contrast agent.

In addition, the resolution in the image is of great importance as in most imaging systems. Better resolution typically demands applying higher transmit frequencies, and there is a trade-off between image resolution and maximum depth of imaging.

1.2.1 Contrast Agent Detection Techniques

Special techniques for detecting the contrast agent in the blood is necessary because the strong linearly scattered tissue signal typically is larger than or of the same order as the scattered contrast agent signal. In small vessels, only a few contrast bubbles will be inside a sample volume and the resulting back-scattered contrast agent signal is weak compared to the surrounding tissue signal whereas in the large blood filled cavities of the heart, the number of contrast bubbles will be large giving a strong back-scattered contrast agent signal from the cavity.

A superior contrast agent detection technique produces a back-scattered contrast agent signal for image reconstruction which is easily and adequately differentiated from the scattered tissue signal and the noise signal of the imaging system. In addition, to obtain high image resolution, the scattered contrast signal used for image reconstruction should have high bandwidth.

Several contrast agent detection techniques have been proposed and I will here give a brief description of some of the most important techniques. Common for all these methods is that they are based on the nonlinear acoustic properties of the contrast agent. As indicated, a problem with all contrast harmonic detection techniques is a spread of contrast signal beyond the actual contrast filled region. The nonlinear part of the contrast signal scattered in the forward propagation direction will add in phase with the transmit field and may then be linearly back-scattered from the tissue. None of the proposed techniques do fulfill the mentioned criteria for the superior detection technique and this superior technique might turn out to be impossible to derive.

The first group of contrast imaging techniques consists of the harmonic imaging methods. These methods are based on transmission of one pulse down each line of sight and then application of various harmonic filters on the received echoes to obtain the desired harmonic components used for image reconstruction.

Second Harmonic Imaging

A pulse centered around a fundamental frequency component is transmitted and the resulting received echos are bandpass filtered around twice this transmit frequency. The received energy at this second harmonic band is then used for image reconstruction. This is the simplest and possibly most robust of the nonlinear detection methods. A limitation is that in order to prevent leakage from the fundamental frequency band into the passband of the second harmonic filter applied, the transmit pulse must be sufficiently narrow-banded resulting in limited range resolution. Also, the received tissue signal typically contains a significant amount of energy at the second harmonic component limiting the CTR. The CNR may also be inadequate, especially when imaging at large depths. Second harmonics from contrast agents are studied and reported in the literature [26] [11] [12].

Higher Harmonic Imaging

These techniques are a generalization of the second harmonic imaging technique applying a different frequency band, for example the third harmonic band, for image reconstruction. The received tissue signal typically contains very little energy at these higher harmonic components and the CTR is better than with the second harmonic technique. The received contrast signal typically also contains less energy at these higher harmonic components and the CNR is a bigger problem than with the second harmonic technique. Design and manufacture of broadband transducers that are efficient over several frequency bands is today very challenging limiting the experimental work carried out using these higher harmonic components.

Sub Harmonic Imaging

Contrast bubbles have the potential to scatter energy at frequencies below the incident driving frequency. Most important is here the scattered energy at half the drive frequency. Subharmonics typically require long drive pulses to develop resulting in degraded range resolution. Results from implementation of subharmonic imaging are reported [34] [15].

Nonlinear Frequency Mixing

If two separated frequency bands are simultaneously transmitted, the nonlinear response will contain energy at the sum and difference frequencies of the two transmitted frequency bands. A strong nonlinear bubble response may, in the same manner as with the other harmonic imaging techniques, be detected in the presence of a weaker nonlinear tissue response.

The second group of contrast imaging techniques can be grouped into what may be called multiple pulse methods where at least two pulses are transmitted down each line of sight. The image reconstruction is then based on combinations of the resulting echoes along each line of sight.

Pulse Inversion Techniques

In its simplest embodiment, the pulse inversion technique consists of transmitting two pulses, where the second pulse is a replica of the first pulse but with inverted polarity, with a relative time delay so that the resulting two echoes are separated. The two echoes are then added together and the image is based on this summation signal. In the ideal case, odd harmonic components in the resulting signal, in particular the fundamental component, are canceled while even harmonic components persist. The pulse inversion technique hence turns out as an alternative way of doing second harmonic imaging. The main advantage relative to the simple second harmonic imaging technique is reduction of leakage from the fundamental band into the second harmonic band, thus allowing for more broadband transmit pulses. The main disadvantage is artifacts resulting from tissue motion between the two transmitted pulses. A combined pulse inversion and Doppler technique has been studied by Simpson *et al* [36].

Power Modulation Techniques

If two transmit pulses with different amplitudes are transmitted, the linear combination of the two resulting echoes can be used for bubble detection. If the tissue response is close to linear, it can be strongly suppressed in the linear combination of the two echoes and mainly the nonlinear contrast echo remains. Also, the fundamental component of the contrast echo in this linear combination is, although significantly reduced, usually not canceled.

Bubble Destruction Methods

If subject to high intensity drive pulses the contrast bubbles, usually encapsulated in a thin stabilizing shell, tend to get destructed due to a rupture of the shell. This rupture results in fragmentation of the bubble into smaller bubbles and/or diffusion of the encapsulating gas. Mechanisms of contrast agent destruction are studied by Chomas *et al* [9]. Such bubble destruction will alter the acoustic scattering properties of the contrast agent. Power Doppler techniques use pulse-to-pulse decorrelation in contrast agent echoes, caused by bubble disruption, to distinguish between contrast agent and tissue using Doppler processing techniques. Kirkhorn *et al* [22] suggested applying a release burst to rupture the contrast bubbles and then using decorrelation methods on contrast signals before and after the release burst to detect the contrast agent.

1.3 Overview of the Thesis

This thesis is made up of four separate papers. In the first paper, the effect of the second harmonic component, introduced due to the nonlinearity of ultrasound wave propagation in soft tissue, in the wave field incident to the contrast agent, is investigated. The second paper investigates a new third harmonic contrast agent detection technique, applying a pulse compression method familiar in radar systems and communication theory. The third paper proposes a new third or fourth harmonic contrast agent detection technique, using dual frequency band transmit pulses and a general form of pulse inversion. And finally, the fourth paper proposes a new detection technique utilizing the total scattered contrast signal for image reconstruction, hence overcoming problems in relation to harmonic imaging methods. This last method is mainly a linear contrast agent detection technique.

The content of the four papers is summarized below.

Paper A

Reduction of Nonlinear Contrast Agent Scattering due to Nonlinear Incident Wave Propagation

Ultrasound wave propagation in tissue and scattering from ultrasound contrast agents are both known to be nonlinear processes at typical frequencies and amplitudes used in medical ultrasound imaging. The nonlinearity of wave propagation manifests itself mainly as a second harmonic component which, due to diffraction, will have a varying phase angle relative to the linear fundamental component in a focused beam commonly used in medical ultrasound imaging. Based on numerical simulations, this paper shows that, depending on the relative phase angle between the fundamental and second harmonic component of the wave field incident to the contrast agent, nonlinear contrast agent scattering may be significantly diminished due to the incident pulse distortion caused by the nonlinearity of wave propagation.

Paper B

Using Barker Codes in Contrast Harmonic Imaging

Ultrasound wave propagation is generally a weak nonlinear process relative to the nonlinearity of ultrasound scattering from contrast agents. This difference in degree of nonlinear response makes higher harmonic imaging techniques interesting. A nonlinear generated harmonic band of the fundamental transmitted band is then used for detecting the contrast agent signal and differentiating it from the tissue signal. Received harmonic components typically contain less energy than the linearly received fundamental component and, in contrast harmonic imaging techniques, the limiting factor is often the noise signal always present in a pulse echo imaging system and not the masking of the contrast signal by the tissue signal. Pulse compression techniques, familiar in radar systems and communication theory, are techniques for increasing the signal level relative to the noise level of the pulse echo imaging system which is assumed to be evenly distributed over all frequencies of interest. The signal level is increased by transmitting an elongated pulse and not by increasing the transmit amplitude. The resulting echoes must then be compressed to restore range resolution. This paper investigates the use of Barker codes, which are a type of pulse compression codes, and their potential to increase the signal level of the received third harmonic component from contrast bubbles relative to the constant noise level.

Paper C

A New Dual Frequency Band Contrast Agent Detection Technique

The fact that the contrast agents respond much more nonlinearly than soft tissue to ultrasound pulses has given rise to the contrast harmonic imaging techniques where a harmonic component of the total scattered signal, typically the second harmonic component, is used for image reconstruction. In a medical ultrasound imaging situation, both the harmonic scattered tissue signal accumulating in the forward propagation direction and the uncorrelated thermal and electronic noise signal will potentially mask the scattered contrast harmonic signal. The present paper deals with a new third and fourth harmonic contrast agent imaging technique, designed to increase the contrast harmonic signal relative to both the noise signal as well as the harmonic tissue signal. In order to achieve this, the new method makes use of dual frequency band transmit pulses, together with a general pulse inversion technique.

Paper D

Linear Contrast Agent Detection through Low Frequency Manipulation of High Frequency Scattering Properties

In medical ultrasound contrast harmonic detection techniques, only a component of the total scattered contrast signal, typically the second harmonic component, is utilized for image reconstruction. These harmonic detection techniques make it possible to differentiate contrast signal and tissue signal scattered from the part of the body being imaged, and as higher harmonic components are utilized, this differentiation typically becomes better. All pulse echo imaging systems are, however, infested by unwanted thermal and electronic noise which usually can be considered uniformly distributed over the frequency range of interest. Received harmonic components are typically reduced in amplitude as higher components are considered, and although the differentiation of contrast signal and tissue signal might be excellent applying these higher harmonics, the contrast signal will be masked by the noise signal. Harmonic imaging techniques also require application of relatively narrowbanded transmit pulses thus degrading range resolution in the ultrasound image. Another problem with all contrast harmonic detection techniques is a spread of contrast signal beyond the actual contrast filled region. The nonlinear part of the contrast signal scattered in the forward propagation direction adds in phase with the transmit pulse and may then be linearly back-scattered from the tissue. The present paper proposes a method applying the total scattered contrast signal for image reconstruction, thus largely overcoming the problems encountered in harmonic imaging techniques. In the new method, the contrast signal and tissue signal are differentiated applying a simple pulse subtraction technique which cancels or significantly reduces the scattered tissue signal. The scattered contrast agent signal is, however, preserved in this process due to transmitted low frequency pulses altering the acoustic scattering properties of the contrast agent in a high frequency range used for image reconstruction. The main mechanism through which this imaging technique selects the contrast agent signal is the linear resonant properties of the contrast bubble.

Chapter 2

Reduction of Nonlinear Contrast Agent Scattering due to Nonlinear Incident Wave Propagation

Abstract

Ultrasound wave propagation in tissue and scattering from ultrasound contrast agents are both known to be nonlinear processes at typical frequencies and amplitudes used in medical ultrasound imaging. The nonlinearity of wave propagation manifests itself mainly as a second harmonic component which, due to diffraction, will have a varying phase angle relative to the linear fundamental component in a focused transmit beam commonly used in medical ultrasound imaging. Based on numerical simulations, this paper shows that, depending on the relative phase angle between the fundamental and second harmonic component of the wave field incident to the contrast agent, nonlinear contrast agent scattering may be significantly diminished due to the incident pulse distortion caused by the nonlinearity of wave propagation.

2.1 Introduction

Wave propagation in tissue is usually a weak nonlinear process at frequencies and amplitudes typically used in medical ultrasound imaging, and the transmit pulse is slightly distorted as it propagates through the medium. Although the local effect of nonlinearity is small, the cumulative effect when the wave has propagated several wavelengths is not negligible. If the wave transmitted from an ultrasound transducer has its energy concentrated in some fundamental frequency band, the nonlinearity of wave propagation gives rise to harmonics of this fundamental band [3, Chapter 12] [30, Chapter 11]. Levels of received second harmonic from tissue is typically found to be around 20 dB below the level of the received fundamental component but this level depends on acoustic parameters in addition to imaging parameters such as frequency, amplitude, and depth of imaging. The second harmonic component accumulates gradually as the wave propagates and will, due to diffraction, have a varying phase angle relative to the fundamental component in a focused transmitted ultrasound beam. This phase angle will be a relatively complex function of both axial and lateral position relative to the ultrasound beam axis [3, Chapter 12.6]. Although much weaker than the second harmonic component, higher harmonics may also exist in the transmit field.

Medical ultrasound contrast agents are typically made as solutions of small gas bubbles (diam $\sim 3\ \mu$m) in a fluid and scattering from such gas bubbles is typically a strong nonlinear process [23] [11] [12]. As indicated, the wave field incident to the contrast agent contains energy in a second harmonic band of the fundamental band transmitted from the ultrasound transducer due to the nonlinear tissue elasticity. Depending on the relative phase angle between the incident fundamental and second harmonic band, the presence of this second harmonic band is in the present paper shown to potentially have a major diminishing effect on the nonlinear response from a contrast bubble.

2.2 Theory

2.2.1 Single Bubble Oscillation

The contrast agent is assumed to be spherical gas bubbles encapsulated in a thin shell. The diameter of the bubble is much less than the wavelength of the incoming wave field and the bubble thus experiences an approximately uniform spatial field and the bubble oscillation is assumed to be purely spherical. Simulations for bubble radius oscillations and acoustic scattering are done using the numerical model developed by Angelsen *et al* [4]. This model includes an equation for the relation between pressure and radial strain in a thin shell encapsulating a gas bubble. The model allows for a finite speed of sound in the medium surrounding the bubble, thus taking radiation losses from the bubble into account. Otherwise it is comparable to the well known Rayleigh-Plesset equation [33] [31] and the two models give similar results for incident pressure pulses and bubble parameters studied in this paper.

The Rayleigh-Plesset equation is a second order nonlinear differential equation. For small amplitudes of the incident drive pressure, the bubble oscillation can be assumed to be approximately linear and we have the following second order linear differential equation for the radial displacement, ψ, around an equilibrium radius a

$$m\ddot{\psi}(t) + b\dot{\psi}(t) + s\psi(t) = -4\pi a^2 p_i(t) \ . \tag{2.1}$$

Here, m is the inertia of the system, b is the damping factor of the system, and s is the

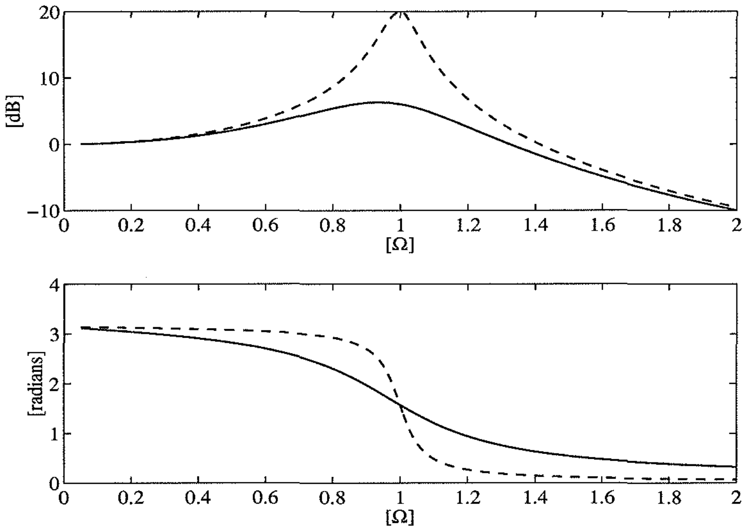

Figure 2.1: Transfer function from drive pressure to radial displacement in Eq. 2.5. The parameter d in Eq. 2.3 is set to 0.5 and 0.1 giving the solid line and dashed line, respectively. Upper panel: Absolute value of transfer function. Lower panel: Phase angle of transfer function.

stiffness of the gas and encapsulating bubble shell. Eq. 2.1 typically describes the forced linear oscillation of a system consisting of a mass m attached on a spring with stiffness s whereas b accounts for the damping in the system. By taking the Fourier Transform of Eq. 2.1 we obtain

$$(-\omega^2 + i\omega\omega_0 d + \omega_0^2)\psi(\omega) = -\frac{4\pi a^2}{m} p_i(\omega) \tag{2.2}$$

where

$$d = \frac{b}{\omega_0 m} \ , \ \omega_0^2 = \frac{s}{m} \ , \ \Omega = \frac{\omega}{\omega_0} \ . \tag{2.3}$$

Rearranging Eq. 2.2 we obtain

$$\psi(\omega) = \frac{4\pi a^2}{s} H(\Omega) p_i(\omega) \tag{2.4}$$

where the transfer function from drive pressure to radial displacement is

$$H(\Omega) = \frac{1}{\Omega^2 - 1 - i\Omega d} \tag{2.5}$$

and where the absolute value and phase angle of $H(\Omega)$ are shown in Fig. 2.1. In the lower panel of this figure, we see that for drive frequencies well below resonance the displacement is π out of phase with the driving pressure. This means that the bubble is expanded and increased in size during the negative pressure cycle while compressed and reduced in size during the positive pressure cycle. For frequencies well above resonance the bubble responds differently to the drive pressure. The displacement and drive pressure are now in phase so that the bubble is increased in size during the positive pressure cycle and vice versa. Around resonance the displacement is approximately $\frac{\pi}{2}$ out of phase with the drive pressure. The absolute value of the amplitude of the transfer function is seen in the upper panel of the figure. Going from frequencies below resonance towards resonance the amplitude increases gradually culminating with a prominent peak around resonance for the situation with low damping ($d = 0.1$) and a considerable smaller peak for the situation with higher damping ($d = 0.5$). In both cases, the amplitude is seen to decrease rapidly above resonance.

2.2.2 Second Harmonic Component in Transmit Field

Wave propagation from a focused ultrasound transducer to the contrast-filled region being imaged is nonlinear because the tissue elasticity responds slightly nonlinearly when subject to an oscillating transmit pulse. The wave incident to the contrast agent will therefore contain second and possibly higher harmonic components. In this context the relative phase angle between the incident fundamental and second harmonic component is of special importance. This phase angle is in the present paper given as a fraction of the temporal period of the second harmonic component. When trying to determine the relative phase angle between the fundamental and second harmonic component, we will here mainly be concerned with pulses where the level of the second harmonic is around 20 dB below the fundamental component and where levels of higher harmonics are so low that these can be neglected. The mentioned phase angle is then found approximately by visual inspection of the pulses in the time domain.

We define the indicated phase angle to zero when the zero-crossings of the fundamental pressure component coincide with every second zero-crossing of the second harmonic pressure component. With this definition, zero phase angle gives a saw-tooth shaped pulse as shown in the upper panel of Fig. 2.2 where the compression period, going from positive to negative values, is less steep than the expansion period, going from negative to positive values. A phase angle of $-\frac{\pi}{2}$, shown in the lower panel of Fig. 2.2, gives a pulse with sharpened crests and rounded troughs where magnitudes of crests are larger than magnitudes of troughs. The actual phase angle in the transmit field from a focused medical ultrasound transducer is a result of wave diffraction. Depending on the axial and lateral position relative to the ultrasound beam axis, this phase angle is usually found to be somewhere between the two indicated cases in Fig. 2.2 [3, Chapter 12.6]. We will in the present paper from now on refer to this phase angle as Φ_{12}.

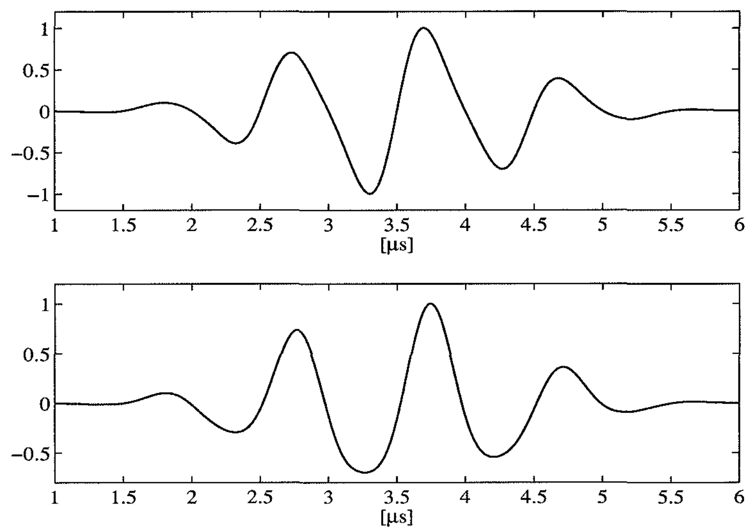

Figure 2.2: Definition of phase angle, Φ_{12}, between incident fundamental and second harmonic component. The sum of a fundamental and a second harmonic component is depicted. Upper panel: Phase angle, Φ_{12}, between fundamental and second harmonic component is zero. Lower panel: Phase angle, Φ_{12}, between fundamental and second harmonic component is $-\frac{\pi}{2}$.

2.3 Results

2.3.1 Simulation of Transmitted Wave Field

A nonlinear simulation program for wave propagation developed in our group [41], is used to calculate the acoustic transmit field. This program is capable of making a 3-dimensional simulation of the acoustic transmit field from an annular transducer taking nonlinear elasticity, frequency dependent absorption, and diffraction into account.

The simulated fundamental and second harmonic transmit field from an annular transducer is displayed in decibel scale in the left and right panel of Fig. 2.3, respectively. The vertical axis in the figure is range direction while the horizontal axis is the lateral direction. The radius of the annular transducer is 1 cm and the geometrical focus was set at 7 cm while the fundamental transmit frequency was set to 1 MHz. Acoustic parameters for muscle found in the literature [13] were used in the simulation. From the fundamental field, shown in the left panel in the figure, it is seen that most of the energy emitted from the transducer follows a geometrical cone in what is usually referred to as the near-field. The acoustic field in this near-field is, due to interference from different parts of the transducer, somewhat irregular, as can be seen from the intensity variations. In the region from about 4 cm to 8 cm, the energy is concentrated in a narrower region and then slowly diverges in the far-field. Acoustic absorption makes the amplitude in the far-field fall more rapidly than the relatively weak diverging effect of the field would suggest. From the right panel in the figure, the second harmonic component is seen to be negligible down to about 2 cm. The generated second harmonic component is somewhat better focused in the focal region and also more collimated in the far-field relative to the fundamental component. These results are in good agreement with analytical considerations [3, Chapter 12.6].

2.3.2 Simulations of Bubble Oscillation

Numerical simulations of bubble oscillations are done using a single bubble with acoustic properties comparable to the contrast agent *Sonazoid* [19]. This agent consists of bubbles containing perfluorcarbon gas encapsulated in a thin surfactant membrane. The bulk modulus of a typical bubble is around 600 kPa which is about 6 times the stiffness of a free gas bubble [19]. The resonance frequency of the bubble used in numerical simulations is around 4 MHz. Simulations for bubble radius oscillations and acoustic scattering are done using the numerical model developed by Angelsen *et al* [4]. As mentioned, this model and the well known Rayleigh-Plesset equation [33] [31] give similar results for drive pressures and bubble parameters studied in the present paper.

First, the bubble is driven into small radius oscillations so that a close to linear response can be assumed. Fig. 2.4(a) depicts the radius response from the bubble (lower panel) when driven well below resonance by a 0.5 MHz pressure pulse (upper panel). We see

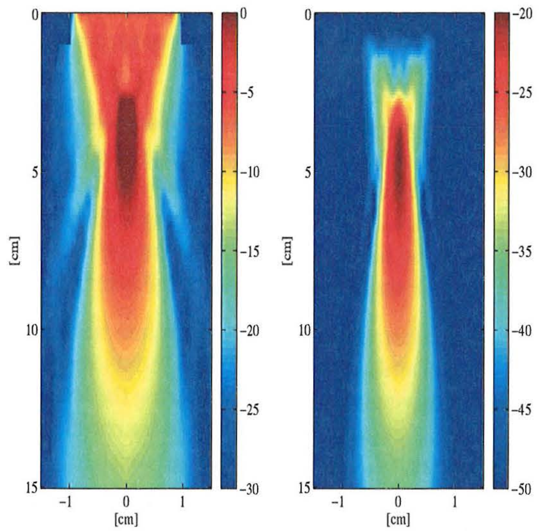

Figure 2.3: Simulated transmit field in decibel scale from an annular transducer with radius equal to 1 cm and geometric focus at 7 cm. Acoustic properties found in the literature for muscle is used [13]. Left panel: Fundamental transmit field. Right panel: Second harmonic transmit field.

that the bubble radius is π out of phase with the drive pressure which is in agreement with our linear considerations that led to Fig. 2.1.

By changing the frequency of our drive pressure to 4 MHz we drive the bubble at resonance and the radius response and drive pressure are displayed in the lower and upper panel of Fig. 2.4(b), respectively. The phase of the radius response relative to the drive pressure has now changed to $\frac{\pi}{2}$ as expected from Fig. 2.1. We also notice that the bubble "rings" for a short period of time after the drive pressure pulse has ended when driven at resonance. Finally, in Fig. 2.4(c), the radius response when driving the bubble well above resonance by a 10 MHz pressure pulse can be seen. The radius oscillation is now almost in phase with the drive pressure meaning that the bubble is expanded during the positive pressure cycle and compressed during the negative pressure cycle. Again, this is in agreement with the linear results from Fig. 2.1.

Similar simulation are then performed with higher amplitudes of the incident drive pressure so that the bubble in each case is driven into nonlinear oscillations. In all cases, the second harmonic component in the radius response is about 20 dB below the fundamental component whereas higher harmonic components are negligible. The phase angle between the fundamental and second harmonic component in the radius oscillation is from now on referred to as Θ_{12} and the same definitions as for Φ_{12} in Fig. 2.2 are used.

Fig. 2.5(a) shows the situation when the bubble is driven into nonlinear oscillations well below resonance. The fundamental component in the radius response is still approximately π out of phase with the drive pressure. By comparing the lower panel of Fig. 2.5(a) with Fig. 2.2, the relative phase angle between the fundamental and second harmonic component in the radius response, Θ_{12}, is found to be around $-\frac{\pi}{2}$.

The bubble is then driven into nonlinear oscillations at resonance and the radius response and drive pressure are shown in Fig. 2.5(b). As in the linear situation, the fundamental component of the radius oscillation is approximately $\frac{\pi}{2}$ out of phase with the drive pressure. We see that, due to the second harmonic component in the radius oscillation, the magnitudes of crests are now lower than magnitudes of troughs and the crests have become rounded while the troughs are sharpened. This is the opposite of what found in the lower panel of Fig. 2.5(a). The reason is that Θ_{12} has changed from $-\frac{\pi}{2}$ to $-\frac{3\pi}{2}$. The total phase shift on Θ_{12} is thus $-\pi$ when changing the drive frequency from well below resonance to resonance.

The result when the bubble is driven well above resonance is depicted in Fig. 2.5(c). We see from the upper panel that a very high pressure amplitude ($\sim$3 MPa) must be used in order to drive the bubble into nonlinear oscillations which agrees with the upper panel in Fig. 2.1 indicating that the amplitude of the transfer function from drive pressure to radius oscillation falls rapidly above resonance. The fundamental component of the radius oscillation is, as in the linear situation, in phase with the drive pressure. The phase angle Θ_{12} is, however, again approaching a value close to $-\frac{3\pi}{2}$.

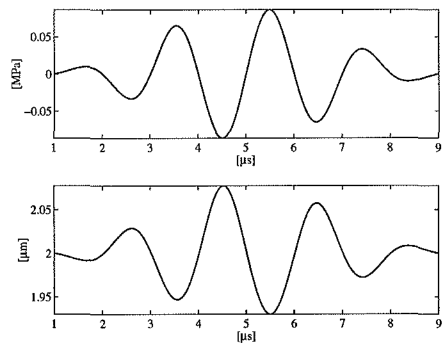

(a) Bubble driven well below resonance.

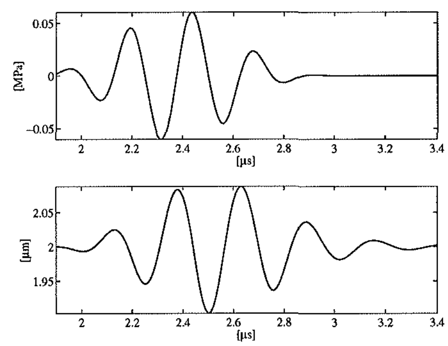

(b) Bubble driven at resonance.

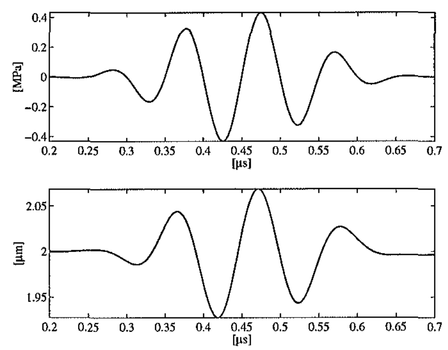

(c) Bubble driven well above resonance.

Figure 2.4: Bubble driven in close to linear oscillations. Upper panel in sub-figures: Drive pressure pulses. Lower panel in sub-figures: Bubble radius responses.

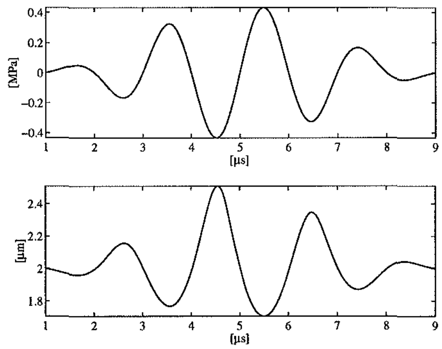

(a) Bubble driven well below resonance.

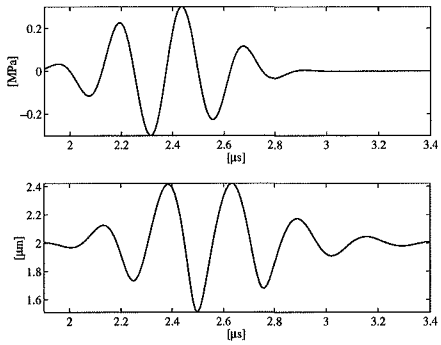

(b) Bubble driven at resonance.

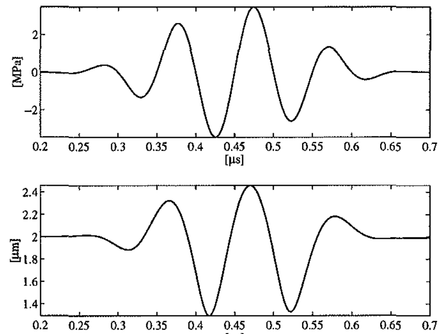

(c) Bubble driven well above resonance.

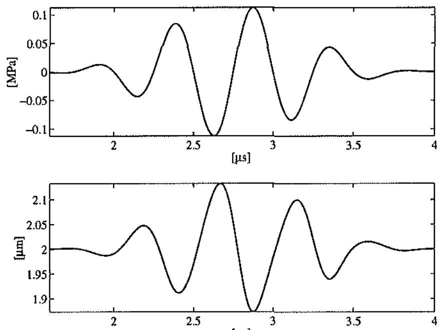

(d) Bubble driven at a normalized frequency, Ω, equal to 0.5.

Figure 2.5: Bubble driven into nonlinear oscillations. Second harmonic in radius oscillation is around 20 dB below fundamental component. Upper panel in sub-figures: Drive pressure pulses. Lower panel in sub-figures: Bubble radius responses.

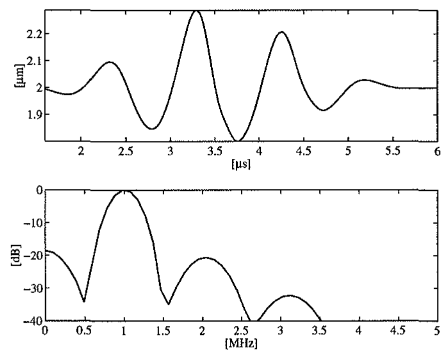

(a) Radius oscillation and amplitude of its frequency spectrum.

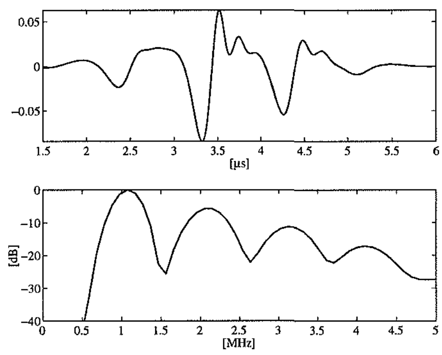

(b) Scattered pressure pulse and amplitude of its frequency spectrum.

Figure 2.6: Bubble driven by non-distorted pressure pulse at $\Omega = 0.25$.

Fig. 2.5(d) shows the bubble response when the bubble is driven at a normalized frequency, Ω, equal to 0.5. In this case Θ_{12} is close to $-\pi$ and magnitudes of crests are approximately equal to magnitudes of the troughs.

When varying the drive frequency from well below resonance to well above resonance the phase on the fundamental component of the radius response relative to the drive pressure changes from being π out of phase to being in phase, respectively. This result was obtained both when driving the bubble in close to linear oscillations and when driving it into nonlinear oscillations and Fig. 2.1 is therefore also a good approximation of the phase of the fundamental radius oscillation relative to the drive pressure for the nonlinear bubble. The radius phase angle Θ_{12} is, however, changing more rapidly when varying the drive frequency from $-\frac{\pi}{2}$ well below resonance to approximately $-\frac{3\pi}{2}$ at resonance. Above resonance, Θ_{12} first decreases towards $-\pi$ and then increases again approaching $-\frac{3\pi}{2}$ well above resonance.

The upper panel of Fig. 2.6(a) shows the radius oscillation in the time domain of the same bubble when driven by a 1 MHz incident pressure pulse. The amplitude of the incident pulse is approximately 250 kPa. In the lower panel of Fig. 2.6(a) the absolute value of the Fourier Transform of the radius oscillation is shown and we clearly see that the radius oscillation is nonlinear and that it mainly has a second harmonic component in addition to the linear fundamental component. The bubble is driven below resonance, at $\Omega = 0.25$, and we see that the phase angle Θ_{12} in the radius oscillation is close to $-\frac{\pi}{2}$. Also, the fundamental component of the radius oscillation is close to π out of phase with the drive pressure.

The far-field component of the scattered pressure from the same bubble is shown in

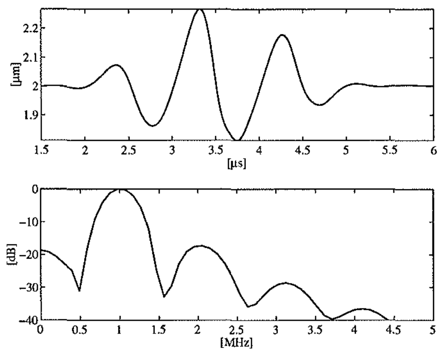

(a) Radius oscillation and amplitude of its frequency spectrum.

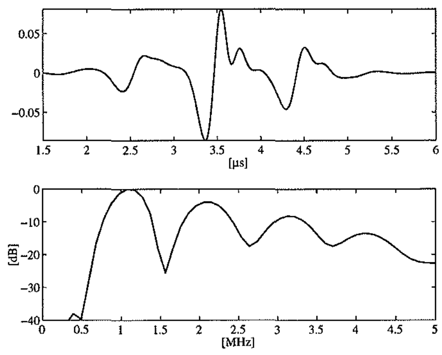

(b) Scattered pressure pulse and amplitude of its frequency spectrum.

Figure 2.7: Bubble driven by distorted pressure pulse at $\Omega = 0.25$. Second harmonic component in drive pressure is 23 dB below fundamental component, while $\Phi_{12} = 0$.

Fig. 2.6(b). This is the pressure component several wavelengths away from the bubble which we may pick up with an ultrasound transducer. The pressure pulse shown has not been modified by acoustic absorption due to wave propagation and we see that it has responded nonlinearly with significant amounts of energy at harmonic components not present in the drive pressure pulse.

We now drive the same bubble with a distorted incident pressure pulse which has the same fundamental component as the pressure drive pulse used in Fig. 2.6 but now also contains a second harmonic component which is 23 dB below the fundamental component. The second harmonic component in the drive pressure has a phase angle Φ_{12}, as defined in Fig. 2.2, equal to zero. The resulting radius response and scattered pressure are displayed in Fig. 2.7(a) and 2.7(b), respectively. Adding the second harmonic component in the drive pressure has slightly increased the second and third harmonic components in the radius response of the bubble as can be seen by comparing Fig. 2.7(a) and 2.6(a). A small fourth harmonic component is now also visible. The effect on the scattered pressure pulse from the bubble is similar, a small increase in all of the scattered harmonic components is found by comparing Fig. 2.7(b) and 2.6(b).

The bubble is then excited with a distorted incident pressure pulse similar to the one applied in Fig. 2.7, the only difference being that the phase angle Φ_{12} in the incident pressure pulse has changed from zero to $-\frac{\pi}{2}$. The upper panel of Fig. 2.8(a) shows the radius oscillation of the bubble in the time domain when driven by this new distorted pressure pulse. In the lower panel, the absolute value of the Fourier Transform of the radius oscillation is depicted and we see that the second harmonic component of the radius oscillation is

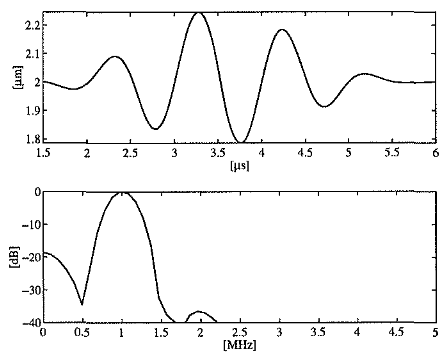

(a) Radius oscillation and amplitude of its frequency spectrum.

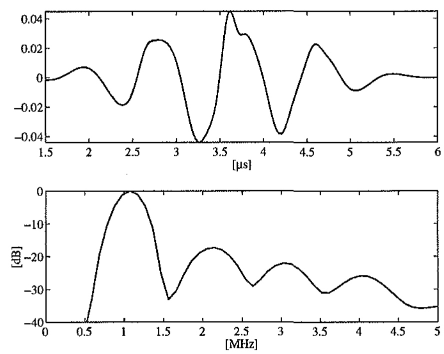

(b) Scattered pressure pulse and amplitude of its frequency spectrum.

Figure 2.8: Bubble driven by distorted pressure pulse at $\Omega = 0.25$. Second harmonic component in drive pressure is 23 dB below fundamental component, while $\Phi_{12} = -\frac{\pi}{2}$.

reduced compared to the lower panel of Fig. 2.6(a).

The fundamental component of the radius oscillation is approximately π out of phase with the fundamental component of the driving pressure. From our linear considerations resulting in Fig. 2.1, we may conclude that the linear radius response to the second harmonic component in the drive pressure, at $\Omega = 0.5$ in this case, is also close to π out of phase. It was seen in the upper panel of Fig. 2.6(a) that Θ_{12} in the radius oscillation was close to $-\frac{\pi}{2}$ when driven by a non-distorted drive pressure. When the bubble then is driven by a distorted pressure pulse containing a second harmonic component with phase angle close to $-\frac{\pi}{2}$ relative to the fundamental component, this distortion will have the potential to linearly cancel out or reduce the second harmonic component in the radius oscillation obtained when driving the bubble with the non-distorted pressure pulse as shown in the lower panel of Fig. 2.6(a).

Also important, is that the third harmonic component inherent in the radius oscillation in the lower panel of Fig. 2.6(a), obtained by using the non-distorted drive pressure, is canceled or significantly reduced when using this new distorted drive pressure as seen from the lower panel in Fig. 2.8(a). This is a nonlinear effect resulting from the mixing of the fundamental and second harmonic component in the distorted drive pressure pulse.

Fig. 2.8(b) displays the scattered pressure from the bubble driven by the new distorted pressure pulse. We observe that the levels of both the second, third, and fourth harmonic components are significantly reduced compared to what we found in the lower panel of Fig. 2.6(b) using a non-distorted driving pressure pulse. The diminishing effects on the third and fourth harmonic components in the scattered pressure pulse are nonlinear.

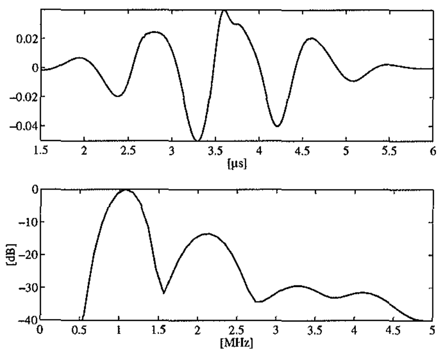

(a) Scattered pressure pulse and amplitude of its frequency spectrum.

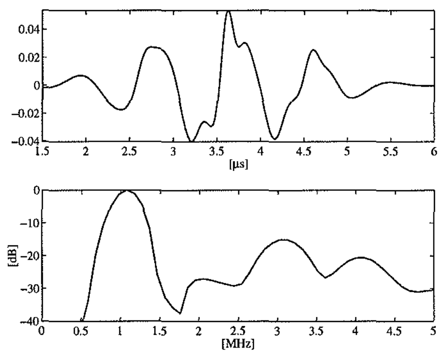

(b) Scattered pressure pulse and amplitude of its frequency spectrum.

Figure 2.9: Bubble driven by distorted pressure pulse at $\Omega = 0.25$. Second harmonic component in drive pressure is 25 dB and 21 dB below fundamental component, left and right panel, respectively, while $\Phi_{12} = -\frac{\pi}{2}$.

The resulting scattered pressure pulse from the bubble when reducing the level of second harmonic in the distorted drive pressure from 23 dB to 25 dB below the fundamental component, while keeping Φ_{12} equal to $-\frac{\pi}{2}$, is seen in Fig. 2.9(a). Comparing the lower panel of this figure with the lower panel of Fig. 2.8(b) we see that there is now a stronger reduction of the scattered third and fourth harmonic components whereas the scattered second harmonic component is somewhat less reduced.

Increasing the level of second harmonic in the distorted drive pressure to 21 dB below the fundamental component, and still not changing Φ_{12}, we obtain the results depicted in Fig. 2.9(b) for the scattered pressure pulse from the bubble. In this case, by comparison with the lower panel in Fig. 2.8(b), the reduction of the scattered second harmonic component is stronger while the third and fourth harmonic components are less diminished.

We now increase our drive frequency to 2 MHz so that $\Omega = 0.5$ for the fundamental component in the drive pressure. The amplitude of the drive pressure is now 180 kPa. Exposing the same bubble to this new drive pressure containing only a fundamental component we obtain the results shown in the upper and lower part of Fig. 2.10(a) for the radius oscillation in the time domain and the absolute value of the Fourier Transform of the radius oscillation, respectively. By comparing the upper panel of this figure with Fig. 2.2 we can conclude that Θ_{12} in the radius oscillation is similar to the situation in the upper panel of Fig. 2.2 where Φ_{12} is equal to zero. The difference is, however, that with our definition, zero phase angle results in a saw-tooth shaped pulse where the compression period from high to low value is less steep than the expansion period from low to

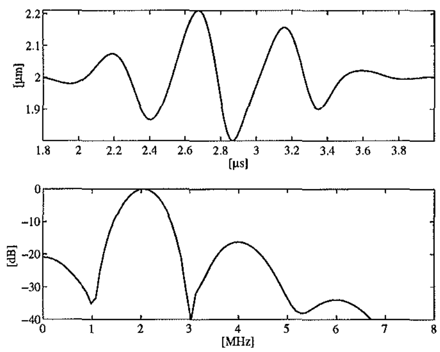

(a) Radius oscillation and amplitude of its frequency spectrum.

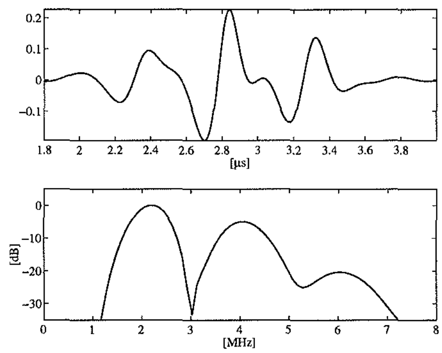

(b) Scattered pressure pulse and amplitude of its frequency spectrum.

Figure 2.10: Bubble driven by non-distorted pressure pulse at $\Omega = 0.5$.

high value. The radius response in Fig. 2.10(a) is a kind of saw-tooth shaped pulse where the compression part is steeper than the expansion part which results in a phase angle Θ_{12} in the radius response that is close to $-\pi$ with our definitions.

Fig. 2.10(b) displays the scattered pressure pulse from the bubble when driven by the non-distorted drive pressure which is seen to be nonlinear.

From Fig. 2.1 the linear radius response when driving the bubble at $\Omega = 0.5$ is close to π out of phase with the drive pressure. A second harmonic component in the drive pressure is now at resonance and for this case the linear radius response is $\frac{\pi}{2}$ out of phase with the drive pressure according to Fig. 2.1. Going from drive pressure to radius oscillation, the fundamental component in the drive pressure, at $\Omega = 0.5$, is shifted approximately π, the second harmonic component in the drive pressure, at $\Omega = 1$, is shifted $\frac{\pi}{2}$, while the phase relation between the fundamental and the second harmonic component of the radius oscillation, Θ_{12}, is close to $-\pi$ according to the upper panel of Fig. 2.10(a). Setting Φ_{12} in the distorted drive pressure equal to $-\frac{\pi}{2}$ will thus potentially cancel out or reduce the inherent second harmonic component in the lower panel of Fig. 2.10(a).

The bubble response is now calculated using the same fundamental component in the drive pressure as in Fig. 2.10 but adding a second harmonic component which is 23 dB below the fundamental component and where Φ_{12} is equal to $-\frac{\pi}{2}$. Radius oscillations resulting from driving the bubble with such a distorted pressure pulse is shown in Fig. 2.11(a). By comparing with Fig. 2.10(a) we notice that the nonlinearity of the radius response has been significantly reduced when driven by the distorted pressure pulse relative to when driven by the non-distorted pressure pulse.

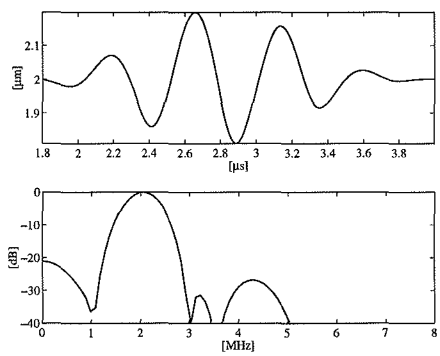

(a) Radius oscillation and amplitude of its frequency spectrum.

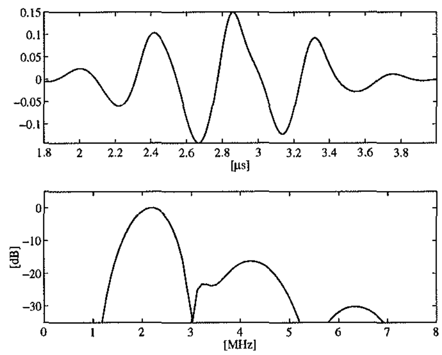

(b) Scattered pressure pulse and amplitude of its frequency spectrum.

Figure 2.11: Bubble driven by distorted pressure pulse at $\Omega = 0.5$. Second harmonic component in drive pressure is 23 dB below fundamental component, while $\Phi_{12} = -\frac{\pi}{2}$.

The scattered pressure from the bubble is displayed in Fig. 2.11(b) and by comparing with Fig. 2.10(b) we can conclude that the bubble response is much less nonlinear when driven by the distorted pressure pulse.

2.3.3 Driving the Bubble with the Simulated Transmit Field

The previous section showed that the presence of a small second harmonic component in the pressure pulse driving the bubble into oscillations potentially has a major diminishing effect on the nonlinear scattering properties of the bubble. It was also seen that the phase relation between the fundamental and second harmonic component in the drive pressure was of crucial importance. The obvious question is therefore if the phase relations found in actual transmit fields are such that a reduction of nonlinear scattering from the bubble will occur relative to what would be obtained if the second harmonic component in the transmit field was removed. In our investigations here we are going to use the acoustic transmit field obtained from numerical simulations with our simulation program for nonlinear wave propagation [41], shown in Fig. 2.3, to drive the contrast bubble. The level of the second harmonic component, shown in the right panel of the figure, is in the near-field too low to have any effect on the scattering from the contrast bubble and the near-field is hence not interesting in the present context.

The calculated pressure pulse at 10 cm on the symmetry axis of the transmit field is shown in Fig. 2.12(a). The solid line is the distorted pressure pulse obtained from the simulation

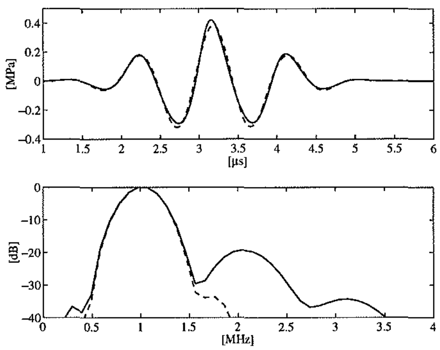

(a) Drive pressure pulses and amplitude of their frequency spectra.

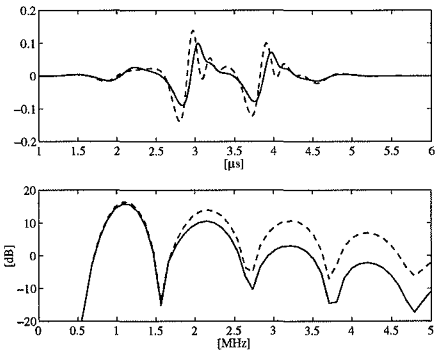

(b) Scattered pressure pulses and amplitude of their frequency spectra.

Figure 2.12: Solid lines: Calculated transmit pressure pulse at 10 cm on the symmetry axis in Fig. 2.3 (left panel) and resulting scattered pressure pulse (right panel). Dashed lines: Fundamental component only of calculated transmit pressure pulse at 10 cm on symmetry axis in Fig. 2.3 (left panel) and resulting scattered pressure pulse (right panel).

program whereas the dashed line represents the fundamental component only of the obtained distorted pressure pulse. In the time domain, in the upper panel of the figure, we see there is a rather small difference between the original and filtered pulse, whereas in the frequency domain, in the lower panel, the graphs are plotted in decibel scale and the difference is more clearly seen.

In Fig. 2.12(b), the scattered pressure pulse from the bubble when driven by the distorted and the filtered pulse in Fig. 2.12(a) is displayed, solid and dashed line, respectively. The level of the scattered fundamental component is similar for the two scattered pulses which is natural since the fundamental component in the two drive pulses are identical. The second harmonic component scattered from the bubble is, however, reduced by approximately 3 dB when driven by the distorted pulse compared to when driven by the pulse containing the fundamental component only. Looking at the third harmonic component scattered from the bubble, we see that the reduction in scattering is somewhat stronger, the reduction now being around 7 dB when driven by the total distorted pressure pulse relative to when driven by the fundamental component only. The scattered fourth harmonic component is even slightly more reduced due to the distortion of the incident drive pulse with a reduction of about 9 dB.

We then take out the simulated pressure pulse at 12 cm but 8 mm to the side of the symmetry axis of the transmit field and this pressure pulse is displayed in Fig. 2.13(a). Again, the solid line is the total distorted pressure pulse obtained while the dashed line represents the

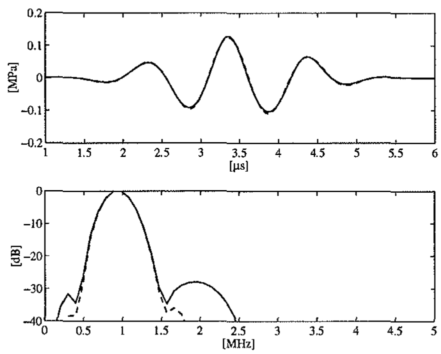

(a) Drive pressure pulses and amplitude of their frequency spectra.

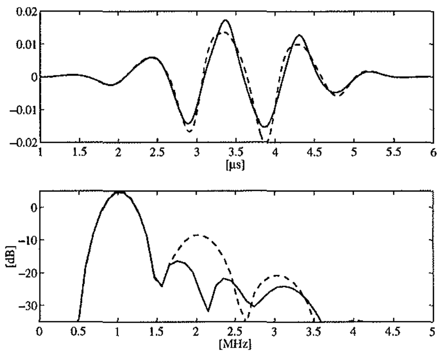

(b) Scattered pressure pulses and amplitude of their frequency spectra.

Figure 2.13: Solid lines: Calculated transmit pressure pulse at 12 cm but 8 mm off the symmetry axis in Fig. 2.3 (left panel) and resulting scattered pressure pulse (right panel). Dashed lines: Fundamental component only of calculated transmit pressure pulse at 12 cm and 8 mm off symmetry axis in Fig. 2.3 (left panel) and resulting scattered pressure pulse (right panel).

fundamental component only of the calculated pressure. In the time domain, in the upper panel of the figure, the original and filtered pulse are now almost indistinguishable due to the low level of second harmonic in the distorted pulse at this location. The difference in scattered pressure from the bubble when driving it with the distorted versus the filtered pressure pulse is, however, significant as shown in Fig. 2.13(b). As seen from the figure, the second harmonic component is now heavily reduced by approximately 10 dB when applying the distorted drive pressure relative to applying the fundamental component only whereas the effect on the scattered third harmonic component is less significant.

In Table 2.1 the results obtained by taking out the simulated transmit pressure pulse at various locations in the transmit field in Fig. 2.3 and applying it on the same contrast bubble are summarized. Unless otherwise noted, pressure drive pulses from the symmetry axis are used. This table shows the reduction of nonlinearly scattered harmonic components from the bubble when driven by the distorted transmit pressure pulse relative to the fundamental component only of the transmit pressure pulse. For the combination of transmit field and contrast bubble used in the present paper, reduction of nonlinear scattering from the bubble using the distorted drive pulse versus fundamental component only, was found to be insignificant using transmit drive pressure pulses in the location between the transducer and down to about 6 cm in Fig. 2.3. Down to about 2 or 3 cm, the level of the second harmonic component in the transmit field is too low to have any significant effect on the scattering from the contrast bubble. Between 3 and 6 cm, a significant amount of second harmonic builds up in the transmit field, as seen in the right panel of Fig. 2.3, but the phase angle Φ_{12} between the fundamental and second harmonic component is such that a reduction of nonlinear scattering from the contrast bubble does not occur. Below 6 cm the effect of the pulse distortion in the transmit field is, however, significant as seen from Table 2.1. At the symmetry axis, the diminishing effect due to the distorted incident drive pulse on the nonlinear scattering from the bubble is most severe on the scattered third and fourth harmonic components whereas the scattered second harmonic component is reduced by 2 or 3 dB. Using drive pulses off the symmetry axis, we see that the diminishing effect on the scattered second harmonic component is stronger.

Table 2.1: Reduction of scattered contrast harmonic components due to incident pulse distortion

	2^{nd} harmonic	3^{rd} harmonic	4^{th} harmonic
6 cm	2 dB	3 dB	3 dB
8 cm	3 dB	5 dB	5 dB
10 cm	3 dB	7 dB	9 dB
12 cm	2 dB	8 dB	15 dB
14 cm	2 dB	4 dB	6 dB
8 cm [a]	3 dB	4 dB	4 dB
10 cm [a]	4 dB	8 dB	8 dB
12 cm [a]	3 dB	12 dB	
14 cm [a]	2 dB	7 dB	
10 cm [b]	8 dB	2 dB	
12 cm [b]	10 dB	3 dB	
14 cm [b]	6 dB	2 dB	

[a] 4 mm off symmetry axis
[b] 8 mm off symmetry axis

2.4 Conclusions

This paper has, based on numerical simulations, investigated bubble radius oscillations and scattered pressure pulses from a contrast bubble driven by various incident pressure pulses. Results from using several distorted incident pressure pulses are compared with the results from using the fundamental component only of the distorted incident drive pressure pulses. The distortion of the pressure pulse incident to the contrast bubble occurs due the the nonlinear nature of tissue elasticity and the relative phase angle between the fundamental and second harmonic component in the transmit field is a result of wave diffraction. A calculated transmit field from an annular ultrasound transducer was obtained using a nonlinear numerical simulation tool developed in our group. Driving a contrast bubble with the distorted transmit field obtained from this simulation program and comparing the resulting scattering with the scattering obtained by driving the same bubble with the fundamental component only of the calculated transmit field clearly indicates that the relatively small distortion introduced due to nonlinear wave propagation has a potentially strong diminishing effect on the nonlinear scattering from the contrast bubble. In the transmit near-field, the pulse distortion is typically very low and its effect on the nonlinear scattering from the bubble is found to be negligible. However, in the focal region and especially in the far-field of the transmit field, the distortion of the pressure pulse incident to the bubble is found to have a significant diminishing effect on its nonlinear scattering properties.

The diminishing effect, due to pulse distortion caused by nonlinear wave propagation, on the scattered second harmonic component from the contrast bubble can to a large extent be explained as a linear process, *i.e.* separately driving the bubble with the fundamental and second harmonic components of the distorted incident drive pulse and then summing the two scattered contributions together. The diminishing effects on the scattered third and fourth harmonic components from the contrast bubble are, however, nonlinear.

2.5 Aknowledgemets

This work was supported by the Research Council of Norway.

Chapter 3

Using Barker Codes in Contrast Harmonic Imaging

Abstract

Received scattered harmonic components typically contain less energy than the linearly received fundamental component and, in contrast harmonic imaging techniques, the limiting factor is often the noise signal always present in a pulse echo imaging system and not the masking of the contrast signal by the tissue signal. Pulse compression techniques, familiar from radar systems and communication theory, are techniques for increasing the signal level relative to the noise level of the pulse echo imaging system which is assumed to be constant and evenly distributed over all frequencies of interest. The transmitted signal level is increased by transmitting an elongated pulse and not by increasing the transmit amplitude. To restore range resolution, the resulting received signals must then be compressed. This paper investigates the use of Barker codes, which are a type of pulse compression codes, and their potential to increase the signal level of the scattered third harmonic component from contrast bubbles relative to the constant noise level.

3.1 Introduction

Medical ultrasound contrast agents are used to enhance the ultrasound signal scattered from blood since ultrasound scattering from blood is much weaker than scattering from soft tissue. The contrast agents are typically made as solutions of small gas bubbles in a fluid and scattering from such gas bubbles is potentially a highly nonlinear process [23] [11] [12].

Ultrasound wave propagation is also known to be a nonlinear process at frequencies and amplitudes commonly used in medical ultrasound imaging. The nonlinearity of the wave propagation is, however, significantly weaker than for the scattering process from the contrast bubbles, and contrast harmonic imaging is thus an interesting imaging technique since scattering from tissue is assumed to be a linear process.

In contrast harmonic imaging, a harmonic band of the fundamental transmitted band is used for bubble detection. The scattered contrast signal is more distorted than the scattered tissue signal and by using higher harmonic components of the received signal for image reconstruction, one would presumably achieve better differentiation between tissue signal and contrast signal. The amplitude of the received tissue harmonics are significantly lower than for the linearly received fundamental component and as higher harmonics are considered, this amplitude drops steeply. The amplitude of the received contrast harmonics are also typically lower than for the received fundamental component. As higher contrast harmonics are considered, the level of the amplitude usually falls although not as fast as for the tissue harmonics.

The ultrasound medical imaging system is a pulse echo imaging system suffering from thermal and electronic noise and, as higher signal harmonics are used for image reconstruction, the level of these harmonics will be comparable to the noise level of the system resulting in image degradation. Application of higher harmonic components implies reduced penetration depth due to the frequency dependent absorption in tissue and a reduction of the received harmonic signal amplitude from the contrast agent.

If the noise level in a pulse echo imaging system is assumed to be constant, the only way to increase the Signal to Noise Ratio (SNR) is by increasing the signal level. In medical ultrasound imaging the transmitted acoustic amplitude cannot be arbitrarily high due to patient safety [8] [5]. Also, the bubbles tend to get destroyed even during imaging at relatively low intensities so that the intensity in the transmit field must be kept relatively low if bubble destruction is unwanted.

Pulse compression techniques, known from radar systems and communication theory, have the ability to improve the SNR without increasing the peak amplitude levels transmitted. A pulse of long duration compared to a conventional transmit pulse is transmitted and the received echo signal is processed with a matched filter [21, Chapter 4.8] [40, Chapter 5.4] to achieve sufficient range resolution. These techniques introduce range sidelobe artifacts which typically are inadequate for medical ultrasound imaging. The range sidelobes can, however, be further reduced with deconvolution type filters.

Barker codes [21, Chapter 6.9] are a type of pulse compression codes where a long pulse is made up of M subpulses which are phase coded and where the phase of the subpulses is either 0 or π. These codes are sequences for which the sidelobes of the autocorrelation function do not exceed $1/M$. Only nine such codes exist, the longest one being of length $M = 13$.

Contrast harmonic imaging using the third harmonic component will typically give superior Contrast to Tissue Ratio (CTR) but inferior Contrast to Noise Ratio (CNR) when compared to second harmonic contrast imaging. The CTR is better due to the high nonlinearity of the scattering from the contrast bubbles compared to the weaker nonlinearity of the wave propagation in soft tissue. CNR will generally be lower due to the relatively lower level of received third harmonics from the bubble assuming the noise level to be constant over the frequency range of interest. By using Barker codes to increase the CNR at the received third harmonic component, it may be possible to achieve adequate CNR and CTR with third harmonic contrast agent imaging.

The contrast bubbles added to the blood flow will, contrary to the situation in radar systems and communication theory, represent a nonlinear, resonant, and unstable medium for scattering of the incident waves. The nonlinear response from the contrast bubbles, utilized in contrast harmonic imaging, depends strongly on the amplitude, frequency, and envelope of the incident pulse. Contrast bubbles are typically encapsulated in a thin stabilizing shell with acoustic properties that may be altered during insonification by ultrasound. Due to the pumping of the heart muscle, the bubbles will have time varying velocities. In addition, there may be interactions between the bubbles and the incident wave field will impose a radiation force on the bubbles with a resulting time varying velocity in the propagation direction of the field. The present paper will try to investigate some of these indicated effects in relation to the application of Barker codes in contrast harmonic imaging.

3.2 Theory

3.2.1 Overview

The motivation for introducing pulse compression techniques in contrast harmonic imaging is a need to increase the CNR, especially at the third or higher harmonic components. Deconvolution of the received signal can be done using a modified inverse filter where the deconvolution kernel for example is based solely on a binary Barker sequence. This deconvolution operation on the received signal is necessary to restore the range resolution which is lost when transmitting an elongated pulse. The idea behind pulse compression techniques is to increase the SNR by increasing the signal level transmitted and assuming the noise level to be constant. The transmitted signal level is increased by transmitting an elongated pulse and not by increasing the amplitude level transmitted. With noise we here mean noise uncorrelated with the transmitted signal such as thermal and electronic noise.

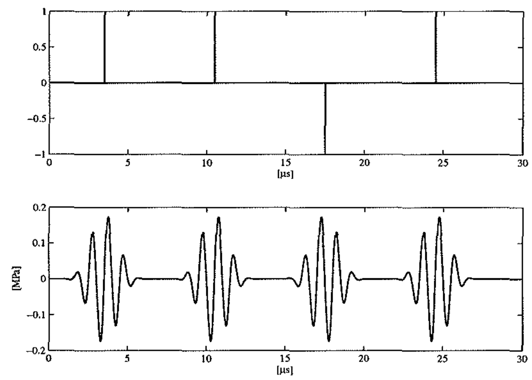

Figure 3.1: Upper panel: Four bit binary Barker sequence. Lower panel: Transmitted four bit Barker sequence.

3.2.2 Barker Codes

The Barker codes are pulse compression codes, made up of M contiguous subpulses, which are modulated in phase. The phase modulation is either 0 or π and the code is a binary sequence taking values 1 and -1. The upper panel of Fig. 3.1 shows an example of a four bit Barker code where the third bit has a phase shift of π relative to the others. In the lower panel, an example of a transmitted four bit Barker code is shown, and the binary four bit code has then been convolved with a conventional transmit pulse. As can be seen, the individual subpulses in the Barker sequence have been somewhat separated in time. This is done to adequately separate the contrast echos from each subpulse since the scattering from contrast bubbles is a highly nonlinear process and the principle of superposition is therefore not valid. If the received signal, obtained using the conventional transmit pulse, is defined as

$$r_1(t) = s(t) + n(t) \tag{3.1}$$

where $s(t)$ is the sum of the tissue signal and contrast signal and $n(t)$ is the noise signal due to thermal and electronic noise, the signal received when transmitting the elongated Barker code, is

$$r_2(t) = b(t) * s(t) + n(t) \tag{3.2}$$

where $b(t)$ is the binary Barker code. Here, the asterisk denotes the convolution operation. The received signal $r_2(t)$ must be processed with a deconvolution filter to restore range resolution. In the noise free case, applying the inverse filter

$$H_I(f) = \frac{1}{B(f)} \tag{3.3}$$

where $B(f)$ is the Fourier Transform of $b(t)$, would produce the same signal as obtained using the conventional transmit pulse. In a real situation where noise is a part of the received signal, this inverse filter would, however, cause a large amplification of the noise signal at frequencies where $|B(f)|$ is low. To compensate for this unwanted effect we may use a stabilized inverse filter instead. This deconvolution filter takes the form

$$H_W(f) = \frac{B^*(f)}{|B(f)|^2 + \frac{max|B(f)|^2}{N}} \tag{3.4}$$

where $B^*(f)$ is the complex conjugate of $B(f)$, and N is a noise parameter, while the term $\frac{max|B(f)|^2}{N}$ can be thought of as the inverse of the SNR of the system. This filter is similar to the optimal Wiener filter [1, Chapter 8.1] [32, Chapter 8.5] obtained performing a least-squares derivation. We see that if N is large compared to $|B(f)|$ the filter is similar to the inverse filter in Eq. 3.3. On the other hand, as N is reduced the filter will approach

$$H_M(f) = N\frac{B^*(f)}{max|B(f)|^2} \tag{3.5}$$

which is the matched filter commonly used in radar imaging [21, Chapter 4.8] [40, Chapter 5.4].

3.2.3 Bubble Oscillation

The contrast bubble is assumed to be a spherical bubble of gas encapsulated in a thin shell. The diameter of the bubble is much less than the wavelength of the incoming wave field and the bubble thus experiences an approximately spatial uniform field and the bubble oscillation is assumed to be purely spherical. Simulations for bubble radius oscillations and acoustic scattering are done using the numerical model developed by Angelsen *et al* [4]. This model includes an equation for the relation between pressure and radial strain in a thin shell encapsulating a gas bubble. The model allows for a finite speed of sound in the medium surrounding the bubble, thus taking radiation losses from the bubble into account. Otherwise it is comparable to the well known Rayleigh-Plesset equation [33] [31] and the two models give similar results for incident pressure amplitudes and bubble parameters studied in this paper.

3.3 Numerical Results

3.3.1 Noise Free Sequence without Harmonic Components

If a noise free Barker sequence, as shown in the lower panel of Fig. 3.1, is processed with the stabilized inverse filter in Eq. 3.4, the range sidelobe level of the compressed sequence can be set arbitrarily by choosing the parameter N. A low range sidelobe level is essential in medical ultrasound imaging where the displayed dynamic range is large to ensure the

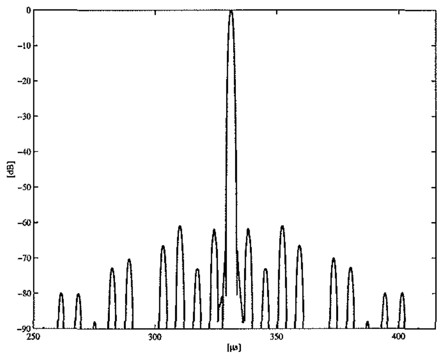

(a) Sidelobes after pulse compression.

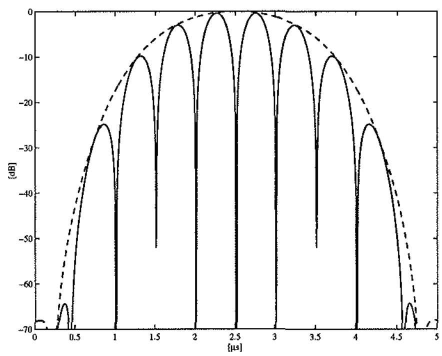

(b) Width of mainlobe after pulse compression.

Figure 3.2: Left panel: Example of a noise free compressed sequence where $B(f)$ is normalized to 1 and N in Eq. 3.4 is set to 10^3. Right panel: Absolute value of one of the subpulses in the Barker sequence shown in the lower panel in Fig. 3.1 (solid line). Range mainlobe after deconvolution of the Barker sequence in the lower panel in Fig. 3.1 with the stabilized inverse filter in Eq. 3.4 (dashed line).

ability to separate strong and weak scatterers. Fig. 3.2(a) shows an example where $B(f)$ is normalized to 1 and the parameter N has been set to 10^3 and the range sidelobe level in the compressed noise free sequence is thus down at 60 dB.

The width of the range mainlobe in the compressed sequence is also an important parameter and should be as small as possible to ensure good range resolution in the ultrasound image. The width of the mainlobe is given by the length of the individual subpulses in the transmitted Barker sequence as shown in Fig. 3.2(b). Here, the solid line is the absolute value of one of the subpulses in the lower panel of Fig. 3.1, while the dashed line depicts the range mainlobe obtained after deconvolution with the stabilized inverse filter in Eq. 3.4. We observe that the mainlobe of the compressed sequence is equal to the envelope of the subpulses processed by the stabilized inverse filter.

In a typical medical ultrasound contrast imaging situation there are several effects which potentially will increase the range sidelobe level shown in Fig. 3.2(a). We will now try to investigate some of the presumably most important effects.

3.3.2 Presence of Several Harmonics in Signal for Processing

Ultrasound scattering from the contrast bubbles is highly nonlinear and the received contrast agent signal will contain energy in several harmonic bands. Although it is possible to use the indicated pulse compression technique without bandpass filtering, *i.e.* on the total received signal, this is not attractive in contrast agent imaging since the strong fundamental component scattered from the tissue would mask the signal scattered from the contrast agent.

Using this form of phase coding on the received second harmonic component would not yield good results as can be seen from the following equation

$$s(t) = \sum_{n=1}^{\infty} a_n(t)p^n(t-\tau) \tag{3.6}$$

where $a_n(t)$ are positive amplitude functions and where the received signal, $s(t)$, is modeled by a simple power expansion of the transmitted pulse, $p(t)$, with a time delay τ. We observe that the second harmonic component is a quadratic effect of the transmitted signal and phase coding with Barker sequences, where the transmitted sequence is phase coded with π, utilizing the second or any other even harmonic component of the received signal is not fruitful. Using this pulse compression technique on the received third harmonic component is, however, interesting. The third harmonic component from tissue is, as previously indicated, low when imaging with relatively low intensity, while the third harmonic component from the contrast agent is considerable due to the high nonlinearity of the ultrasound scattering from gas bubbles.

Using the scattered third harmonic component means that a third harmonic bandpass filter must be applied on the received signal in addition to the stabilized inverse filter in Eq. 3.4. The upper panel of Fig. 3.3 shows an example of a four bit Barker code consisting of three harmonic components according to Eq. 3.6, and in the lower panel we see the absolute value of the Fourier transform of the time sequence in the upper panel. The special appearance of the three harmonic components in frequency domain is a result of the combing effect introduced by the Barker sequence.

The third harmonic component of the sequence is obtained with a third harmonic bandpass filter and the stabilized inverse filter is then applied to compress the code. Results using two different bandwidths in the third harmonic bandpass filter are shown in Fig. 3.4. The solid line is the ideal compressed code obtained for an imagined case when there is no fundamental or second harmonic component present in the received signal, *i.e.* only $a_3(t)$ is different from zero in Eq. 3.6. The dotted line is obtained using a third harmonic Gaussian filter with a -6 dB bandwidth equal to 0.4 MHz (narrowband) on the signal in Fig. 3.3, while the dashed line is obtained using a similar filter with a -6 dB bandwidth equal to 0.85 MHz (broadband) on the same signal. For the dashed line, the range sidelobe level has increased significantly compared to the ideal situation when there is only a third harmonic component present in the total signal. The reason is an overlap from the second

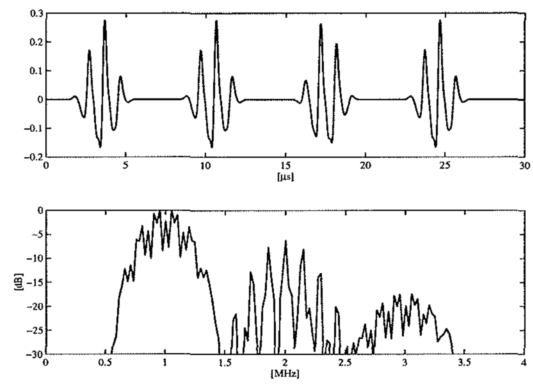

Figure 3.3: Upper panel: Four bit Barker sequence consisting of three harmonic components according to Eq. 3.6. Lower panel: Absolute value of Fourier transform of the sequence in the upper panel.

harmonic component into the third harmonic band processed by the stabilized inverse filter.

This overlap in frequency is seen in Fig. 3.5 which displays the absolute value of the Fourier Transform of one of the subpulses in the upper panel of Fig. 3.3. When using the broadband third harmonic bandpass filter (dotted line with circles) the level of second harmonic (dashed line) in the passband of the filter is much higher than when the narrowband third harmonic bandpass filter (dotted line with diamonds) is applied. The presence of a second harmonic component in the signal fed to the stabilized inverse filter easily increases the range sidelobes, as seen from Fig. 3.4, due to the fact that this second harmonic component is not phase coded as previously explained. When the narrowband filter is used we see from Fig. 3.4 that the increase in range sidelobes is not so drastic. Applying the narrowband filter there is, however, a significant increase in the width of the mainlobe which will degrade range resolution and hence the ability to separate targets which are close.

3.3.3 Effect of Acoustic Power Absorption

Both the forward propagating transmit pulse and the scattered pulses from the contrast bubbles propagating back to the ultrasound transducer will be modified by a frequency dependent absorption in the tissue. This frequency dependent absorption will, depending of number of wave lengths propagated, shift the scattered pulses somewhat down in frequency. In the lower panel of Fig. 3.6, it is shown how the normalized third harmonic component of a subpulse affected by an absorption of 10 dB/MHz (dashed line) may appear compared to one not affected by absorption (solid line). The upper panel of Fig. 3.6

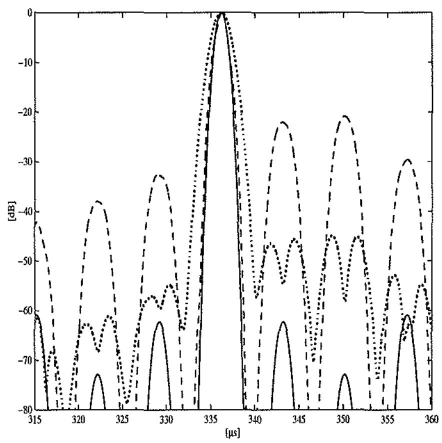

Figure 3.4: Effect of bandwidth in the third harmonic bandpass filter on range sidelobe levels and width of mainlobe. Solid line is the results after pulse compression for the ideal case without a fundamental or second harmonic component present in the original sequence. The dashed line is obtained using the broadband third harmonic Gaussian filter on the sequence in Fig. 3.3 while the dotted line is obtained using the narrowband third harmonic Gaussian filter on the same sequence.

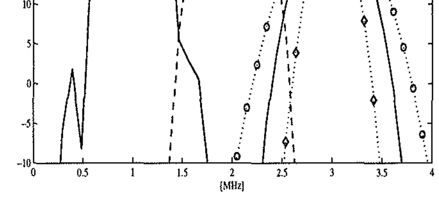

Figure 3.5: Pulse consisting of three harmonic bands, second harmonic band displayed as dashed line. Third harmonic Gaussian filters, broadband and narrowband, dotted line with circles and dotted line with diamonds, respectively.

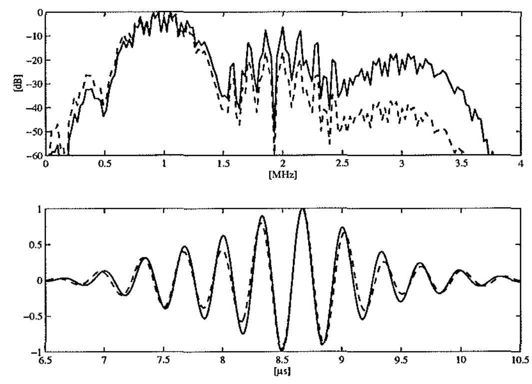

Figure 3.6: Upper panel: Normalized absolute value of Fourier transform of Barker sequence not affected by absorption (solid line) and affected by an absorption of 10 dB/MHz (dashed line). Lower panel: Normalized third harmonic component of one of the subpulses in a Barker sequence not affected by absorption (solid line) and one affected by an absorption of 10 dB/MHz (dashed line).

depicts the absolute value of the Fourier transform of the Barker sequences before the third harmonic filter is applied where the solid line is the original sequence and the dashed line is the sequence affected by absorption. The two sequences have been normalized to the same maximum value.

In Fig. 3.7 the results after applying the stabilized inverse filter on the original sequence not affected by absorption and on the one affected by an absorption of 10 dB/MHz are shown. The upper panel is for the case when the broadband third harmonic Gaussian filter is used while the lower panel shows results obtained using the narrowband third harmonic bandpass filter. We see that when applying the narrowband and broadband third harmonic bandpass filter, the frequency dependent absorption increases the range sidelobe level by around 3 and 8 dB, respectively.

3.3.4 Bubble Signal with Infinite CNR

The upper panel of Fig. 3.8 shows the scattered pressure pulse from a bubble with resonance frequency around 4 MHz when driven by the acoustic pressure pulse in the lower panel of Fig. 3.1 which has a center frequency of 1 MHz. In the lower panel of Fig. 3.8, the absolute value of the Fourier Transform of the sequence in upper panel is displayed and the scattered pressure pulse is clearly seen to contain energy at several harmonic bands. The third harmonic component of the scattered pressure pulse is obtained using the two harmonic Gaussian filters from Fig. 3.5 and the filtered sequences are processed

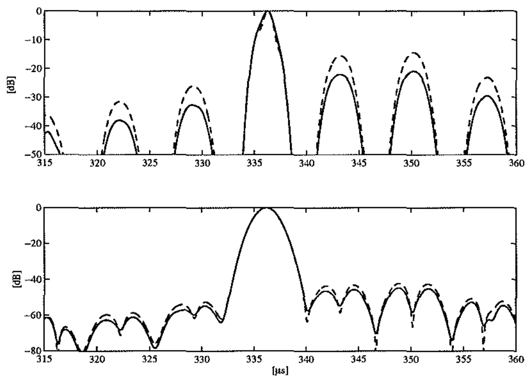

Figure 3.7: Effect of absorption on range sidelobe level. Solid line is obtained from the original sequence while the dashed line is obtained from the sequence affected by an absorption of 10 dB/MHz. Upper panel: The broadband Gaussian third harmonic bandpass filter has been applied. Lower panel: The narrowband third harmonic Gaussian filter has been applied.

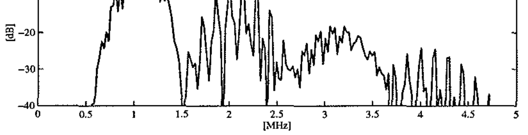

Figure 3.8: Upper panel: Scattered pressure pulse from a 4 μm bubble with resonance frequency around 4 MHz when driven by the acoustic pulse in the lower panel of Fig. 3.1. Lower panel: Absolute value of the Fourier Transform of the time sequence in the upper panel.

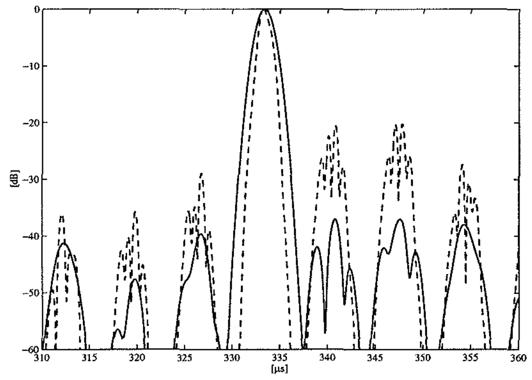

Figure 3.9: Results after applying the stabilized inverse filter on the third harmonic component of the scattered pressure pulse shown in Fig. 3.8. Solid line is obtained using the narrowband third harmonic filter while the dashed line is obtained using the broadband third harmonic bandpass filter.

with the stabilized inverse filter from Eq. 3.4.

Results after deconvolution are depicted in Fig. 3.9 where the solid and dashed lines are obtained using the narrowband and broadband third harmonic bandpass filter, respectively. After deconvolution, the sidelobe level is approximately down at 40 and 20 dB using the narrowband and broadband bandpass filter, respectively. These results are obtained on sequences for which uncorrelated noise still has not been added and the sidelobe level in the compressed pulse is mainly due to the presence of second (and fourth) harmonic signal components in the filtered signals processed by the stabilized inverse filter. From Fig. 3.4 it was seen that the presence of a second harmonic component in the signal fed to the stabilized inverse filter significantly increased the range sidelobe level in the compressed signal relative to the imagined situation having only the third harmonic signal component.

Also, as seen from the lower panel of Fig. 3.8, the harmonic components scattered below resonance are somewhat shifted up in frequency relative to harmonics of the drive frequency which is centered around 1 MHz. The upward frequency shift of the scattered third harmonic component is opposite to the downward frequency shift displayed in the upper panel of Fig. 3.6 obtained due to absorption. This frequency shift will thus also contribute somewhat to the sidelobe level obtained in Fig. 3.9 in a similar manner as the absorption increased the sidelobes in Fig. 3.7.

In addition, as discussed in the next section, the response from the nonlinear, resonant bubble will depend on the bandwidth of the incident drive pulse and the bubble may respond differently on the third subpulse where the polarity is inverted relative to the three other subpulses. The incident drive pulse in the lower panel of Fig. 3.1 is, however,

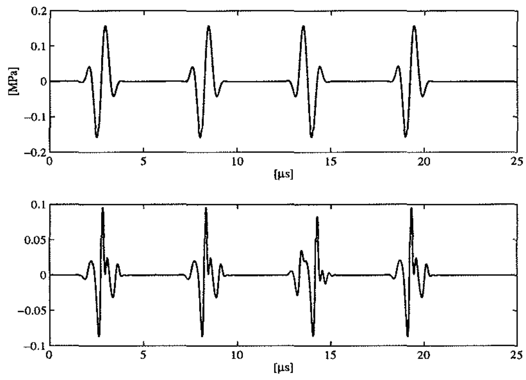

Figure 3.10: Upper panel:Broadband incident Barker sequence. Lower panel: Resulting scattered pressure pulse from a 4 μm bubble.

sufficiently narrowbanded for this effect to be marginal.

3.3.5 Transmit Pulse Bandwidth

The contrast bubble represents a highly nonlinear and resonant medium for scattering of the incident transmit pulse. For a wide bandwidth incident pulse consisting of only a few half periods, the bubble may respond differently when the incident oscillation begins with a rarefaction period rather than a compression period [29] [28]. In addition, problems with the presence of second (and fourth) harmonic signal components in the passband of the third harmonic bandpass filter discussed in Sec. 3.3.2 will be bigger applying broadband transmit pulses.

Fig. 3.10 displays an example of a broadband transmit Barker sequence, upper panel, and the resulting scattered pressure pulse from the bubble, lower panel.

In the upper panel of Fig. 3.11 we see the third harmonic envelope, obtained with the narrowband bandpass filter, of the scattered pulse from the lower panel of Fig. 3.10 as the solid line. The dashed line shows the resulting third harmonic envelope obtained by using a drive pulse similar to the one in the upper panel of Fig. 3.10 but without the phase shift on the third subpulse, *i.e.* consisting of four identical subpulses. The nonlinear response from the bubble when driven by the broadband subpulse with inverted polarity is clearly seen to be different from results obtained with the three other subpulses. We notice that the third harmonic envelope from the third subpulse in the scattered Barker sequence is somewhat time delayed and has lower amplitude relative to the other scattered subpulses.

In the lower panel of Fig. 3.11, the result after pulse compression is depicted and we see that the sidelobe level is very high compared to Fig. 3.9 obtained by using the more

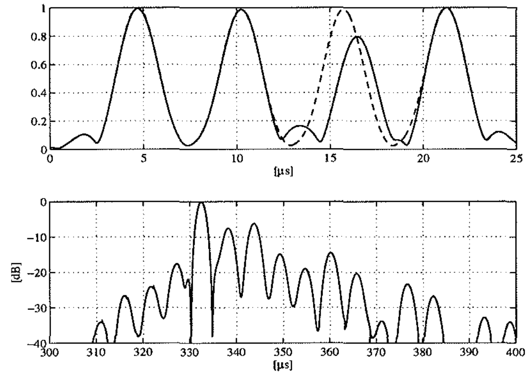

Figure 3.11: Upper panel: Third harmonic envelope of scattered signal from lower panel of Fig. 3.10, solid line. Dashed line represents third harmonic envelope obtained by driving the bubble with four identical subpulses. Lower panel: Result after pulse compression of scattered broadband Barker sequence.

narrowbanded incident drive pulse from the lower panel of Fig. 3.1.

A new broadband Barker sequence, similar to the one in the upper panel of Fig. 3.10 but with higher amplitude, is then used to drive the bubble. The new incident Barker sequence and the resulting scattered pressure pulse from the bubble can be seen in the upper and lower panel of Fig. 3.12, respectively.

The third harmonic envelope, obtained with the narrowband bandpass filter, is displayed as the solid line in the upper panel of Fig. 3.13. Again, the dashed line represents the result obtained by using a drive pulse similar to the one in the upper panel of Fig. 3.12 but with no phase inversion on the third subpulse. Comparing the upper panels of Fig. 3.11 and Fig. 3.13, we notice that the third harmonic envelope of the third subpulse in the scattered Barker sequences have similar time shifts when the broadband incident Barker sequences of different amplitudes are applied. By inspecting the scattered pulses in the lower panel of Fig. 3.10 and 3.12, it is clear that the third subpulse starts with mainly low frequency signal components while the main contributions to the high frequency components occur later in the subpulse.

The amplitude of the third harmonic envelope was in the upper panel of Fig. 3.11 seen to be lower for the third subpulse when using the low amplitude broadband incident Barker sequence. Using the high amplitude broadband incident Barker sequence, the amplitude of the third harmonic envelope is, however, higher for the subpulse with inverted polarity even if the amplitude of the total scattered signal in the lower panel of Fig. 3.12 is lower for this subpulse.

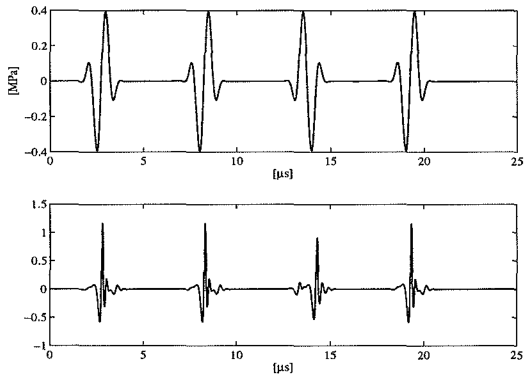

Figure 3.12: Upper panel: Broadband incident Barker sequence. Lower panel: Resulting scattered pressure pulse from a 4 μm bubble.

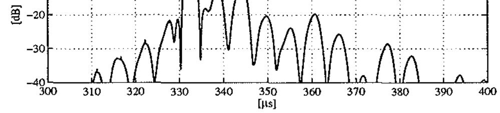

Figure 3.13: Upper panel: Third harmonic envelope of scattered signal from lower panel of Fig. 3.12, solid line. Dashed line represents third harmonic envelope obtained by driving the bubble with four identical subpulses. Lower panel: Result after pulse compression of scattered broadband Barker sequence.

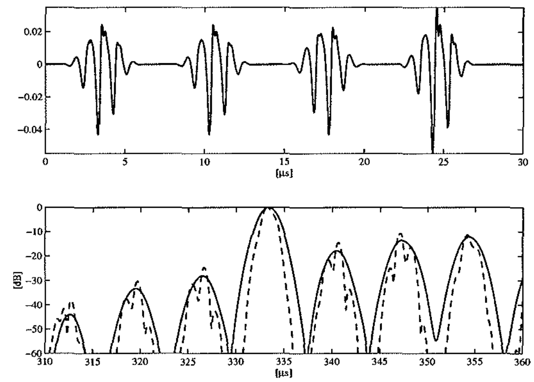

Figure 3.14: Upper panel: Signal scattered from bubble driven by the acoustic pulse in the lower panel of Fig. 3.1 where the equilibrium bubble radius is increased by 5 % for the last subpulse. Lower panel: Results after third harmonic bandpass filtering on the the pulse in the upper panel and compressing using the stabilized inverse filter. Solid line is obtained using the narrowband bandpass filter and the dashed line is obtained using the broadband bandpass filter.

3.3.6 Variable Acoustic Bubble Parameters

Contrast agent gas bubbles are not entirely stable and as the bubbles are subjected to the incident pressure pulses they may, to some degree, change their acoustic properties. The thin shell encapsulating the gas bubble dramatically changes the acoustic properties and stability of the contrast bubble compared to a free gas bubble not encapsulated by this shell [19]. The properties of the shell hence, to a large extent, determine the acoustic properties of the bubble. When the bubble is subjected to a Barker sequence it is therefore, contrary to the situation in Power Doppler techniques, important for the shell to maintain its properties for the entire duration of the sequence.

The upper panel in Fig. 3.14 shows an example of the scattered pressure pulse from a bubble when the bubble has increased its equilibrium radius by 5 % for the last subpulse compared to the three first subpulses. This increase in radius could for example be due to a change in the properties of the encapsulating shell or a heating of the gas inside the shell. The radius increase results in a small reduction of the resonance frequency of the bubble. In the lower panel of Fig. 3.14 we see the results after the third harmonic component of the sequence in the upper panel has been filtered out and processed by the stabilized inverse filter. Compared to results obtained in Fig. 3.9, range sidelobe levels are significantly increased both when applying the broadband bandpass filter (dashed line) and the narrowband bandpass filter (solid line).

Fig. 3.15 depicts the normalized envelope of the third harmonic component in the last sub-

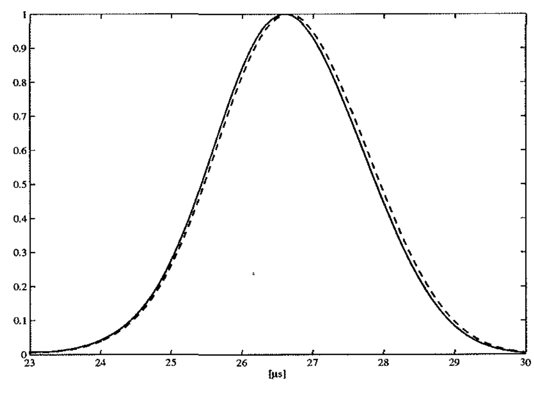

Figure 3.15: Normalized envelope of the third harmonic component in the last subpulse in the upper panel of Fig. 3.8 and 3.14, solid and dashed line, respectively.

pulse in the upper panel of Fig. 3.8 and 3.14, solid and dashed line respectively. A small change in the equilibrium radius of the bubble slightly changes the acoustic properties, and hence the resonance frequency of the bubble. This has an effect on the scattered third harmonic component envelope. The envelope of the third harmonic component in the subpulse scattered from the bubble with the increased equilibrium radius (dashed line) is somewhat delayed and stretched relative to the envelope obtained from the subpulse scattered from the bubble with the unchanged original equilibrium radius (solid line). The amplitude of the third harmonic component scattered from the increased bubble is around 3 dB larger than from the original bubble. In addition to this amplitude variation, the small delay and stretch of the third harmonic envelope significantly increases the range sidelobe level in the compressed pulse as shown in the lower panel of Fig. 3.14.

If instead the bubble radius is increased by 5 % for the first scattered subpulse, while the three last subpulses are scattered from the original 4 μm bubble, we obtain the results displayed in Fig. 3.16. Again, the solid and dashed lines in the lower panel of the figure is obtained using the narrowband and broadband third harmonic bandpass filter, respectively. In the lower panel of Fig. 3.14 the sidelobes to the left of the mainlobe are significantly lower than the sidelobes to the right and one might initially expect the sidelobes in the lower panel of Fig. 3.16 to appear in an exactly opposite manner. The sidelobes to the left of the mainlobe in the lower panel of Fig. 3.16 are, indeed, somewhat higher than the sidelobes to the right but the sidelobes at the left and right of the mainlobe are significantly more balanced in level than what was found in the lower panel of Fig. 3.14. Also, the highest sidelobe level in Fig. 3.16 is somewhat lower than what found in Fig. 3.14.

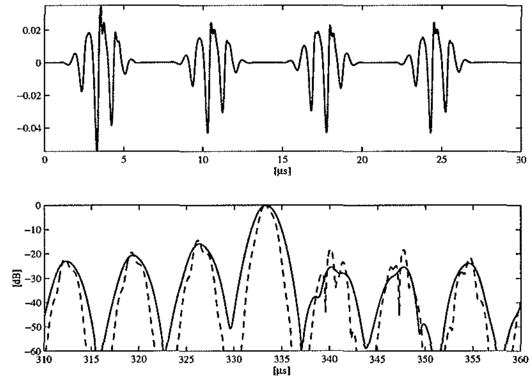

Figure 3.16: Upper panel: Signal scattered from bubble driven by the acoustic pulse in the lower panel of Fig. 3.1 where the equilibrium bubble radius is increased by 5 % for the first subpulse. Lower panel: Results after third harmonic bandpass filtering on the the pulse in the upper panel and compressing using the stabilized inverse filter. Solid line is obtained using the narrowband bandpass filter and the dashed line is obtained using the broadband bandpass filter.

3.3.7 Bubble Movement

The contrast agent in a medical ultrasound imaging situation is usually moving due to blood flow. Even though the blood flow velocity is low compared to the speed of sound it may have a degrading effect on the range sidelobe level obtained after pulse compression of a Barker sequence. The movement of the contrast bubble will cause a Doppler shift according to the following equation

$$f_d = 2f\frac{v}{c} \tag{3.7}$$

where f is the transmit frequency, v is the velocity of the contrast agent in the beam direction, and c is the speed of sound in the medium. Setting $v = 1$ m/s gives a Doppler frequency around 5 kHz for the third harmonic component with a transmit frequency equal to 1 MHz which is rather low compared to the frequency shifts obtained from absorption (upper panel in Fig. 3.6) and scattering (lower panel in Fig. 3.8). The frequency shift due to the Doppler effect is thus not believed to have a significant effect on the range sidelobe level obtained in the compressed pulse.

When the contrast bubble is subjected to an incident pressure wave it is also affected by a radiation pressure due to the fact that the bubble absorbs and scatters parts of the energy in the incoming wave. This radiation pressure will have the potential to introduce a velocity to the bubble in the direction of the incoming wave. The intensity of a plane or spherical incident wave can be calculated as

$$I = \frac{p^2}{2Z} \tag{3.8}$$

where p is the acoustic pressure amplitude and Z is the acoustic impedance. The energy absorbed and scattered by the bubble during a time interval Δt is $I\sigma_e\Delta t$ where σ_e is the extinction cross section of the bubble. Extinction cross section is the sum of the scattering cross section and the absorption cross section and is thus the total loss of energy from the incident pressure wave. The work done on the bubble during Δt is $F_r c\Delta t$ where F_r is the radiation force on the bubble and c is the speed of sound in the medium. Equating the energy absorbed/scattered by the bubble and the work done on the bubble we obtain

$$F_r = \frac{I\sigma_e}{c} \tag{3.9}$$

where values for σ_e for the agent *Sonazoid* can be estimated [19, pp. 152-157]. If the flow around the bubble is assumed to be laminar and the shape of the bubble is assumed to be purely spherical, the bubble velocity due to the radiation force can be calculated as [42, pp. 183-184]

$$U = \frac{F_r}{4\pi a\mu_v} \ . \tag{3.10}$$

Here, a is the bubble radius, and μ_v is the viscosity of the ambient fluid. Inserting typical numerical values gives a velocity caused by radiation forces which is of the same order as common velocities due to regular blood flow and this effect is therefore not negligible.

Dayton *et al* [10] examined the magnitude of radiation forces on ultrasound contrast agents taking a more rigorous approach than done here. A velocity of up to 0.5 m/s due to radiation forces on a 4 μm bubble insonified with similar pressure amplitudes as in the present paper ($\sim$ 0.1 MPa) and a transmit frequency around 2.25 MHz was then obtained. The velocity introduced due to radiation forces will be time-varying.

If the velocity of the bubble is assumed to be 1 m/s, the bubble will have moved a distance of 25 μm in a time period of 25 μs (which is approximately the duration of the four bit Barker sequence used). In a pulse echo imaging system this will introduce a time shift equal to 33 ns if the speed of sound is set equal to 1500 m/s. Due to the pumping of the heart muscle and the presence of radiation forces, the blood flow will not be stationary and the upper panel in Fig. 3.17 shows an example where the last subpulse in the scattered Barker sequence has been time shifted by an amount equal to 30 ns relative to the original sequence in the upper panel of Fig. 3.8. Here, the solid line is the normalized third harmonic envelope of the original unshifted last subpulse, while the dashed line is the normalized third harmonic envelope of the resulting time-shifted subpulse. In the lower panel it is shown how this time shift effects the range sidelobe level obtained after the stabilized inverse filter is applied. We see that the Barker sequence is very sensitive to even a minor time shift between its subpulses.

The compressed pulse in the lower panel of Fig. 3.14, obtained by slightly changing the acoustic properties of the contrast bubble for the last subpulse, and the compressed

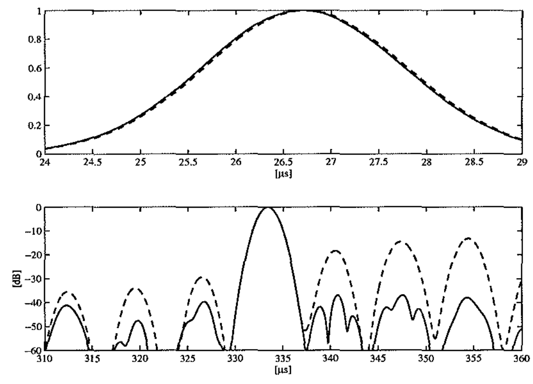

Figure 3.17: Upper panel: Normalized envelope of third harmonic component from two subpulses where one of them has been time shifted by an amount equal to 30 ns relative to the other. Lower panel: Dashed line show effect on range sidelobe level introduced by time shifting the last subpulse of a four bit Barker sequence by an amount equal to 30 ns relative to the sidelobe level obtained from the original unshifted sequence (solid line).

pulse in the lower panel of Fig. 3.17, obtained by slightly time shifting the last subpulse, are seen to be very similar. As seen in Fig. 3.15, an important effect introduced by slightly changing the acoustic properties of the bubble was a time shift of the scattered third harmonic envelope which explains the similarities in the lower panels of Fig. 3.14 and Fig. 3.17.

3.3.8 Effect of Having a Finite CNR

In an actual ultrasound imaging situation, there will always be a finite CNR and the motivation for introducing Barker sequences was to improve the CNR at the received third harmonic component from the contrast agent. Two different levels of uncorrelated noise are now added to the original scattered four bit Barker sequence displayed in Fig. 3.8. In both cases the noise level is so high that the resulting sidelobes in the compressed sequence is limited by the noise signal and not the effects discussed in relation to Fig. 3.9.

In the upper panel of Fig. 3.18, the envelope of the scattered third harmonic component of the Barker sequence, when the narrowband bandpass filter has been applied, is displayed as the solid line. The dashed line represents the envelope of the third harmonic component of an uncorrelated noise signal and the CNR before applying the stabilized inverse filter is around 4 dB. In the lower panel of the same figure, the results after pulse compression are shown. The solid line is the result obtained feeding the sum of the two signals in the upper panel to the stabilized inverse filter while the dashed line is the result obtained

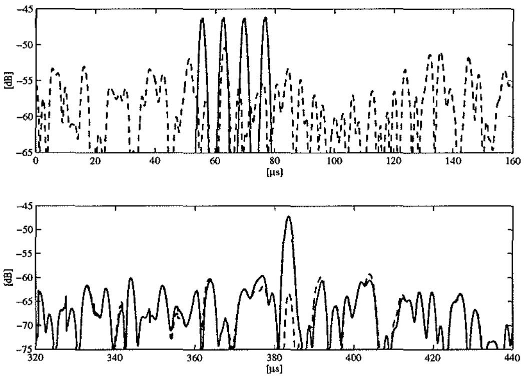

Figure 3.18: Upper panel: Envelope of scattered third harmonic component, obtained with narrowband bandpass filter, from a 4 bit Barker sequence (solid line) and envelope of third harmonic uncorrelated noise signal (dashed line). Third harmonic CNR is approximately 4 dB before pulse compression. Lower panel: Result after applying the stabilized inverse filter on the sum of the two sequences in the upper panel (solid line) and on the noise signal only (dashed line). Third harmonic CNR is approximately 13 dB after pulse compression.

processing only the noise signal in the upper panel. The CNR after pulse compression is approximately 13 dB and the increase in CNR achieved using the Barker sequence is thus around 9 dB.

In Fig. 3.19 the added noise signal has been somewhat reduced. The solid line in the upper panel shows the envelope of the scattered third harmonic Barker sequence while the dashed line represents the envelope of the third harmonic component of the noise signal when the narrowband filter is used. The third harmonic CNR before the stabilized inverse filter is applied is now approximately 13 dB. In the lower panel we see the results after pulse compression. Again, the solid line is obtained processing the sum of the two signals in the upper panel and the dashed line is obtained from the noise signal only in the upper panel. An increase of about 7 dB in the third harmonic CNR is now achieved after pulse compression is performed.

3.4 Experimental Results

In vitro measurements are done on a tissue mimicking phantom using an annular transducer consisting of 5 rings. The outer ring is a low frequency ring used for transmitting the ultrasound signal while the four inner rings are high frequency rings used for receiving the scattered third harmonic components of the transmitted signal. A signal similar to the one in the lower panel of Fig. 3.1, with a center frequency equal to 1.3 MHz, is stored

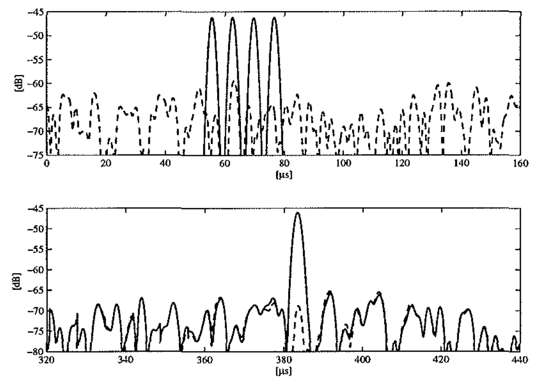

Figure 3.19: Upper panel: Envelope of scattered third harmonic component, obtained with narrowband bandpass filter, from a 4 bit Barker sequence (solid line) and envelope of third harmonic uncorrelated noise signal (dashed line). Upper panel: Third harmonic CNR is approximately 13 dB before pulse compression. Lower panel: Result after applying the stabilized inverse filter on the sum of the two sequences in the upper panel (solid line) and on the noise signal only (dashed line). Third harmonic CNR is approximately 20 dB after pulse compression.

in a signal generator and used as an excitation pulse on the outer ring of the ultrasound transducer. The tissue mimicking phantom contains a small polyethylene tube with inner diameter equal to 0.28 mm through which a solution of water and contrast agent may flow. The contrast agent *Sonazoid* [19] which has a resonance frequency around 4 MHz, was used in the present measurements. Measurements were conducted on a System FiVe ultrasound scanner made by GE Vingmed Ultrasound and the contrast bubbles were subjected to relatively low amplitude ultrasound pulses with an amplitude around 0.1 MPa. The narrowband third harmonic bandpass filter shown in Fig. 3.5 with a center frequency equal to 3.9 MHz was used on the received signals to obtain the scattered third harmonic component.

The upper panel of Fig. 3.20 depicts the third harmonic envelope from a received Barker sequence where the CNR is around 4 dB. We notice that for the third subpulse, occurring at around 29 μs on the time axis, the signal level is particularly reduced. This reduction is most likely due to destructive interference with the uncorrelated noise signal and not a change in the acoustic properties of the bubble since for the last subpulse, occurring at around 35 μs, the signal level is again increased. In the lower panel of Fig. 3.20, the result after the stabilized inverse filter has been applied is shown and the CNR is now approximately 13 dB.

Fig. 3.21 shows another example of a received scattered Barker sequence from the contrast bubbles flowing through the tissue mimicking phantom. In the upper panel of the figure,

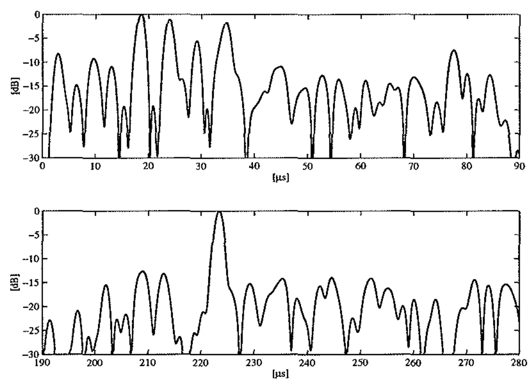

Figure 3.20: Upper panel: Envelope of measured third harmonic component, obtained with the narrowband bandpass filter, from a 4 bit Barker sequence. Third harmonic CNR is approximately 4 dB before pulse compression. Lower panel: Result after applying the stabilized inverse filter on the signal in the upper panel. Third harmonic CNR is approximately 13 dB after pulse compression.

the third harmonic envelope is displayed and the CNR is for this case around 10 dB. The lower panel of the figure shows the result after pulse compression and the CNR is now seen to be approximately 17 dB. There is a gradual increase in the received signal level from the first to the third subpulse occurring between 27 and 38 μs on the time axis. This increase is also most likely due to interference between the bubble signal and the noise signal since for the last subpulse, occurring at around 43 μs, the signal level is slightly reduced.

Fig. 3.22 depicts yet another example of a received scattered Barker sequence. In the upper panel, before pulse compression, the CNR is seen to be around 16 dB. In the lower panel, after pulse compression, the CNR has increased to around 23 dB.

The previous three figures show examples of received scattered Barker sequences where the presence of uncorrelated noise is believed to be the limiting factor regarding the sidelobe level obtained after pulse compression is performed. The bubbles are hence assumed to maintain rather constant values with respect to acoustic properties and bubble movement is believed not to cause a limitation on the sidelobe level obtained.

In the upper panel of Fig. 3.23, we see an example of a received sequence where the signal level from the contrast agent is seen to gradually increase from the first subpulse occurring at around 27 μs, to the last subpulse occurring at around 42 μs. This steady increase in signal level may indicate a gradual change of the acoustic properties of the contrast agent inside the sample volume. One plausible explanation might be that the thin encapsulating shell gets slightly more flexible during the oscillations of each subpulse and thus results

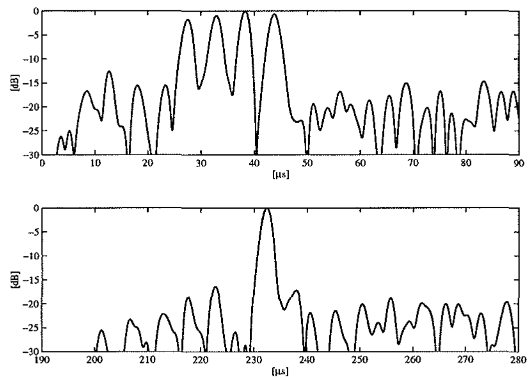

Figure 3.21: Upper panel: Envelope of measured third harmonic component, obtained with the narrowband bandpass filter, from a 4 bit Barker sequence. Third harmonic CNR is approximately 10 dB before pulse compression. Lower panel: Result after applying the stabilized inverse filter on the signal in the upper panel. Third harmonic CNR is approximately 17 dB after pulse compression.

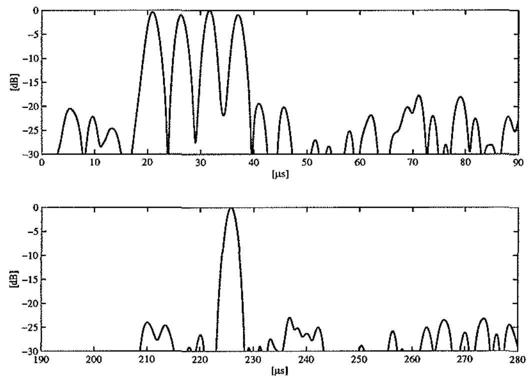

Figure 3.22: Upper panel: Envelope of measured third harmonic component, obtained with the narrowband bandpass filter, from a 4 bit Barker sequence. Third harmonic CNR is approximately 16 dB before pulse compression. Lower panel: Result after applying the stabilized inverse filter on the signal in the upper panel. Third harmonic CNR is approximately 23 dB after pulse compression.

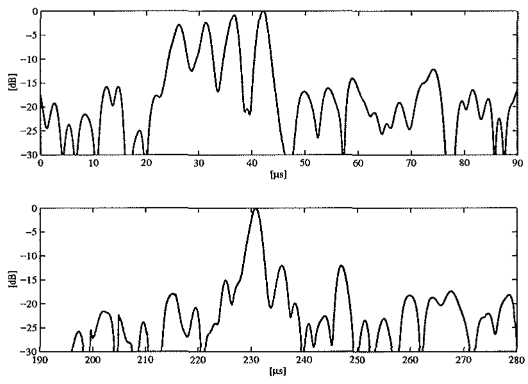

Figure 3.23: Upper panel: Envelope of measured third harmonic component, obtained with the narrowband bandpass filter, from a 4 bit Barker sequence. Lower panel: Result after applying the stabilized inverse filter on the signal in the upper panel.

in a slight increase in the scattering cross section from the contrast agent. The lower panel of Fig. 3.23 shows the result after pulse compression and by comparing with the upper panel in the figure, we see that the CNR is approximately the same before and after pulse compression is performed.

The upper panel of Fig. 3.24 shows a final example of the third harmonic envelope from a received scattered Barker sequence. We notice that the two last received subpulses, occurring between 29 and 37 μs on the time axis, are significantly lower in amplitude than the two first subpulses in the sequence. This effect might also be a result of a change in the acoustic properties of the contrast agent. The CNR in the upper panel is approximately 19 dB for the two first subpulses and hence too high to explain the significant reduction in amplitude of the two last subpulses in the sequence as resulting from destructive interference between the contrast signal and the noise signal. In the lower panel of Fig. 3.24, we see the result after applying the stabilized inverse filter. We notice that, again, there is little or no improvement in the CNR in the compressed sequence relative to the uncompressed sequence.

3.5 Conclusions

The application of a four bit Barker code to increase the CNR for third harmonic contrast agent imaging has been studied numerically and experimentally. Results from numerical simulations, adding various levels of uncorrelated noise to a four bit Barker sequence scattered from a contrast bubble and applying a stabilized inverse filter indicated an increase in the third harmonic CNR between 6 and 9 dB after pulse compression. *In vitro* measure-

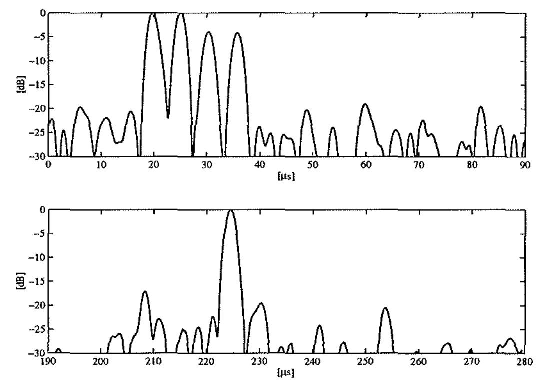

Figure 3.24: Upper panel: Envelope of measured third harmonic component, obtained with the narrowband bandpass filter, from a 4 bit Barker sequence. Lower panel: Result after applying the stabilized inverse filter on the signal in the upper panel.

ments performed on a tissue mimicking phantom with the contrast agent *Sonazoid*, carried out using the same four bit Barker sequence, typically gave similar improvements in the third harmonic CNR when the acoustic properties of the contrast agent were assumed to be close to constant for the whole Barker sequence, and results from measurements were hence in good agreement with the numerical results. Received sequences for which the acoustic properties of the contrast bubbles were believed to change during insonification by the Barker sequence showed little or no improvement in CNR when comparing the compressed and uncompressed signals. A longer Barker sequence would have the potential to further increase the CNR. Using a significantly longer sequence one would, however, also presumably encounter problems regarding bubble motion during insonification by the sequence. The possibility that the contrast bubbles would, to some extent, change their acoustic properties during insonification by such a long sequence is also greater than for the shorter code. Both these effects are in the present paper shown to potentially have a major degrading effect on the range sidelobe level obtained in the final compressed pulse. For sequences with a low CNR before pulse compression, the adjustable stabilized inverse filter is set so that the filter is shifted towards a matched filter, while for sequences with higher CNR before pulse compression, the filter more closely resembles the inverse filter.

3.6 Acknowledgments

This work was supported by the Research Council of Norway.

Chapter 4

A New Dual Frequency Band Contrast Agent Detection Technique

Abstract

Ultrasound wave propagation in soft tissue and scattering from ultrasound contrast agents are both known to be nonlinear processes at frequencies and amplitudes commonly applied in medical ultrasound imaging. The fact that the contrast agents usually respond much more nonlinearly than soft tissue has given rise to the contrast harmonic imaging techniques where only a harmonic component of the total scattered signal, typically the second harmonic component, is used for image reconstruction. In a medical ultrasound imaging situation, both the harmonic scattered tissue signal and the uncorrelated thermal and electronic noise signal will potentially mask the scattered contrast harmonic signal. The present paper deals with a new contrast harmonic imaging technique, designed to increase the contrast harmonic signal relative to both the noise signal as well as the harmonic tissue signal. In order to achieve this, the new method makes use of dual frequency band transmit pulses, together with a general pulse inversion technique.

4.1 Introduction

Wave propagation in soft tissue is usually a weak nonlinear process for frequencies and amplitudes typically used in medical ultrasound imaging, and the transmitted pulse is slightly distorted as it propagates through the medium. Although the local effect of nonlinearity is small, the cumulative effect when the wave has propagated several wavelengths is not negligible. If the wave transmitted from an ultrasound transducer has its energy concentrated in some fundamental frequency band, the nonlinearity of wave propagation gives rise to harmonics of this fundamental band [3, Chapter 12] [30, Chapter 11]. The level of received second harmonic component from tissue is typically found to be around 20 dB below the level of the fundamental component but this level depends on acoustic parameters in addition to imaging parameters such as frequency, amplitude, and depth of imaging.

Ultrasound scattering from soft tissue is assumed to be a linear process so that the energy received from tissue outside the fundamental transmitted band is generated in the forward nonlinear propagation of the wave unless a spreading of scattered contrast signal beyond the actual contrast-filled region occurs. Although much weaker than the second harmonic component, higher harmonics may also exist in the scattered tissue signal.

Medical ultrasound contrast agents are typically made as solutions of small gas bubbles (diam $\sim 3\ \mu$m) in a fluid and scattering from such gas bubbles is potentially a strong nonlinear process [23] [11] [12]. The high compliance of the gas bubbles relative to soft tissue make them highly effective scatterers of acoustic energy.

A spherical gas bubble in a liquid undergoing simple harmonic motion has a natural or resonance frequency first calculated by Minnaert [27]. When driven by acoustic pulses used in medical ultrasound imaging, and especially when subjected to pulses with frequency components close to or below its resonance frequency, the gas bubble represents a highly nonlinear scatterer of ultrasound giving rise to the contrast harmonic imaging techniques [35].

The Contrast to Tissue Ratio (CTR), or specificity, is defined as the ratio of signal power from the contrast agent in a region to the signal power from the tissue in that region. In order to adequately differentiate contrast signal and tissue signal it is therefore necessary with a high CTR. Contrast bubbles generally respond much more nonlinearly than soft tissue when subjected to ultrasound pulses and the CTR typically increases as higher harmonic components are considered.

Ultrasound pulse echo imaging systems are infested by thermal and electronic noise and the Contrast to Noise Ratio (CNR), or sensitivity, is defined as the ratio of signal power from the contrast agent in a region to the noise power in that region. The thermal and electronic noise signal (noise not correlated with the transmitted signal) can be considered constant over the frequency range of interest in medical ultrasound imaging. In the received signal from a contrast bubble, the amplitude of harmonic components typically decreases as higher harmonic components are considered and the CNR thus decreases for higher harmonic components.

In an imagined imaging situation without tissue, the best CNR would be achieved transmitting a high amplitude pulse and then using the total received signal for image reconstruction of the contrast agent. A high amplitude transmit pulse is, however, limited by patient safety [5] [8]. Also, the bubbles tend to get destroyed even during insonification by relatively low amplitude ultrasound pulses.

On the other hand, in an imagined noise free situation, the best CTR would be achieved by transmitting a low amplitude pulse, making the tissue behave approximately linearly while still driving the bubbles into nonlinear oscillations and using the third or higher harmonic component of the received signal for image reconstruction. In an actual imaging situation, tissue signals and noise signals are present, and the CTR and CNR both need to be as high as possible in order to construct a reliable and adequate image of the contrast agent added to the blood.

The present paper describes a new contrast harmonic imaging method designed to significantly increase the CNR at the third or fourth harmonic component while maintaining, or even increasing, the potentially good CTR found for these harmonic components.

4.2 Method

4.2.1 Wave Propagation and Scattering from Soft Tissue

Ultrasound wave propagation in soft tissue can, as indicated, be considered a weak nonlinear process for amplitudes and frequencies common in medical ultrasound imaging. The local nonlinearity is low but the distortion accumulates gradually in the forward propagating wave. The tissue elasticity behaves slightly nonlinearly and by doing a Taylor series expansion of the equation of state $P = P(\rho, s)$ along an isentrope $s = s_0$ [16, Chapter 2], where P is the sum of the ambient and acoustic pressure and ρ is the density of the medium, we can include this nonlinearity. By discarding terms of order higher than the second in the Taylor series expansion, we obtain the following nonlinear tissue elasticity equation [3, Chapter 12.3]

$$-\nabla \cdot \vec{\psi}(\vec{r}, t) = \kappa p(\vec{r}, t) - \beta\{\kappa p(\vec{r}, t)\}^2 + h \underset{t}{*} \kappa p(\vec{r}, t) \tag{4.1}$$

where $\vec{\psi}$ is particle displacement, κ is the compressibility of the medium, p is the acoustic pressure, β is a nonlinearity parameter, h is a causal lowpass filter, and $\vec{r}$ and t are the space and time coordinates, respectively. The first and second term on the right-hand side of Eq. 4.1 represent the linear and nonlinear tissue elasticity, respectively, while the last convolution term is taking care of acoustic absorption. By applying this nonlinear tissue elasticity equation we may derive the following nonlinear equation for wave propagation [3, Chapter 12.3]

$$\nabla^2 p - \frac{1}{c^2}\frac{\partial^2 p}{\partial t^2} - \frac{1}{c^2} h \underset{t}{*} \frac{\partial^2 p}{\partial t^2} = -\beta\kappa \frac{1}{c^2}\frac{\partial^2 p^2}{\partial t^2} \tag{4.2}$$

where c is the speed of sound in the propagation medium. We observe that the nonlinearity described by this wave equation is produced by a quadratic effect and that this effect enters as a source term in the homogeneous wave equation obtained by setting the term on right-hand side in Eq. 4.2 equal to zero.

First calculating the transmitted fundamental field from the homogeneous wave equation and using this field as a source term in Eq. 4.2 to calculate the transmitted second harmonic field is often referred to as the quasi-linear approximation of the nonlinear wave equation. This quasi-linear approximation, which is a first approximation to the nonlinear wave equation, is typically good when the nonlinear distortion is relatively low as in absorbing soft tissue.

The signal scattered from soft tissue is a result of the inherent inhomogeneous nature of the propagation medium. There is a spatial variation of the mass density and compressibility on several scales resulting in scattering of the transmitted acoustic wave. The acoustic scattering process from soft tissue is assumed to be linear and the presence of higher harmonic components in the scattered tissue signal is, unless spreading of scattered contrast agent signal beyond a contrast-filled region occurs, therefore a result of the nonlinearity in the forward propagating wave [3, Chapter 7].

4.2.2 Scattering from Contrast Agents

Ultrasound contrast agents generally respond much more nonlinearly than soft tissue when subject to an imaging ultrasound pulse. Higher order terms will not be negligible in the scattered signal and a quasi-linear approximation of the nonlinearity, as explained in Sec. 4.2.1, is therefore usually not a good approximation for the contrast agent. A well known nonlinear equation for the fluid surrounding a spherical pulsating gas bubble is the Rayleigh-Plesset equation [33] [31]. The radius oscillation of the bubble is in this equation expressed as

$$\rho(a\ddot{a} + \frac{3}{2}\dot{a}^2) = p(a,t) - P_0 - p_i(t) \tag{4.3}$$

where a is the radius, $\dot{a}$ and $\ddot{a}$ is the velocity and acceleration of the bubble radius, ρ is the density of the surrounding fluid, P_0 is the ambient equilibrium pressure, $p_i(t)$ is the incident driving pressure, and $p(a,t)$ is the pressure at the bubble surface. Nonlinear elasticity of the gas and the encapsulating thin shell, surface tension, and viscosity may be incorporated in the first term on the right-hand side in Eq. 4.3.

A numerical model derived by Angelsen et al [4] has been used for calculating bubble radius oscillations and scattered pressure in the present paper. This model includes an equation for the relation between pressure and radial strain in a thin shell encapsulating a gas bubble. The model also allows for a finite speed of sound in the medium surrounding the bubble, thus taking radiation losses from the bubble into account. Otherwise this model is comparable to the well known Rayleigh-Plesset equation and the two models give similar results for small amplitude radius oscillations of the contrast bubble.

4.2.3 A New Pulse Inversion Technique

In the conventional pulse inversion technique [20], two single frequency band pulses are transmitted, scattered, and received separately where the polarity of the second transmitted pulse is inverted relative to the first. The two received pulses are then added together and, in the ideal situation, all odd harmonic components in the summed signal, including the fundamental component, are canceled while the even harmonic components are preserved. In this way the conventional pulse inversion technique typically turns out as a second harmonic technique, using the second harmonic component for image reconstruction. The second harmonic component is, in the summation, ideally increased by 6 dB for the contrast signal as well as the tissue signal, hence increasing the Contrast to Noise Ratio (CNR) by 3 dB assuming a white noise signal, but giving the same Contrast to Tissue Ratio (CTR) relative to the second harmonic imaging technique where only one transmit pulse is applied and the received second harmonic signal component is filtered out and used for image reconstruction.

The present paper deals with a new and more contrast specific pulse inversion technique where dual frequency band pulses, with frequency components overlapping in time, are transmitted. First, a pulse containing two frequency bands, in particular a fundamental band and its second harmonic band, is transmitted, and the scattered signal is received and stored. Then a second pulse is transmitted, where the polarity on either the first or second frequency band is inverted relative to the first transmitted pulse, and a general form of pulse inversion is performed on the received scattered signals.

By performing this new pulse inversion technique, nonlinearities described by the quasi-linear approximation are canceled. This greatly favors imaging, and in particular third or fourth harmonic imaging, of a region containing contrast agents embedded in soft tissue since the contrast agents are assumed to respond much more nonlinearly than the soft tissue when subject to the transmit pulses. The two transmitted pulses may for example be expressed as

$$p_1(t) = a_1(t)sin(\omega t) + a_2(t)sin(2\omega t + \phi) \tag{4.4}$$

$$p_2(t) = a_3(t)sin(\omega t) - a_4(t)sin(2\omega t + \phi) \tag{4.5}$$

where $a_n(t)$ are positive amplitude functions, ω is the angular frequency, and ϕ is an arbitrary phase angle. The fact that $a_3(t)$ may be different from $a_1(t)$ and $a_4(t)$ may be different from $a_2(t)$ gives the flexibility to further utilize the assumption of strong versus weak nonlinearity of the propagation medium. If the received signals are modeled as power series expansions of the transmitted signal, they may be written

$$s_t(t) = \sum_{n=1}^{2} b_n(t)p^n(t-\tau) \tag{4.6}$$

$$s_c(t) = \sum_{n=1}^{\infty} c_n(t)p^n(t-\tau) \tag{4.7}$$

for the tissue signal and contrast signal, respectively. Here p is the transmitted signal, $b_n(t)$ and $c_n(t)$ are amplitude functions, and τ is a time delay. If $a_3(t) = a_1(t)$ and $a_4(t) = a_2(t)$ in Eq. 4.4 and 4.5, summing the two received signals, s_{t1} and s_{t2}, from a region of soft tissue not containing contrast agents, and where nonlinearities hence are assumed to be described by the quasi-linear approximation, gives

$$\begin{aligned} s_{t1}(t) + s_{t2}(t) &= 2b_1(t)a_1(t)sin(\omega t) \\ &+ 2b_2(t)a_1^2(t)sin^2(\omega t) \\ &+ 2b_2(t)a_2^2(t)sin^2(2\omega t + \phi) \ . \end{aligned} \tag{4.8}$$

Here, the first term on the right-hand side is the linear component in the summed signal while the second and third terms are the first order nonlinear harmonic components, *i.e.* the result of the quadratic effect in Eq. 4.2. The linear component of the transmitted second harmonic band is canceled in the summation process, due to the phase inversion in Eq. 4.4 and 4.5, whereas the linear component of the transmitted fundamental band is doubled. The two nonlinear terms consist of a second harmonic component from the transmitted fundamental band and a second harmonic component from the transmitted second harmonic band (*i.e.* a fourth harmonic component). The nonlinear sum and difference frequencies, producing third and fundamental harmonic components, have hence been canceled in the pulse inversion process for a propagation medium of weak nonlinearity, such as soft tissue.

Strong nonlinear scatterers, such as contrast agents, will not be adequately described by the quasi-linear approximation of the nonlinearity and scattered third harmonic components from the bubbles will not be canceled in the resulting pulse inversion process.

In addition, adjusting the arbitrary phase angle in Eq. 4.4 and 4.5 one is, when inverting the polarity of the second harmonic component, able to produce two asymmetric transmit pulses with respect to positive and negative pressure amplitudes, hence altering the acoustic scattering properties of the contrast agent for the two transmitted pulses as shown in Sec. 4.3.3.

If we instead subtract the two received signals, s_{t1} and s_{t2}, from a region of soft tissue not containing contrast agents, and where nonlinearities hence are assumed to be described by the quasi-linear approximation, we obtain

$$\begin{aligned} s_{t1}(t) - s_{t2}(t) &= 2b_1(t)a_2(t)sin(2\omega t + \phi) \\ &+ 4b_2(t)a_1(t)a_2(t)sin(\omega t)sin(2\omega t + \phi) \ . \end{aligned} \tag{4.9}$$

Now, the linear transmitted fundamental band is canceled in the pulse inversion process while the linear transmitted second harmonic band is doubled. The first order nonlinear term, second term on the right-hand side in Eq. 4.9, now consists of a nonlinear mixing term between the linear transmitted fundamental and second harmonic components producing nonlinear fundamental and third harmonic components. Performing a subtraction instead of a summation of the received scattered signals hence cancels the first order nonlinear fourth harmonic components from the soft tissue.

Both the first order nonlinear third and fourth harmonic tissue components can potentially be canceled by subtracting the scattered signals from two identical dual frequency band transmit pulses where there is no phase inversion on either the fundamental nor the second harmonic band. Subtracting the scattered signals from two such identical transmit pulses would, however, probably also significantly reduce the scattered third and fourth harmonic components from the contrast agent.

4.3 Numerical Simulations

Numerical simulation of nonlinear wave propagation has been done using a simulation tool developed in our group [41]. The simulation program is capable of making a 3-dimensional simulation of the acoustic transmit field from an annular transducer including effects of nonlinear wave propagation, frequency dependent absorption, and diffraction. The nonlinear elasticity effect of the propagation medium is in the simulation program not limited by the quasi-linear approximation discussed in Sec. 4.2.1.

An annular transducer with radius equal to 1 cm and a geometric focus at 8 cm was used to calculate the transmit field when using acoustic properties of muscle found in the literature [13]. The transmit field on the symmetry axis of the transducer is then in Sec. 4.3.2 and 4.3.3 used to calculate the scattered signal from an inserted "tissue scatterer" and a contrast bubble, respectively.

Bubble radius oscillations and scattered far-field pressure pulses were calculated using the numerical model developed by Angelsen *et at* [4]. Acoustic properties found in the literature [37] [18] for the contrast agent *Sonazoid* were used for the contrast bubble. The equilibrium radius was set to 1.5 μm and the resonance frequency of the bubble is then around 4 MHz.

4.3.1 The Transmit Field

First, a single frequency band 1 MHz transmit pulse, described by Eq. 4.4 where $a_2(t) = 0$, is used as a source on the annular transducer and the axisymmetric transmit field is calculated. Fig. 4.1 depicts the obtained fundamental and second harmonic transmit field in decibel scale, left and right panel, respectively. The horizontal axis is the lateral direction while the vertical axis is the range direction. The dynamic range is 30 dB in both panels but the second harmonic field is plotted in a dynamic scale which is 20 dB below the fundamental field. We notice that the second harmonic field builds up gradually in range direction and that its intensity is around 25 dB below the intensity of the fundamental field.

A dual frequency band pulse, described by Eq. 4.4 where now $a_2(t) \neq 0$ and where $a_1(t)$

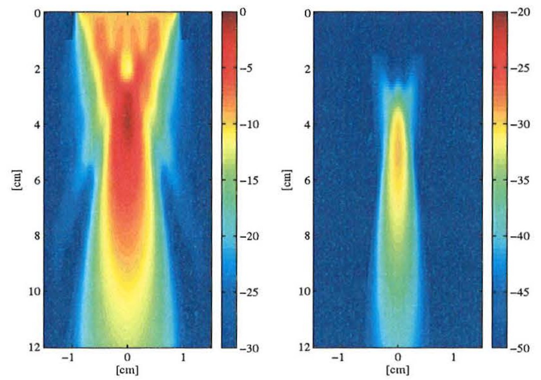

Figure 4.1: Transmit field from single frequency band source pulse. Left panel: Fundamental field. Right panel: Second harmonic field.

is unchanged relative to the previous pulse, is then used as a source on the transducer. This dual frequency band pulse consists of a 1 MHz and a 2 MHz pulse which are overlapping in time. The obtained transmit fields for the fundamental (1 MHz) and second harmonic (2 MHz) components are displayed in Fig. 4.2, left and right panel, respectively. The dynamic range in the plots are still 30 dB but the two fields are now plotted in the same dynamic scale. We observe that the intensity of the fundamental and second harmonic field is of the same order. The second harmonic field is now mainly a result of the linear propagation of the second harmonic source at the transducer and not a first order nonlinear effect as in the right panel of Fig. 4.1. By comparing the left panel in Fig. 4.1 and 4.2 we observe that the transmitted fundamental field is very similar in the two situations.

In Fig. 4.3, the obtained third and fourth harmonic fields using the dual frequency band source pulse are shown, left and right panel, respectively. These two harmonic fields are displayed in the same dynamic scale as the second harmonic field in the right panel of Fig. 4.1. The third and fourth harmonic fields from the dual frequency band source pulse are of the same order as the second harmonic field from the single frequency band source pulse which is natural since they all mainly are results of the first order nonlinear effect discussed in Sec. 4.2.1.

A second dual frequency band pulse, described by Eq. 4.5, where the polarity of the transmitted second harmonic component is inverted relative to the first dual frequency band pulse, and where $a_3(t) = a_1(t)$ and $a_4(t) = a_2(t)$, is then used as a source on the transducer and the transmit field is calculated. The two transmit fields, obtained by using the two different dual frequency band sources on the transducer, are then summed together in a pulse inversion process. Since scattering from tissue is assumed to be a linear process, the signal obtained by adding these two transmit fields gives an impression of how the pulse summation process will affect the resulting received tissue signals.

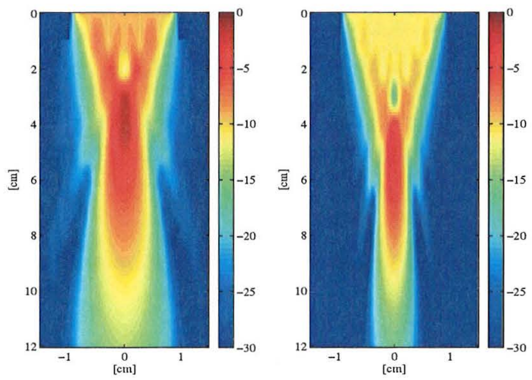

Figure 4.2: Transmit field from dual frequency band source pulse. Left panel: Fundamental field. Right panel: Second harmonic field.

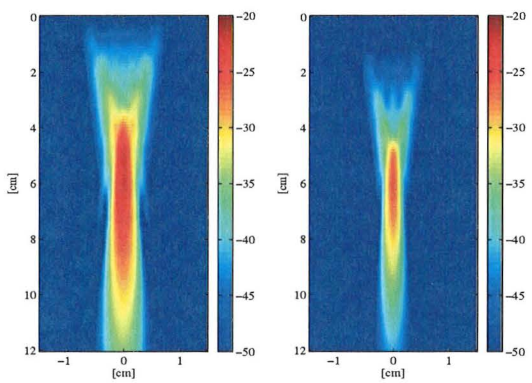

Figure 4.3: Transmit field from dual frequency band source pulse. Left panel: Third harmonic field. Right panel: Fourth harmonic field.

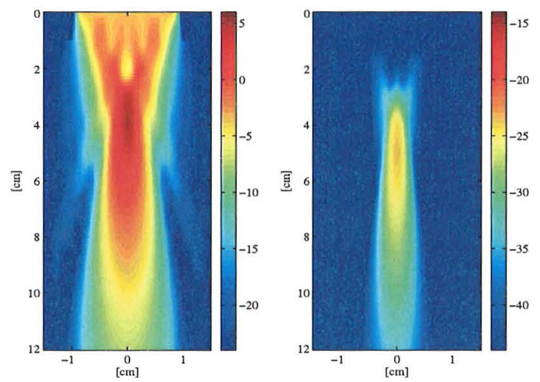

Figure 4.4: Wave field obtained as sum of transmit fields from two dual frequency band sources with identical fundamental components and inverted polarity on second harmonic components. Left panel: Fundamental field. Right panel: Second harmonic field.

In Fig. 4.4, the fundamental and second harmonic field obtained after pulse summation is shown, left and right panel, respectively. The dynamic range is still 30 dB but the dynamic level has been increased by 6 dB in both panels relative to Fig. 4.1. Comparing the left panels in Fig. 4.4 and 4.1 we see that the intensity of the fundamental component is increased by around 6 dB in the pulse summation process relative to the situation applying a single frequency band source. This is due to the fact that the phase and amplitude of the fundamental components in the two transmitted dual frequency band pulses are identical, and the intensity of the fundamental component in the summed signal is hence doubled as shown in Eq. 4.8. Comparing the right panels in Fig. 4.4 and 4.1 we observe that the second harmonic component in the signal obtained after pulse summation also has increased its intensity by approximately 6 dB relative to the situation when a single frequency band source is used. Again, this is in agreement with Eq. 4.8.

In Fig. 4.5 the third and fourth harmonic field obtained from the pulse summation process are displayed, left and right panel, respectively. The dynamic scale in the left panel has been reduced by 20 dB relative to the left panel in Fig. 4.3 while the dynamic scale in the right panel has been increased by 6 dB relative to the right panel in Fig. 4.3. By comparing the left panels in Fig. 4.3 and 4.5 we can conclude that the third harmonic component is significantly reduced in the pulse summation process as expected from Eq. 4.8. Finally, comparing the right panels in Fig. 4.3 and 4.5 we observe that the fourth harmonic field has increased by an expected 6 dB in the pulse summation process relative to the field obtained from the dual frequency band source pulse.

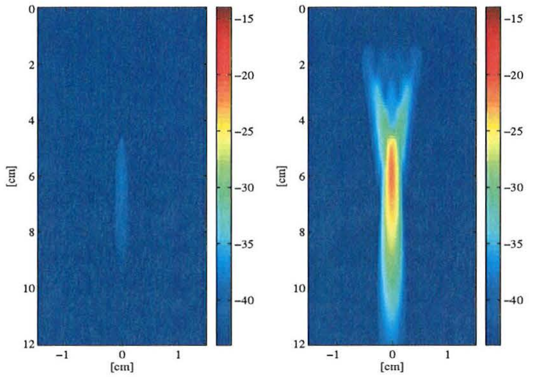

Figure 4.5: Wave field obtained as sum of transmit fields from two dual frequency band sources with identical fundamental components and inverted polarity on second harmonic components. Left panel: Third harmonic field. Right panel: Fourth harmonic field.

4.3.2 Scattering from Tissue

The calculated transmit field at the symmetry axis is now used to calculate the scattered signal from a "tissue scatterer" inserted at various locations along the symmetry axis. The scattering from soft tissue is assumed to be a linear process proportional with the frequency.

Only the relative levels of scattered harmonic components are considered in the present paper and absolute levels of scattered tissue signals and contrast bubble signals are hence not given.

First, the obtained transmit field from the single frequency band source pulse, described by setting $a_2(t) = 0$ in Eq. 4.4, is used to calculate the scattered signal from tissue. The intensity of the scattered tissue signal along the symmetry axis is displayed as the dashed lines in Fig. 4.6. The panels in this figure indicate scattered harmonic components, going from the fundamental component in the left panel, to the fourth harmonic component in the right panel. The dynamic range in all panels is set to 30 dB whereas the dynamic level varies between the panels. As seen in the first panel, the scattered tissue signal is normalized so that the fundamental component at 8 cm is set to 0 dB. In the second panel we see that the scattered second harmonic tissue component is around 20 dB below the scattered tissue fundamental component, while the scattered third harmonic component is in the third panel found to be around 35 dB below the scattered fundamental component.

The solid lines in Fig. 4.6 are harmonic tissue components of the pulse summation signal. This pulse summation signal is acquired by summing the two scattered tissue signals obtained by applying the two dual frequency band sources, described by Eq. 4.4 and 4.5, where $a_3(t) = a_1(t)$ and $a_4(t) = a_2(t)$. In the left panel, we observe that the intensity

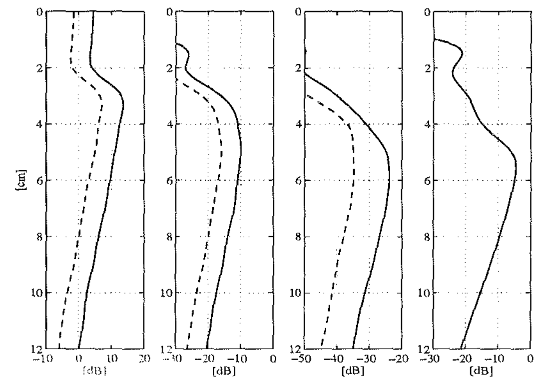

Figure 4.6: Scattered harmonic tissue signal along symmetry axis based on calculated transmit fields, going from fundamental component in left panel to fourth harmonic component in right panel. Dashed lines: Single frequency band source pulse used. Solid lines: Two dual frequency band source pulses used, phase inversion on second harmonic component, with pulse summation of scattered signals.

of the fundamental tissue component is increased by approximately 6 dB in the pulse summation process of the two scattered dual frequency band source signals relative to the scattered single frequency band source signal. In the second panel, the second harmonic component of the pulse summation signal is also seen to be around 6 dB above the signal obtained using the single frequency band source pulse. The third harmonic component, displayed in the third panel, is significantly higher than the scattered third harmonic component obtained using the single frequency band source pulse. However, by comparing with the scattered fourth harmonic component of the pulse summation signal in the fourth panel, we see that the scattered third harmonic pulse summation signal is significantly reduced in the pulse summation process. These are all expected results in reasonable agreement with Eq. 4.8.

If the two scattered signals, obtained using the two dual frequency band sources, are time shifted relative to each other by a small amount before summation, the resulting third harmonic component in the pulse summation signal can be further reduced.

In Fig. 4.7 the two scattered signals have been time shifted relative to each other by up to 10 ns before pulse summation is performed. Fig. 4.7 represents the same as Fig. 4.6 and the displayed dynamic range and scale are identical in the two figures. By comparing these two figures we observe that the small time shifts introduced before pulse summation have little or no effect on the fundamental and fourth harmonic pulse summation components. This is due to the fact that these harmonic components are in phase when summed together and a small time shift, relative to the wave length, will not have a major effect on the results of the summation. The second and third harmonic components are, however, close

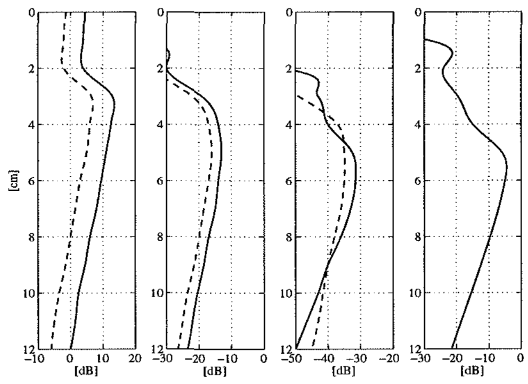

Figure 4.7: Same as Fig. 4.6 but with small time shifts between the two scattered dual frequency band pulses before pulse summation.

to π out of phase when summed together and the small time shifts introduced are seen to have major effects on these harmonic components. Relative to the situation without time shifts between the two scattered pulses as in Fig. 4.6, both these components are reduced when introducing the small time shifts with a 3 dB reduction for the second harmonic component and a major reduction for the third harmonic component. With the introduced time shifts, the third harmonic component after pulse summation is of the same order as obtained from the single frequency band source pulse (dashed line).

If instead the two scattered signals from the dual frequency band sources are subtracted, the scattered fourth harmonic component from tissue may be reduced as previously indicated in relation to Eq. 4.9.

The dashed lines in Fig. 4.8 still indicate the scattered level obtained by using a single frequency band source and the scattered fundamental component in the left panel is normalized to 0 dB at 8 cm as in the two previous figures. The solid lines in the panels indicate harmonic levels obtained after pulse subtraction of the scattered tissue signals obtained from the two dual frequency band sources, described by Eqs. 4.4 and 4.5, where $a_3(t) = a_1(t)$ and $a_4(t) = a_2(t)$. In the left panel we clearly see that the fundamental component is heavily reduced in the pulse subtraction process relative to the case using a single frequency band source. The linear transmitted fundamental component is canceled in the process and only a nonlinear fundamental component, second term on the right-hand side in Eq. 4.9, remains. A strong linear transmitted second harmonic component, first term on the right-hand side in Eq. 4.9, is evident in the second panel. In the third panel, a significant first order nonlinear third harmonic component, second term on the right-hand side in Eq. 4.9, also remains after the pulse subtraction process. The fourth harmonic component in the last panel is, although significantly reduced compared to Fig. 4.6, still relatively strong.

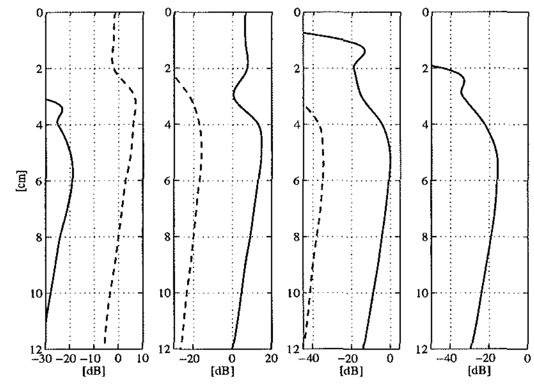

Figure 4.8: Scattered harmonic tissue signal along symmetry axis based on calculated transmit fields, going from fundamental component in left panel to fourth harmonic component in right panel, Dashed lines: Single frequency band source pulse used. Solid lines: Two dual frequency band source pulses used, phase inversion on second harmonic component, with pulse subtraction of scattered signals.

To further reduce the fourth harmonic component in Fig. 4.8, small time shifts and amplitude corrections must be introduced in the two scattered pulses before they are combined in the pulse inversion process. In Fig. 4.9, a time shift of up to 22 ns and amplitude corrections up to 4 dB are introduced before pulse subtraction. We notice that the effects on the resulting fundamental and fourth harmonic components, are of special importance. The fourth harmonic component in the right panel is heavily reduced by approximately 20 dB compared to what was obtained in Fig. 4.8 without the time and amplitude compensations whereas the resulting fundamental component, in the left panel, is significantly increased by around 20 dB.

In Fig. 4.6 and 4.8, we saw that the scattered third or fourth harmonic tissue components, mainly introduced due to application of dual frequency band sources, could be significantly reduced by performing the simple pulse summation or pulse subtraction process according to Eq. 4.8 and 4.9. Introducing small time shifts and amplitude corrections in the two scattered pulses before summation or subtraction, the third or fourth harmonic components could, however, be further reduced. The need to introduce these compensations in the scattered signals before performing the pulse inversion process is a consequence of the fact that the resulting wave propagation from the applied sources deviates somewhat from the quasi-linear approximation discussed in Sec. 4.2.1.

In Table 4.1, the resulting third and fourth harmonic signal components along the symmetry axis for the two dual frequency band transmit fields are compared. Two sources described by Eq. 4.4 and 4.5, where $a_3(t) = a_1(t)$ and $a_4(t) = a_2(t)$ and $\phi = 0$, are used as sources on the indicated transducer.

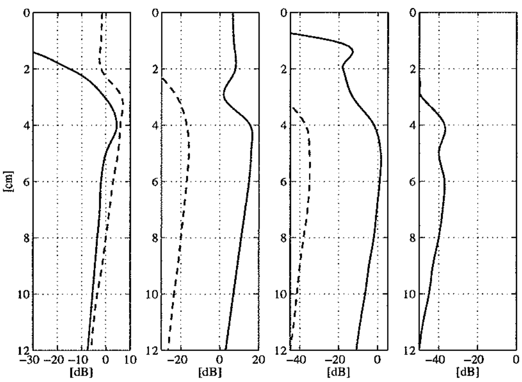

Figure 4.9: Same as Fig. 4.8 but with time shifts and amplitude corrections between the two scattered dual frequency band pulses before subtraction.

Inspecting the third harmonic components we observe that the relative time shifts between the two transmit fields are almost constant from around 6 cm in range direction and that differences in amplitudes generally are small.

Changing to the fourth harmonic components, we see that differences in amplitudes are much larger and in Fig. 4.9, amplitude compensations had to be included in order to further suppress the fourth harmonic component in the pulse subtraction signal.

The deviations between the full nonlinear wave propagation and the quasi-linear approximation can be further examined by using our simulation program in a quasi-linear mode to calculate the two quasi-linear wave fields resulting from the two dual frequency band sources. These two transmit wave fields are then calculated by first using the dual frequency band source pulse described by Eq. 4.4 on the transducer and then applying the source described by Eq. 4.5, where $a_3(t) = a_1(t)$ and $a_4(t) = a_2(t)$ and $\phi = 0$. Keeping in mind that the scattering from tissue is assumed to be a linear process, the two transmit fields are then combined in the pulse inversion process and compared with the previous results obtained by performing a full nonlinear solution of Eq. 4.2.

Fig. 4.10 displays a comparison of the third harmonic pulse summation transmit fields obtained from the the full nonlinear solution of the nonlinear wave equation and the quasi-linear solution of the nonlinear wave equation, left and right panel, respectively. We observe that the third harmonic level from the quasi-linear solution is significantly lower than from the full nonlinear solution. Comparisons of the two transmit fields obtained from the full nonlinear solution of the wave equation resulted in time delays and amplitude variations shown in Table 4.1, which are not present in the quasi-linear solution of the wave equation.

From Eq. 4.8, the third harmonic component of the pulse summation signal should, in the quasi-linear situation, ideally be totally canceled. In the right panel of Fig. 4.10,

Table 4.1: Relative time delays and amplitude variations along symmetry axis for the two dual frequency band transmit fields.

	3rd harmonic	3rd harmonic	4th harmonic	4th harmonic
1 cm		0.2 dB		0.7 dB
2 cm		0.4 dB		1.3 dB
3 cm	-2 ns	0.6 dB	-2 ns	2.6 dB
4 cm	5 ns	0.1 dB	24 ns	4 dB
5 cm	6 ns	0.5 dB	15 ns	2.9 dB
6 cm	8 ns	0.5 dB	15 ns	3 dB
7 cm	9 ns	0.5 dB	15 ns	3.2 dB
8 cm	9 ns	0.5 dB	16 ns	3.4 dB
9 cm	9 ns	0.5 dB	18 ns	3.6 dB
10 cm	9 ns	0.5 dB	19 ns	3.8 dB
11 cm	9 ns	0.4 dB	20 ns	3.9 dB
12 cm	10 ns	0.3 dB	22 ns	4 dB

the third harmonic component is, however, not fully canceled. The resulting second and fourth harmonic components which are not that strongly suppressed in the pulse summation signal will, depending on the bandwidth of the transmitted fundamental and second harmonic components and the bandwidth of the third harmonic filter applied, introduce weak signal components in the passband of the third harmonic filter.

In Fig. 4.11 we see a comparison between the fourth harmonic pulse subtraction transmit fields obtained from the the full nonlinear solution of the nonlinear wave equation and the quasi-linear solution of the nonlinear wave equation, left and right panel, respectively. We observe that the intensity of the fourth harmonic field obtained from the quasi-linear approximation of the nonlinear wave equation is significantly lower in the resulting pulse subtraction signal.

4.3.3 Scattering from a Contrast Bubble

We now proceed to investigate the scattering from a contrast bubble. The main goal now is twofold. First, to compare the signal scattered from the bubble when driven by a conventional single frequency band pulse and the signal obtained after pulse inversion using dual frequency band drive pulses. And second, to compare the relative level of harmonic components in the dual frequency band pulse inversion bubble signal and the dual frequency band pulse inversion soft tissue signal from the previous section. Ultrasound contrast bubbles have much higher compliance than soft tissue and the bubble will respond differently relative to soft tissue when driven by the dual frequency band pulses.

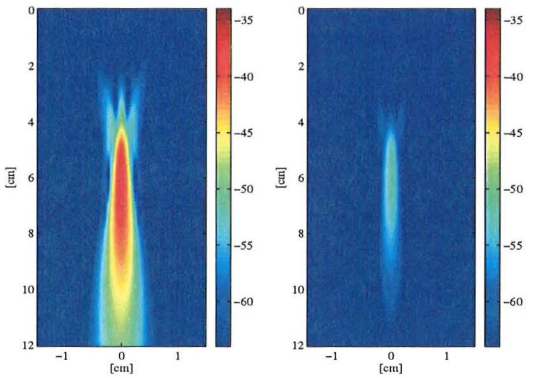

Figure 4.10: Wave field obtained as summation of transmit fields from two dual frequency band sources with identical fundamental components and inverted polarity on second harmonic components. Left panel: Third harmonic field obtained from full nonlinear solution of Eq. 4.2. Right panel: Third harmonic field obtained from quasi-linear solution of Eq. 4.2.

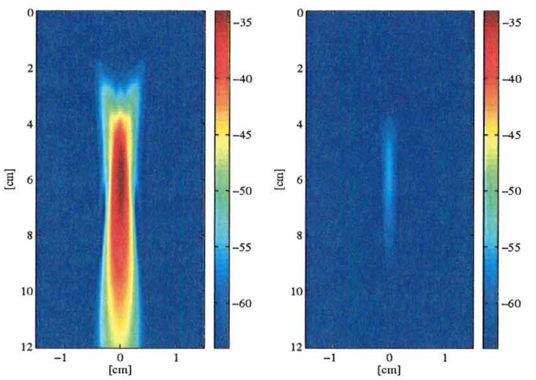

Figure 4.11: Wave field obtained as difference of transmit fields from two dual frequency band sources with identical fundamental components and inverted polarity on second harmonic components. Left panel: Fourth harmonic field obtained from full nonlinear solution of Eq. 4.2. Right panel: Fourth harmonic field obtained from quasi-linear solution of Eq. 4.2.

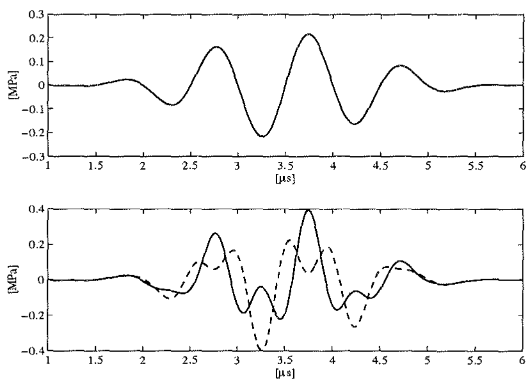

Figure 4.12: Upper panel: Single frequency band pulse. Lower panel: Dual frequency band pulses with identical fundamental components and phase inversion on second harmonic components.

The upper panel in Fig. 4.12 shows an example of a 1 MHz single frequency band source pulse where $a_2(t)$ in Eq. 4.4 is set to zero. If $a_1(t)$ in Eq. 4.4 is unchanged and $a_2(t)$ now is different from zero, so that a 2 MHz pulse is added, we can get the solid line in the lower panel of Fig. 4.12 representing a dual frequency band source pulse. Then, simply by inverting the polarity on the added 2 MHz pulse while keeping the 1 MHz pulse unchanged, we can construct the pulse displayed as the dashed line in the lower panel of the figure. These two pulses, in the lower panel, represent the two dual frequency band pulses used in the explained pulse inversion technique. We notice that these pulses are asymmetric with respect to positive and negative pressure amplitudes and the contrast bubble will presumably respond differently when driven by one of them relative to the other.

In Fig. 4.13, the solid lines display the absolute value of the Fourier Transform of the scattered bubble signal from a 3 μm bubble with resonance frequency around 4 MHz when driven by the single frequency band pulse in the upper panel of Fig. 4.12. We clearly see that the bubble has responded nonlinearly to the drive pulse with significant amounts of scattered energy at harmonic components.

The scattered bubble signal is then calculated using the two dual frequency band pulses in the lower panel of Fig. 4.12 as drive pulses.

Adding the resulting two scattered pulses, we obtain the dashed line in the upper panel of Fig. 4.13. All scattered harmonic components are increased in the pulse summation process relative to when using the single frequency band drive pulse (solid line). We particularly notice the increase on the fundamental and third harmonic component, approximately 6 and 15 dB, respectively.

If we instead subtract the two scattered bubble signals from the dual frequency band

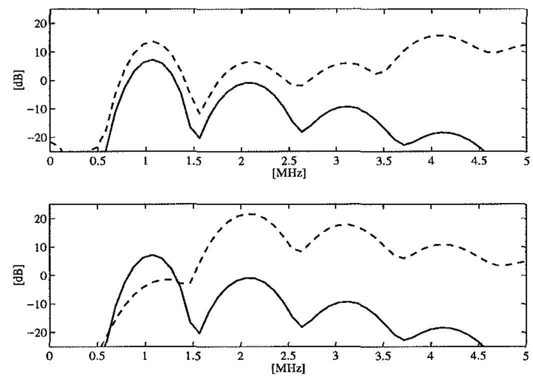

Figure 4.13: Absolute value of Fourier Transform of scattered bubble signal. Solid line: Single frequency band drive pulse from upper panel in Fig. 4.12 used. Dashed line upper panel: Sum of scattered pulses when driven by the two pulses in lower panel of Fig. 4.12. Dashed line lower panel: Subtraction of the scattered pulses when driven by the two pulses in lower panel of Fig. 4.12.

drive pulses, we obtain the dashed line in the lower panel of Fig. 4.13. All scattered harmonic components except from the fundamental, are now increased relative to when using the single frequency band drive pulse (solid line). Here, we particularly notice the major increase on the scattered fourth harmonic component of about 30 dB.

In Fig. 4.14, the dashed lines display harmonic components scattered from a contrast bubble when driven by the calculated transmit field from Sec. 4.3.1 obtained with a single frequency band source pulse described by Eq. 4.4 where $a_2(t) = 0$. As previously, the scattered fundamental component in the left panel is normalized to 0 dB at 8 cm. Both the dynamic range and scale varies between the panels due to the fact that the level of scattered harmonic bubble signal depends strongly on the amplitude of the incident drive pulse.

Similar to Fig. 4.7, the solid lines in Fig. 4.14 show the scattered harmonic components obtained using the transmit fields from the dual frequency band source pulses in Eqs. 4.4 and 4.5 to drive the bubble, and then summing the two scattered signals in a pulse summation process. The small time shifts introduced between the two scattered signals before the pulse summation process in Fig. 4.7 have also been applied in Fig. 4.14 and it is therefore of special interest to compare these two figures. Introducing the indicated time shifts to the scattered bubble signals before summation do, however, only have marginal effects on the obtained pulse summation signal.

Starting with the scattered fundamental components in the left panel we see that the level is increased by around 6 dB in the pulse summation process relative to the level obtained using a single frequency band source for the contrast bubble (Fig. 4.14) as well as for the soft tissue (Fig. 4.7).

The second harmonic bubble signal obtained after pulse summation is seen to lie from around 10 to 2 dB above the bubble signal achieved using a single frequency band source pulse whereas for soft tissue, there is an almost constant 3 dB increase in scattered signal level applying the pulse summation process.

The third harmonic pulse summation bubble signal is increased significantly by 15 to 20 dB (at depths from 4 to 12 cm) relative to when applying a conventional single frequency band source pulse. The third harmonic pulse summation tissue signal, on the other hand, is around the same level as for the single frequency band signal as previously seen. This implicates that the new method, consisting of transmitting two dual frequency band source pulses and performing a pulse summation process, is capable of significantly increasing both the CNR and CTR at the third harmonic component relative to when applying the conventional single frequency band source pulse.

Looking at the fourth harmonic components in the right panel, we notice that there is a major increase in signal level for both the contrast bubble and the soft tissue applying the dual frequency source pulses with the pulse summation technique. Using this new pulse summation method on the fourth harmonic component would therefore result in a major increase in CNR but also a strong reduction in CTR relative to using a single frequency band source pulse.

It is also interesting to compare the third harmonic CNR obtained with the new pulse summation technique and the second harmonic CNR achieved using conventional second harmonic imaging with a single frequency band source pulse. The solid line in the third panel and the dashed line in the second panel of Fig. 4.14 are then to be compared. When comparing the CNR at two different harmonic components, the effect of absorption due to wave propagation from the scatterer to the transducer should be included, and in the present comparison, an absorption of 0.5 dB/cm/MHz was used. At 4 cm, the third harmonic CNR with the new method is around 13 dB above the second harmonic CNR obtained with a single frequency band source pulse. At 6 and 8 cm, the increase in CNR is approximately 10 and 5 dB, respectively, while at 10 cm, the third and second harmonic CNR are about the same.

The new pulse summation technique is seen to perform best in the near-field and focal region where the transmit amplitude is higher than in the far-field. Looking at Fig. 4.2 the transmit amplitude is seen to fall rather steeply in the far-field. The new pulse summation technique would probably have performed better in the far-field applying a transmit field more collimated in the far-field. This can for example be achieved by increasing the radius of the annular transducer to 1.5 cm and the geometric focus to 10 cm.

Also, acoustic absorption increases with frequency when not measured as number of wave lengths traveled hence working against higher harmonic imaging techniques at large depths.

The new method, transmitting dual frequency band source pulses and performing a general form of pulse inversion, may also be used applying the scattered fourth harmonic

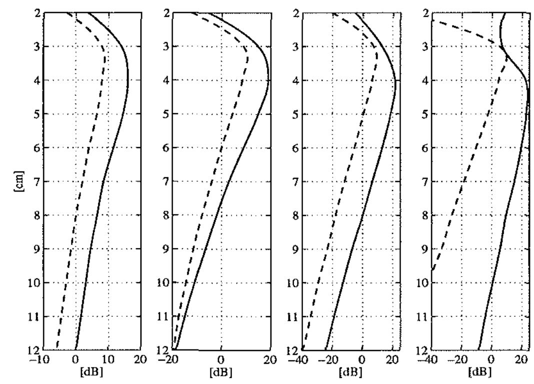

Figure 4.14: Scattered harmonic bubble signal along symmetry axis based on calculated transmit fields, going from fundamental component in left panel to fourth harmonic component in right panel. Dashed lines: Single frequency band source pulse used. Solid lines: Two dual frequency band source pulses used, phase inversion on second harmonic component. Pulse summation of scattered signals with same time shift as in Fig. 4.7.

component for image reconstruction. Then, in order to reduce the resulting fourth harmonic components from the soft tissue as seen in Sec. 4.3.2, the two scattered pulses should be subtracted.

Fig. 4.15 shows the results after the resulting scattered bubble signals have been subtracted in a pulse subtraction process. The two scattered bubble signals have been time shifted and amplitude corrected relative to each other by the same amount as was used in Fig. 4.9 and it is therefore of special interest to compare Fig. 4.9 and 4.15. As before, the dashed lines indicate the scattered harmonic levels obtained from the single frequency band source pulse from soft tissue and a contrast bubble, respectively. In Fig. 4.9, we see that all harmonic components from soft tissue, except the fourth harmonic, are very strong and thus only fourth harmonic imaging is interesting with this pulse subtraction technique due to the resulting limitations in CTR using the other harmonic components.

Investigating the fourth harmonic component in the right panel in Fig. 4.15, we notice that the increase in signal level applying dual frequency band source pulses and the pulse subtraction process is significant. We thus conclude that using two dual frequency band source pulses in combination with the pulse subtraction process significantly increases the CNR at the fourth harmonic component relative to applying a single frequency band source pulse. Also, from Fig. 4.9 we see that the fourth harmonic tissue signal resulting from the pulse subtraction process is very low giving a high CTR.

Here, it is also interesting to compare the fourth harmonic CNR obtained with the new pulse subtraction technique and the second harmonic CNR achieved using conventional second harmonic imaging with a single frequency band source pulse. The solid line in the

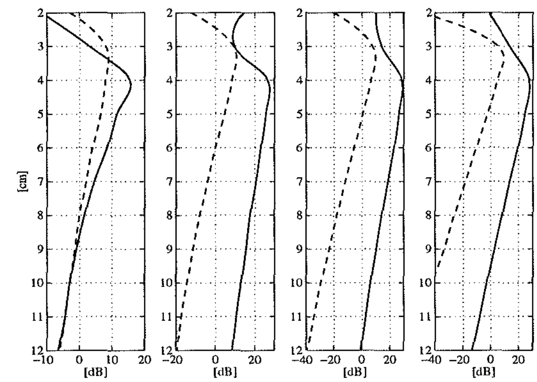

Figure 4.15: Scattered harmonic bubble signal along symmetry axis based on calculated transmit field, going from fundamental component in left panel to fourth harmonic component in right panel. Dashed lines: Single frequency band source pulse used. Solid lines: Two dual frequency band source pulses used, phase inversion on second harmonic component. Pulse subtraction of scattered signals with same relative time shifts and amplitudes as in Fig. 4.9.

fourth panel and the dashed line in the second panel of Fig. 4.15 are then to be compared. An absorption equal to 0.5 dB/cm/MHz is included in the present comparison. At 4 cm, the fourth harmonic CNR is about 18 dB above the second harmonic CNR obtained with the single frequency band source. The increase in CNR using the new pulse subtraction method is reduced to around 15, 8, and 3 dB at 6, 8, and 10 cm, respectively.

Again, as indicated previously, the new pulse subtraction technique would probably have performed better in the far-field applying a transmit field more collimated in the far-field. The effects of the acoustic absorption mechanisms will be stronger for the fourth harmonic signal components from the pulse subtraction method than for the third harmonic signal components from the pulse summation method.

4.4 Conclusions

The present paper has described and discussed a new contrast harmonic imaging method designed to increase the scattered harmonic contrast signal relative to both the scattered harmonic tissue signal and the noise signal always present in a pulse echo imaging system. To achieve this, the new method consists of transmitting dual frequency band pulses where in particular, a fundamental band and its second harmonic component are transmitted overlapping in time. This dual frequency band transmit pulse boosts up the scattered third and fourth harmonic contrast signal and tissue signal components. The increase in scattered third and fourth harmonic tissue signal is then removed or reduced transmitting a second dual frequency band pulse and performing a general pulse inversion process. Transmitting dual frequency band pulses, one is capable of constructing two asymmetric transmit pulses with respect to positive and negative pressure amplitude and thus preventing the scattered third or fourth harmonic contrast signal from being significantly reduced in the pulse inversion process.

4.5 Further Work

Presented results based on numerical simulations are interesting and suggest that experimental studies should be carried out to further validate the new contrast harmonic imaging method. The main obstacle in conducting these experiments is the design and manufacture of a new multiband ultrasound transducer capable of transmitting a fundamental and second harmonic imaging pulse while receiving the scattered third and possibly fourth harmonic components. One interesting transducer design is an annular transducer consisting of several independent rings. Then, the outer rings might be used in transmit mode while the inner rings, having a different frequency response, could be used in receive mode.

4.6 Acknowledgments

This work was supported by the Research Council of Norway.

Chapter 5

Linear Contrast Agent Detection through Low Frequency Manipulation of High Frequency Scattering Properties

Abstract

The present paper proposes a new method applying the total scattered contrast signal for image reconstruction, thus largely overcoming the problems encountered in harmonic imaging techniques. In the new method, the contrast signals and the tissue signals are differentiated applying a simple pulse subtraction technique which cancels or significantly reduces the scattered tissue signal, whereas the scattered contrast signal, due to assisting transmitted low frequency pulses altering the acoustic scattering properties of the contrast agent, is preserved in this process. The main mechanism through which this imaging technique selects the contrast agent signal is the linear resonant properties of the contrast bubble and the new method is thus mainly a linear contrast agent detection technique.

5.1 Introduction

Medical ultrasound wave propagation is typically a weak nonlinear process [3, Chapter 12]. Ultrasound scattering from soft tissue is assumed to be a linear process and energy received from soft tissue outside the fundamental transmitted frequency band is hence generated in the forward propagation of the ultrasound wave unless a spreading of contrast agent signal beyond the contrast-filled region, as discussed below, occurs. Ultrasound contrast agents are introduced to increase the ultrasound scattering from blood which is weak compared to the scattered tissue signal [13, Table 4.21-4.22]. The contrast agents are usually made as solutions of gas bubbles in a fluid which is injected into the blood flow. Ultrasound scattering from the added gas bubbles in the blood is usually strong and highly nonlinear, hence increasing the scattered blood signal.

The strong nonlinear response from the contrast bubbles when driven by an ultrasound pulse has given rise to the contrast harmonic imaging techniques [35] [11] [12], where only a harmonic component of the total scattered bubble signal is used for image reconstruction. As higher scattered harmonic components are considered, one is able to obtain a better differentiation of the received contrast signal and the received tissue signal due to the weaker nonlinear distortion of the received tissue signal. In addition to the fact that only a fraction (a harmonic component) of the total scattered contrast signal is used for image reconstruction, the contrast harmonic imaging techniques do have important unwanted aspects, some of which we are briefly going to discuss here.

First, as higher harmonic signal components are considered, the received contrast harmonic signal is, although increased relative to the harmonic tissue signal, typically significantly reduced in amplitude. The reduction in amplitude of the received contrast harmonic components has important consequences in a pulse echo imaging system where electronic and thermal noise always is present, and as higher contrast harmonic components are considered, the amplitude of these will be of the same order as the noise in the imaging system.

Second, for the contrast bubbles to respond with strong scattered harmonic components, the frequency of the transmitted drive pulses should be well below the resonance frequency of the contrast agent. Also, for the bubble to respond with distinct harmonic components, the transmit pulse has to be relatively narrowbanded. These constraints on transmit frequency and pulse length impose restrictions in the range resolution of the ultrasound image which is inversely proportional to the length of the transmit pulse.

Third, the part of the contrast signal scattered in the forward propagation direction adds in phase with the transmit pulse and introduces an extra distortion of the transmit field due to the strong nonlinearity of scattering from the bubbles. This extra distortion of the transmit field may then be linearly back-scattered from tissue regions and falsely interpreted as contrast signal. This unwanted spread of contrast agent signal is especially troublesome for tissue regions which in range direction lies beyond large blood vessels or the large blood filled heart cavities.

And finally, the design and manufacture of broadband ultrasound transducers capable of efficiently receiving higher than the scattered second harmonic component, is today very challenging.

The present paper deals with a new contrast agent detection technique, using the total scattered contrast signal, and in particular the linear component of this, for image reconstruction. By not being dependent on the scattered contrast harmonic components, the new detection technique largely overcomes the mentioned unwanted aspects resulting from the contrast harmonic imaging techniques. The new method accomplishes this by making use of transmitted assisting low frequency pulses which purpose are to manipulate the acoustic scattering properties of the resonant contrast bubbles. In addition, a simple pulse subtraction method is applied to cancel or significantly reduce the scattered tissue signal hence making it possible to efficiently differentiate the scattered contrast signal and the scattered tissue signal.

5.2 Theory

5.2.1 Wave Propagation and Scattering from Soft Tissue

Wave propagation in soft tissue can be considered a weak nonlinear process for amplitudes and frequencies common in medical ultrasound imaging. The tissue elasticity responds slightly nonlinearly giving rise to the nonlinearity of ultrasound wave propagation. The local nonlinearity is low but the distortion accumulates gradually in the forward propagating wave, manifesting itself mainly as a second harmonic component. By doing a Taylor series expansion of the equation of state $P = P(\rho, s)$ along an isentrope $s = s_0$, where ρ is the density of the medium, we can account for this nonlinearity. By discarding terms of order higher than the second in the Taylor series expansion, we obtain [16, Chapter 2]

$$p = A\frac{\rho_1}{\rho_0} + \frac{B}{2}\frac{\rho_1^2}{\rho_0^2} \ . \tag{5.1}$$

Here, ρ_0 is the density in the unstrained material while $\rho_1 = \rho - \rho_0$. The acoustic pressure is defined as $p = P - P_0$ where P_0 is the ambient pressure, and the parameters A and B are defined as

$$A = \rho_0 \frac{\partial P}{\partial \rho}\bigg|_{0,s} \ , \quad B = \rho_0^2 \frac{\partial^2 P}{\partial \rho^2}\bigg|_{0,s}$$

where the subscripts in the partial derivatives indicate that they are evaluated at the unstrained state for an isentropic process. We may then derive the following tissue elasticity equation [3, Chapter 12.3]

$$p(\vec{r}, t) = -A\nabla \cdot \vec{\psi}(\vec{r}, t) + A\beta \left(\nabla \cdot \vec{\psi}(\vec{r}, t)\right)^2 \tag{5.2}$$

where $\vec{\psi}$ is particle displacement and β is a nonlinearity parameter defined as

$$\beta = 1 + \frac{B}{2A} \ .$$

Eq. 5.2 is a nonlinear material elasticity equation where the nonlinearity parameter can be found experimentally for various materials. In the one-dimensional case, the equation for conservation of momentum gives

$$\rho_0 \frac{\partial^2 \psi(z, t)}{\partial t^2} = -\frac{\partial p(z, t)}{\partial z} \ . \tag{5.3}$$

From Eq. 5.2, we can for the one-dimensional case, omitting the coordinate dependency, write the material equation as

$$p = -A\frac{\partial\psi}{\partial z} + A\beta\left(\frac{\partial\psi}{\partial z}\right)^2 \tag{5.4}$$

or alternatively

$$\frac{\partial\psi}{\partial z} = -\kappa p + \beta(\kappa p)^2 \tag{5.5}$$

where the compressibility κ is defined as the inverse of the parameter A. We may now derive the one-dimensional nonlinear wave equation as

$$\frac{\partial^2\psi}{\partial t^2} = c_0^2\left(1 - 2\beta\frac{\partial\psi}{\partial z}\right)\frac{\partial^2\psi}{\partial z^2} \tag{5.6}$$

where the linear propagation velocity is defined as

$$c_0 = \sqrt{\frac{A}{\rho_0}} = \frac{1}{\sqrt{\rho_0\kappa}} \ .$$

We notice that the nonlinear propagation velocity varies with the volume compression of the material according to

$$\begin{aligned} c &= c_0\sqrt{1 - 2\beta\frac{\partial\psi}{\partial z}} \\ &= c_0\sqrt{1 + 2\beta\kappa p - 2\beta^2(\kappa p)^2} \\ &\approx c_0\sqrt{1 + 2\beta\kappa p} \approx c_0(1 + \beta\kappa p) \end{aligned} \tag{5.7}$$

where the last approximations are valid for the case when $\kappa p << 1$. Eq. 5.7 is later used in Sec. 5.5 to analyze the propagation of two transmitted dual frequency band pulses.

The signal scattered from soft tissue is a result of the inherent inhomogeneous nature of the medium. There is a spatial variation of the mass density and compressibility on various scales resulting in scattering of the transmitted acoustic wave. The acoustic scattering process from soft tissue is assumed to be linear and the presence of harmonic components in the scattered tissue signal is, if spreading of contrast agent signal beyond the actual contrast-filled regions does not occur, therefore a result of the nonlinearity in the forward propagating wave [3, Chapter 7].

In medical ultrasound imaging, soft tissue is a non-resonant medium, the wave propagation is a weak nonlinear process while the resulting scattering is a linear process.

5.2.2 Contrast Agent Scattering

The contrast agent is assumed to be gas bubbles encapsulated in a thin shell. The diameter of the bubble is much less than the wavelength of the incoming wave field and the bubble thus experiences an approximately uniform spatial field and the bubble oscillation is assumed to be purely spherical.

Simulations for bubble radius oscillations and acoustic scattering are done using the numerical model developed by Angelsen *et al* [4]. This model includes an equation for the relation between pressure and radial strain in a thin shell encapsulating a gas bubble. The model allows for a finite speed of sound in the medium surrounding the bubble, thus taking radiation losses from the bubble into account. Otherwise it is comparable to the well known Rayleigh-Plesset equation [33] [31] and the two models give similar results for incident pressure pulses and bubble parameters studied in this paper.

The Rayleigh-Plesset equation is a second order nonlinear differential equation for the fluid surrounding a spherical pulsating gas bubble. This equation describes the radius oscillation of the bubble as [33] [31]

$$\rho_0(a\ddot{a} + \frac{3}{2}\dot{a}^2) = p(a,t) - P_0 - p_i(t) \tag{5.8}$$

where a is the radius, $\dot{a}$ and $\ddot{a}$ is the velocity and acceleration of the bubble radius, ρ_0 is the density of the surrounding fluid, P_0 is the ambient pressure, $p_i(t)$ is the incident driving pressure, and $p(a,t)$ is the pressure at the bubble surface. Nonlinear elasticity of the gas and encapsulating thin shell, surface tension, and viscosity may be incorporated in the first term on the right-hand side in Eq. 5.8.

For small amplitudes of the incident drive pressure, the bubble oscillation can be assumed to be approximately linear and we have the following second order linear differential equation for the radial displacement, ψ, around an equilibrium radius a

$$m\ddot{\psi}(t) + b\dot{\psi}(t) + s\psi(t) = -4\pi a^2 p_i(t) \ . \tag{5.9}$$

Here, m is the inertia of the surrounding fluid, b is a damping constant, and s is the stiffness of the gas and encapsulating bubble shell. Eq. 5.9 typically describes the forced linear oscillation of a system consisting of a mass m attached on a spring with stiffness s whereas b accounts for the damping in the system. By taking the Fourier Transform of Eq. 5.9 we obtain

$$\psi(\omega) = \frac{4\pi a^2}{s} H_1(\Omega) p_i(\omega) \tag{5.10}$$

where we have defined the transfer function from drive pressure to radial displacement as

$$H_1(\Omega) = \frac{1}{\Omega^2 - 1 - i\Omega d} \tag{5.11}$$

and where

$$d = \frac{b}{\omega_0 m}\ , \quad \omega_0^2 = \frac{s}{m}\ , \quad \Omega = \frac{\omega}{\omega_0}\ . \tag{5.12}$$

Here, ω is the angular frequency of the Fourier Transform, and ω_0 is the resonance frequency. The absolute value and phase angle of $H_1(\Omega)$ are shown in Fig. 5.1. We see that

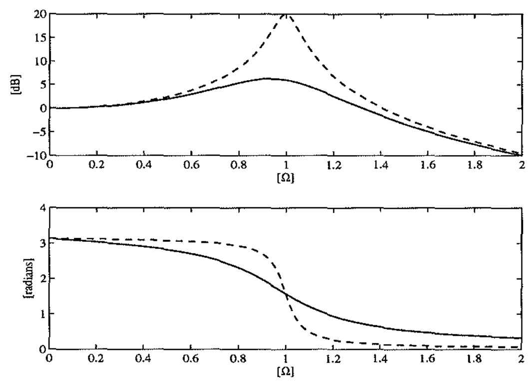

Figure 5.1: Transfer function from drive pressure to radial displacement in Eq. 5.11. The parameter d in Eq. 5.12 is set to 0.5 and 0.1 giving the solid line and dashed line, respectively. Upper panel: Absolute value. Lower panel: Phase angle.

for drive frequencies well below resonance the displacement is π out of phase with the driving pressure. For frequencies well above resonance, the bubble responds differently and the displacement and drive pressure are now in phase. Around resonance the displacement is approximately $\frac{\pi}{2}$ out of phase with the drive pressure.

The absolute value of the amplitude of the transfer function is seen in the upper panel of Fig. 5.1. Going from frequencies below resonance towards resonance the amplitude increases gradually culminating with a prominent peak around resonance for the situation with low damping ($d = 0.1$) and a considerable smaller peak for the situation with higher damping ($d = 0.5$). In both cases, the amplitude is seen to decreases rapidly above resonance.

The far-field pressure at a distance r from the source, radiated from a time harmonic oscillating bubble behaving as a monopole source is a diverging spherical wave that may be written

$$p(r) = \frac{p(a)a}{r} e^{-ik(r-a)} \tag{5.13}$$

where a is the bubble radius and k is the wave number. By assuming pure radial incompressible oscillations and neglecting the nonlinear convective acceleration term, the Navier-Stokes Equations reduce to [42]

$$\rho_0 \frac{\partial u_r}{\partial t} = -\frac{\partial p}{\partial r} \tag{5.14}$$

where u_r is the radial velocity. We particularly notice that the viscous terms have vanished for the situation with pure radial incompressible fluid motion. We may now write the pressure gradient as

$$-\frac{\partial p(r)}{\partial r} = \frac{p(a)}{r}\left(\frac{a}{r} + ika\right) . \tag{5.15}$$

At the bubble surface, $u_r = \dot{\psi}$ and $r = a$, and we thus get

$$p(a,\omega) = -\frac{\rho_0 a}{1+ika}\omega^2\psi(\omega) \ . \tag{5.16}$$

Assuming that the source is much less than the wave length which is typically the case for ultrasound contrast bubbles, $ka << 1$, we get

$$p(a,\omega) \approx -\rho_0 a\omega^2\psi(\omega) \ . \tag{5.17}$$

Applying the result from Eq. 5.10 we finally obtain the following relation between the drive pressure and the scattered pressure

$$p(a,\omega) = \rho_0\frac{4\pi a^3}{m}H_2(\Omega)p_i(\omega) \tag{5.18}$$

where the transfer function from drive pressure to scattered pressure is given by

$$H_2(\Omega) = \frac{\Omega^2}{1-\Omega^2+i\Omega d} \ . \tag{5.19}$$

The upper and lower panel of Fig. 5.2 display the absolute value and phase angle of $H_2(\Omega)$, respectively. As previously, the dashed lines are results obtained setting the parameter d equal to 0.1 while the solid lines are obtained for d equal to 0.5. The amplitude of the scattered pressure, as seen from the upper panel in Fig. 5.2, significantly increases when going from drive frequencies below resonance towards resonance. For drive frequencies above resonance, the scattered amplitude approaches a constant level.

In the lower panel of the figure, we see that for drive frequencies well below resonance, the scattered pressure is in phase with the driving pressure. This means that the bubble is dominated by s, the stiffness of the gas and shell. For frequencies well above resonance, the bubble responds differently and is now dominated by m, the inertia of the co-oscillating mass. The scattered pressure and drive pressure are now π out of phase. Around resonance the scattered pressure is approximately $\frac{\pi}{2}$ out of phase with the drive pressure.

In medical ultrasound imaging, the contrast bubble is typically a resonant scatterer and contrast agent scattering is a highly nonlinear process.

5.3 Method

The new contrast agent detection method is performed by consecutively transmitting two ultrasound pulses, both containing two frequency bands which are overlapping in the time domain. These two transmitted pulses contain a low frequency band and a high frequency band, where the purpose of the transmitted low frequency band is to manipulate,

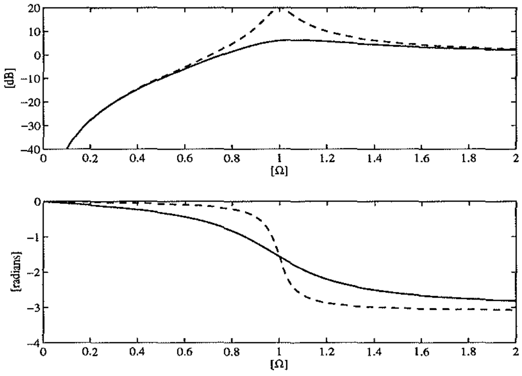

Figure 5.2: Transfer function from drive pressure to scattered pressure in Eq. 5.19. The parameter d in Eq. 5.12 is set to 0.5 and 0.1 giving the solid line and dashed line, respectively. Upper panel: Absolute value. Lower panel: Phase angle.

by expanding and compressing the bubble, the acoustic scattering properties of the contrast agent at the transmitted high frequency band. The two transmitted pulses may be expressed as

$$p_1(t) = a_1(t)sin(\omega_1 t) + a_2(t)sin(\omega_2 t + \phi_1) \quad (5.20)$$

$$p_2(t) = -a_3(t)sin(\omega_1 t) + a_4(t)sin(\omega_2 t + \phi_2) \quad (5.21)$$

where a_n are positive amplitude functions, ω_n is the angular frequency, and ϕ_n are selected phase angles. In the simplest embodiment of the new imaging technique, $a_3 = a_1$, $a_4 = a_2$, and $\phi_2 = \phi_1$.

First, the pulse described by Eq. 5.20 is transmitted and the scattered pulse is received and stored. Then the pulse in Eq. 5.21 is transmitted, where the phase of the low frequency components not used for image reconstruction are inverted, and the received scattered signal is subtracted from the first received pulse. The non-resonant soft tissue and the resonant contrast bubble will respond differently on the two transmitted dual frequency band pulses.

We assume that the time duration of the transmitted high frequency pulse is less than the time duration of a half period of the transmitted low frequency pulse. If the high frequency components ω_2 in the first transmitted pulse are placed in the negative half period of the low frequency components ω_1, then in the second transmitted pulse, they will due to the phase inversion be placed in the positive half period of the low frequency components. The transmitted low frequency components are well below the resonance frequency of the contrast agent. In the first scattered bubble signal, the high frequency components will hence be scattered from an expanded bubble relative to equilibrium size, whereas in the second scattered bubble signal, the high frequency components will be scattered from a compressed bubble (see lower panel of Fig. 5.1).

We saw in the lower panel of Fig. 5.2 that the phase of the transfer function from drive pressure to scattered pressure changes rapidly for drive frequencies around the resonance frequency of the bubble. If the transmitted high frequency components then are placed around the equilibrium resonance frequency of the contrast bubble, the resulting two scattered high frequency pulses from the contrast bubble will be somewhat time shifted relative to each other. Also, from the upper panel of Fig. 5.2 the amplitude of the two scattered bubble signals will be somewhat different. The two received signals from soft tissue will not have this relative time shift and amplitude difference and the soft tissue signal is thus canceled in the pulse subtraction process of the two received signals while the received contrast agent signal is preserved.

5.4 Bubble Oscillations

Simulations of bubble radius oscillations and acoustic scattering are done using the numerical model developed by Angelsen *et al* [4]. Results from this model are, as indicated, similar to results obtained using the well-known Rayleigh-Plesset equation [33] [31] for pressure amplitudes and bubble parameters used in the present paper. Simulations are done using a single bubble with acoustic parameters similar to the contrast agent *Sonazoid*. The equilibrium resonance frequency of the contrast bubble is around 5 MHz.

Fig. 5.3 shows an example of two transmit pulses described by Eq. 5.20 and 5.21 where a low frequency 0.5 MHz and a high frequency 5 MHz pulse are transmitted simultaneously. The high frequency pulse in the upper panel of the figure appears during the negative half period of the low frequency pulse. In the lower panel, the phase of the low frequency pulse is inverted relative to the upper panel, whereas the high frequency pulse is unchanged, and the high frequency pulse now appears during the positive half period of the low frequency pulse. These two transmit pulses are now used to drive the contrast bubble which equilibrium resonance frequency is around 5 MHz.

In Fig. 5.4 the bubble radius responses from the two transmitted drive pulses are shown in the upper and lower panel, respectively. The low frequency drive pulse is much below the equilibrium resonance frequency of the bubble and the radius response is thus π out of phase with the low frequency drive pulse as expected from the lower panel of Fig. 5.1. In the first transmitted pulse, the high frequency drive pulse occurs for an expanded bubble while in the second transmitted pulse, the high frequency drive pulse occurs when the bubble is compressed. Relative to equilibrium conditions, the resonance frequency is somewhat reduced and increased for the expanded and compressed bubble, respectively. We notice that the radius oscillations due to the high frequency pulse are larger in magnitude for the less stiff, expanded bubble than for the stiffer, compressed bubble.

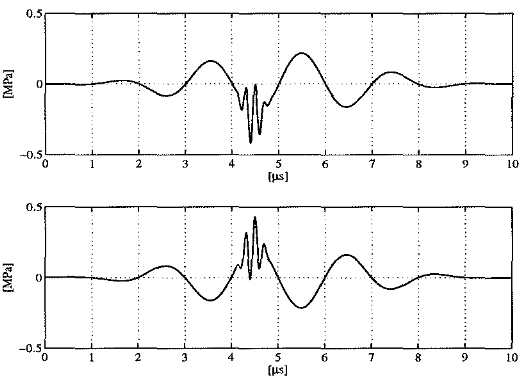

Figure 5.3: Dual frequency band drive pulses. Upper panel: High frequency components occur during negative half period of low frequency components. Lower panel: High frequency components occur during positive half period of low frequency components.

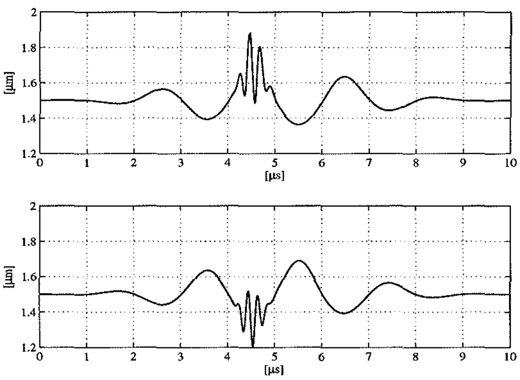

Figure 5.4: Bubble radius oscillations due to drive pulses in upper and lower panel of Fig. 5.3, respectively.

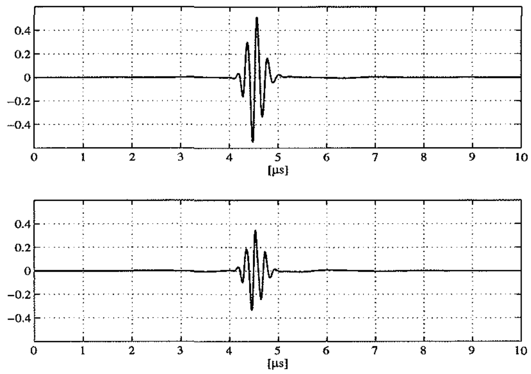

Figure 5.5: Scattered pressure pulses due to drive pulses in upper and lower panel of Fig. 5.3, respectively.

Simulations of scattered pressure pulses due to the two drive pulses are displayed in Fig. 5.5, upper and lower panel, respectively. First, we notice that the scattered low frequency components, almost invisible in this figure, are much lower in amplitude than the scattered high frequency components. This is in agreement with our linear theoretical considerations culminating in Fig. 5.2, where the amplitude in the upper panel was seen to increase significantly when going from drive frequencies below resonance towards resonance. We also see that the scattering of the high frequency components are somewhat larger in amplitude for the expanded bubble than for the compressed one. This is due to the larger high frequency radius oscillations of the expanded bubble seen in the previous figure.

The two scattered pressure pulses are depicted together in the upper panel of Fig. 5.6. Here, the solid line is the pulse scattered from the expanded bubble, upper panel of Fig. 5.5, while the dashed line is the scattered pulse from the compressed bubble, lower panel of Fig. 5.5, and we clearly see the difference in amplitude indicated. Also important, we see that even if the two transmitted high frequency pulses occur at the exact same relative time, the two scattered high frequency pulses are time shifted relative to each other. This effect is due to the rapid change of the phase around resonance of the transfer functions for radial displacement and scattered pressure seen in the lower panels of Fig. 5.1 and Fig. 5.2.

The lower panel of Fig. 5.6 displays the result obtained when subtracting the two scattered high frequency pulses in the upper panel. Due to the relative time shift between the two scattered pulses, the signal obtained after subtraction is not canceled or significantly reduced.

The same bubble is now driven by the high frequency components only in Fig. 5.3 and the resulting radius oscillation and scattered pressure pulse are shown in the upper and

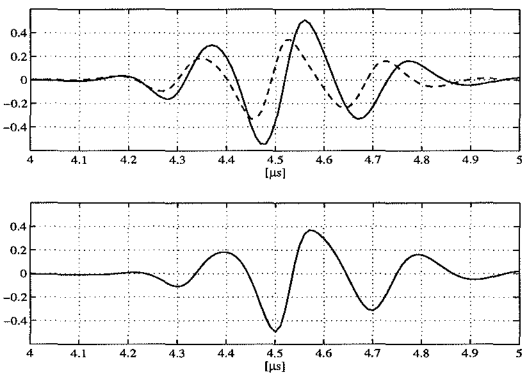

Figure 5.6: Upper panel: Scattered pressure pulses due to drive pulse in upper (solid line) and lower (dashed line) panel of Fig. 5.3. Lower panel: Pulse subtraction of the two pulses in the upper panel.

lower panel of Fig. 5.7, respectively. The scattered pressure pulse in the lower panel is in magnitude seen to lie between the two scattered pressure pulses in Fig. 5.5 obtained from the expanded and compressed bubble.

The upper panel of Fig. 5.8 shows the absolute value of the Fourier Transform of the pulses in the upper panel in Fig. 5.6. As previously indicated, we see that the scattered high frequency fundamental component is somewhat larger for the expanded bubble (solid line) than for the compressed bubble (dashed line). The nonlinearity of the high frequency scattering process is, however, stronger for the compressed bubble. Also, the harmonic components scattered from the expanded bubble are shifted slightly down in frequency due to the lowering of the resonance frequency relative to equilibrium conditions.

In the lower panel of Fig. 5.8, the solid line displays the absolute value of the Fourier Transform of the pulse in the lower panel in Fig. 5.6. As indicated, there are only marginal changes in the high frequency components of the pulse subtraction signal relative to the individual scattered pulses, and the total pulse subtraction signal may thus be used for image reconstruction.

The dashed line in the lower panel of Fig. 5.8 depicts the absolute value of the Fourier Transform of the pulse in the lower panel in Fig. 5.7, *i.e.* when the low frequency components have been removed from the drive pressure. As seen, the pulse subtraction signal obtained from the two dual frequency band drive pulses is very similar to the result obtained applying only one single high frequency band drive pulse. Applying only one such single high frequency band drive pulse, the scattered tissue signal can, however, not be efficiently removed and will hence mask the scattered contrast signal.

Simulations for radius oscillation and scattered pressure using the same low frequency pulse as in Fig. 5.3 but varying the amplitude of the high frequency pulse were also carried

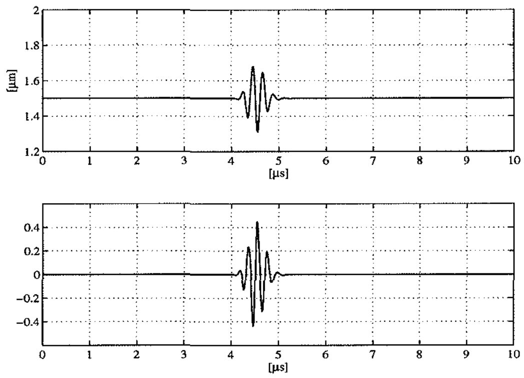

Figure 5.7: Upper panel: Bubble radius oscillation when driven by high frequency component only in Fig. 5.3. Lower panel: Scattered pressure pulse resulting from radius oscillation in upper panel.

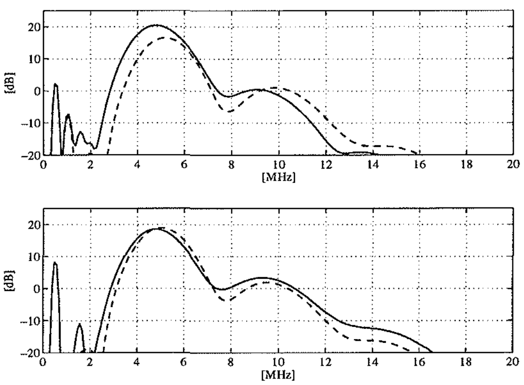

Figure 5.8: Upper panel: Absolute value of the Fourier Transform of the pulses in the upper panel of Fig. 5.6. Lower panel: Absolute value of the Fourier Transform of the pulse in the lower panel of Fig. 5.6, solid line, and the pulse in the lower panel of Fig. 5.7, dashed line.

out. When increasing and decreasing the amplitude of the high frequency drive pulse by 6 dB, the resulting amplitude of the fundamental component of the high frequency pulse subtraction signal increased and decreased by approximately 6 dB, respectively. It is mainly the linear acoustic properties of the oscillating resonant bubble which are utilized in this new contrast agent detection technique, and the performance of the technique is hence not sensitive to the amplitude of the high frequency pulse. As discussed in the next section, the amplitude of the transmitted high frequency pulse may vary considerably in the range direction due to acoustic absorption.

The transmitted low frequency components alter the acoustic scattering properties of the contrast bubble at the transmitted high frequency components and the described technique will be sensitive to the amplitude of these low frequency pulses. If the same high frequency pulse as in Fig. 5.3 is used to drive the bubble whereas the amplitude of the low frequency pulse is increased and decreased by 6 dB, respectively, we get the results displayed in the upper and lower panel of Fig. 5.9, respectively. This figure depicts the absolute value of the Fourier Transform of the obtained pulse subtraction signal just as the solid line in the lower panel of Fig. 5.8 and it is interesting to compare with this graph.

In the upper panel of Fig. 5.9 the amplitude of the low frequency pulse is increased by 6 dB to 400 kPa and we see that the high frequency fundamental component of the pulse subtraction signal has increased by around 3 dB relative to the solid line in the lower panel of Fig. 5.8. The level of the high frequency second harmonic component in the pulse subtraction signal is close to unchanged when increasing the low frequency amplitude.

The low frequency amplitude is then reduced by 6 dB to 100 kPa and the resulting high frequency fundamental component of the pulse subtraction signal in the lower panel of Fig. 5.9 is seen to suffer a reduction of around 6 dB relative to the solid line in the lower panel of Fig. 5.8. The high frequency second harmonic component in the pulse subtraction signal is now reduced by approximately 4 dB.

Reducing the low frequency amplitude by another 6 dB to 50 kPa results in a further reduction in the high frequency fundamental component of the pulse subtraction signal of around 6 dB. As the amplitude of the manipulating low frequency drive pulse is further reduced the two scattered high frequency pulses will become more and more similar.

5.5 Propagation of Transmitted Pulses

We will now briefly investigate the forward wave propagation of the two dual frequency band transmit pulses. Due to the large difference in transmitted frequency (a factor 10 was used in the previous section), the effects of diffraction, absorption, and nonlinearity will all appear very different for the two transmitted frequency bands. It may today be challenging to design and manufacture an ultrasound transducer capable of efficiently transmitting for example a low frequency 0.5 MHz pulse and a high frequency 5 MHz pulse. One solution is to use an annular transducer made up of several independent rings which may have different thicknesses and thus different resonance frequencies.

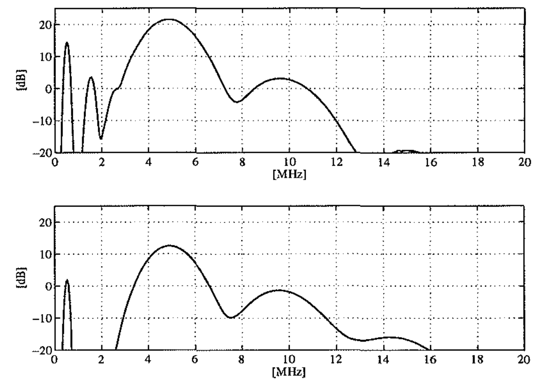

Figure 5.9: Absolute value of the Fourier Transform of the pulse subtraction signal obtained by increasing and decreasing the amplitude of the low frequency drive pulse by 6 dB, upper and lower panel, respectively.

First, we examine the effects of wave diffraction from such an axisymmetric annular transducer consisting of a low frequency and a high frequency ring. Fig. 5.10 displays the calculated low frequency (0.5 MHz) and high frequency (5 MHz) fields in decibel scale, left and right panel, respectively. A Finite Difference Method was used in the calculation of the wave diffraction. The low frequency pulse is transmitted from an unfocused outer ring with inner and outer radius equal to 0.5 cm and 1 cm, respectively, whereas the high frequency pulse is transmitted from a focused inner element with radius equal to 0.5 cm and geometric focus at 8 cm. The vertical axis in the figure represents range direction while the horizontal axis represents the lateral direction in the field.

The sharp edges occurring down to 1 cm in range in the left panel of Fig. 5.10 are unphysical and only a result of the way the calculated field is stored and visualized. The calculated low frequency wave field is only stored at each centimeter in range direction and hence has to be interpolated in range when visualized. We see, from the left panel in the figure, that the low frequency field is relatively constant in amplitude around the symmetry axis from 1 cm and down to 10 cm.

Our intention is that the high frequency field propagates in either a positive or a negative half period of the assisting low frequency field. For this to happen, the phase of the low frequency field has to change little in range direction along the symmetry axis. The phase shifts on the high frequency components are marginal in comparison due to their much higher frequency and resulting shorter temporal period.

Fig. 5.11 displays the normalized transmit low frequency pulse in the retarded time domain at the symmetry axis at various locations in range direction. The upper panel of this figure shows the pulse at the transducer (0 cm). In the middle panel, the resulting pulse at 2 cm and 5 cm, solid and dashed line, respectively, are shown while the lower panel

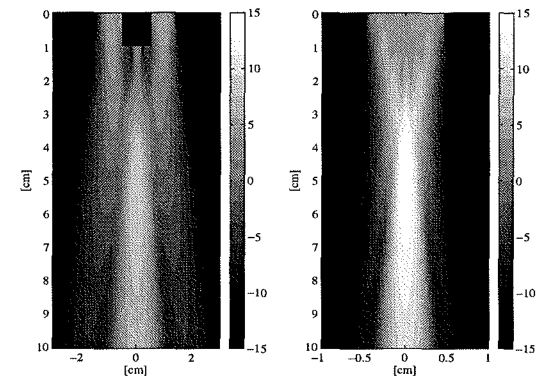

Figure 5.10: Calculated low frequency, left panel, and high frequency, right panel, transmit fields resulting from wave diffraction only. Low frequency source is an unfocused ring with radius from 0.5 cm to 1 cm. High frequency source is a focused disc with radius equal to 0.5 cm and focus at 8 cm. Fields displayed in decibel scale.

depicts the pulse at 7 cm and 10 cm, solid and dashed line, respectively.

At 2 cm the phase shift of the low frequency pulse is around $\frac{\pi}{3}$ relative to the pulse at the transducer which is significant. This means that if at the transducer, the high frequency pulse was centered around a normalized low frequency amplitude equal to 1 in the positive half period of the low frequency pulse, indicated by the vertical line in the upper panel of the figure, at 2 cm it would be centered in the same positive half period of the low frequency pulse but around a normalized amplitude equal to 0.5.

From 5 cm down to 10 cm, however, the phase shift is less than $\frac{\pi}{6}$ which can be considered little in the present context.

A possible solution for this specific case is to divide the range direction into two separate regions, one from the transducer and down to 4 or 5 cm, and one from 4 or 5 cm and down to 10 cm. The high frequency components dedicated to the first region should then be time shifted by approximately $\frac{\pi}{3}$ relative to the peak of the low frequency amplitude at the transducer to occur around peak positive or peak negative low frequency amplitude in the region of interest. This means that a total of four pulses must be transmitted down each line of sight instead of just two.

Acoustic absorption will also affect the two calculated wave fields in Fig. 5.10 very differently. Absorption increases with frequency when measured as a function of propagation distance and a typical experimental value for soft tissue is a power reduction of 0.5 dB/cm/MHz. Using this value, the intensity of the low frequency 0.5 MHz pulse is reduced by only 2.5 dB at 10 cm, while the intensity of the high frequency 5 MHz pulse is reduced by a massive 25 dB.

As indicated earlier, ultrasound wave propagation in tissue is usually a weak nonlinear

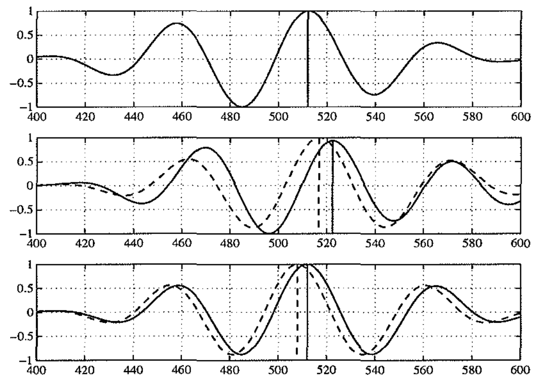

Figure 5.11: Normalized low frequency pulse taken out at various locations along the symmetry axis in the left panel of Fig. 5.10 and plotted in the retarded time domain as functions of sample number. Upper panel: Pulse at the transducer. Middle panel: Pulse at 2 cm and 5 cm, solid and dashed line, respectively. Lower panel: Pulse at 7 cm and 10 cm, solid and dashed line, respectively.

process. The tissue elasticity behaves slightly nonlinearly, getting stiffer during compression and less stiff during expansion relative to a linear behavior. This results in the fact that the ultrasound wave propagation velocity will be a function of the pressure and will hence not be constant. In the new imaging technique described in the present paper, this effect results in the possibility that the high frequency pulse propagating in the expansion cycle of the low frequency pulse (upper panel of Fig. 5.3) will propagate with a somewhat lower velocity than the high frequency pulse propagating in the compression cycle of the low frequency pulse (lower panel of Fig. 5.3).

In Eq. 5.7 we derived an expression for the variation of the propagation velocity with respect to the pressure for a plane wave approximation. Using typical values for the parameters in this equation, $\beta = 5$ and $\kappa = 400 \cdot 10^{-12}$ m^2/N, we are able to calculate the difference in propagation velocity $\triangle c$ for the two transmit high frequency pulses in Fig. 5.3 assuming the transmitted low frequency pulses to propagate as plane waves. The difference in pressure, due to the low frequency pulses, for these two high frequency pulses is around 0.5 MPa and we may here use the last approximation in Eq. 5.7, valid when $\kappa p << 1$. With $c_0 = 1500$ m/s we get a $\triangle c$ equal to 1.5 m/s using the indicated numerical values. At a depth equal to 10 cm, the high frequency pulse in the upper panel of Fig. 5.3 would then arrive around 67 ns after the high frequency pulse in the lower panel of this figure which is about one third of the period of the 5 MHz high frequency pulse. When subtracting the two received scattered pulses in order to cancel the scattered high frequency tissue components, a time shift around one third of the period is enough to prevent the cancellation of the tissue signal. The time shifts between the two received pulses can, due to the fact that the transmitted low frequency pulses propagate mainly as plane waves, relatively easily be compensated for by applying the approximation in Eq. 5.7 to calculate the proper time shifts and introducing them in the received signals before the subtraction process is performed.

5.6 Conclusions

The present paper has described a new method for detection of contrast agents utilizing the total scattered signal for image reconstruction, hence overcoming the problems in relation to harmonic detection techniques. In its simplest embodiment, the new method is performed by transmitting two dual frequency band pulses, both containing a low frequency band and a high frequency band which are overlapping in the time domain. The purpose of the transmitted low frequency band is to manipulate the acoustic scattering properties of the resonant contrast bubble at the transmitted high frequency band, which is used for image reconstruction. The resonant contrast bubble will respond differently on the two transmitted dual frequency band pulses relative to the non-resonant soft tissue. This is utilized to efficiently differentiate scattered contrast signal and scattered tissue signal in a simple pulse subtraction process. Mainly the linear acoustic properties of the oscillating resonant bubble are then utilized. Presented results show that the total scattered high frequency signal from the contrast bubble is preserved in the method. If the tissue elasticity is assumed to respond linearly to the transmitted pressure pulses, the scattered high frequency tissue signal can be canceled by the simple pulse subtraction process. Due to the weak nonlinear nature of the tissue elasticity, small time compensations must be introduced to the received signals before performing the pulse subtraction process to ensure that the scattered high frequency tissue components are completely removed.

5.7 Further Work

Based on numerical simulations and theoretical considerations, the proposed new contrast detection method appears interesting and should be further validated by experimental measurements. A possible annular transducer design, consisting of distinct rings with variable thicknesses, capable of transmitting the dual frequency band pulses used is indicated in relation to Fig. 5.10. It is also possible to use two separate transducers with overlapping transmit fields for the transmitted low and high frequency pulses. The resulting phase relations between the transmitted low frequency and high frequency pulses would then be somewhat more complex than for the transducer indicated in relation to Fig. 5.10.

5.8 Acknowledgments

This work was supported by the Research Council of Norway.

Bibliography

[1] H. Andrews. *Digital Image Restoration.* Prentice-Hall, New Jersey, 1992.

[2] B. A. J. Angelsen. *Ultrasound Imaging vol I.* Emantec, Norway, 2000. http: www.ultrasoundbook.com.

[3] B. A. J. Angelsen. *Ultrasound Imaging vol II.* Emantec, Norway, 2000. http: www.ultrasoundbook.com.

[4] B. A. J. Angelsen, T. F. Johansen, and L. Hoff. Simulation of gas bubble scattering for large mach-numbers. In *1999 IEEE Ultrasonics Symposium Proceedings*, pages 505–508. IEEE, 1999.

[5] R. Apfel and C. Holland. Gauging the likelihood of cavitation from short-pulse, low-duty cycle diagnostic ultrasound. *Ultrason. Med. Biol*, 17(2):179–185, 1991.

[6] M. A. Averkiou, D. R. Roundhill, and J. E. Powers. A new imaging technique based on the nonlinear properties of tissue. *Proc. IEEE Ultrason. Symp.*, 2:1561–1566, 1997.

[7] K. Caidal, E. Kazzam, J. Lidberg, G. Neumann Andersen, J. Nordanstig, S. Rantapaa Dahlqvist, A. Waldenstrom, and R. Wikh. New concepts in echocardiography: Harmonic imaging of tissue without use of contrast agents. *Lancet*, 352(9136):1264–1270, 1998.

[8] S. Child, C. Hartman, L. Schery, and E. Carstensen. Lung damage from exposure to pulsed ultrasound. *Ultrason. Med. Biol.*, 16(8):817–825, 1990.

[9] J. E. Chomas, P. Dayton, J. Allen, K. Morgan, and K. W. Ferrara. Mechanisms of contrast agent destruction. *IEEE Trans. Ultrason., Ferroelectr., Freq. Contr.*, 48(1):232–248, 2001.

[10] P. Dayton, J. S. Allen, and K. W. Ferrara. The magnitude of radiation force on ultrasound contrast agents. *J. Acoust. Soc. Am.*, 112(5):2183–2192, 2002.

[11] N. de Jong and R. Cornet. Higher harmonics of vibrating gas-filled microspheres. Part one: Simulations. *Ultrasonics*, 32:447–453, 1994.

[12] N. de Jong and R. Cornet. Higher harmonics of vibrating gas-filled microspheres. Part two: Measurements. *Ultrasonics*, 32:455–459, 1994.

[13] F. Duck. *Physical Properties of Tissue*. Academic Press, London, 1990.

[14] D. H. Evans, W. N. McDicken, R. Skidmore, and J. P. Woodcock. *Doppler Ultrasound, Physics, Instrumentation, and Clinical Applications*. John Wiley & Sons, Inc., New York, 1989.

[15] F. Forsberg, W. T. Shi, R. Y. Chiao, , A. L. Hall, S. D. Lucas, and B. Goldberg. Implementation of subharmonic imaging. *IEEE Ultrason. Symp.*, pages 1673–1676, 1999.

[16] M Hamilton and D. Blackstock. *Nonlinear Acoustics*. Academic Press, San Diego, 1998.

[17] L. M. Hinkelman, T. D. Mast, L. A. Metlay, and R. C. Waag. The effect of abdominal wall morphology on ultrasonic pulse distortion. I. Measurements. *J. Acoust. Soc. Am.*, 104:3635–3650, 1998.

[18] L. Hoff. Nonlinear response of sonazoid, numerical simulations of pulse-inversion and subharmonics. In *2000 IEEE Ultrasonics Symposium Proceedings*, volume 2, pages 1885–1888. IEEE, 2000.

[19] L. Hoff. *Acoustic Characterization of Contrast Agents for Medical Ultrasound Imaging*. Kluwer Academic Publishers, Dordrecht, 2001.

[20] Siemens Medical Systems Inc. Ultrasound imaging system employing phase inversion subtraction to enhance the image. U.S. Pat. No. 5,632,277.

[21] S. Kingsley and S. Quegan. *Understanding Radar Systems*. McGraw-Hill, London, 1992.

[22] J. Kirkhorn, P. J. A. Frinking, N. de Jong, and H. Torp. Three-stage approach to ultrasound contrast detection. *IEEE Trans. Ultrason., Ferroelectr., Freq. Contr.*, 48:1013–1022, 2001.

[23] T. G. Leighton. *The Acoustic Bubble*. Academic Press, San Diego, 1994.

[24] S.-E. Måsøy, T. F. Johansen, and B. A. Angelsen. Correction of ultrasonic wave aberration with a time delay and amplitude filter. *J. Acoust. Soc. Am.*, 113(4):2009–2020, 2003.

[25] T. D. Mast, L. M. Hinkelman, M. J. Orr, and R. C. Waag. The effect of abdominal wall morphology on ultrasonic pulse distortion. II. Simulations. *J. Acoust. Soc. Am.*, 104:3651–3664, 1998.

[26] D. Miller. Ultrasonic detection of resonant cavitation bubbles in a flow tube by their second harmonic emissions. *Ultrasonics*, 22:217–224, 1981.

[27] M. Minnaert. On musical air-bubbles and sounds of running water. *Phil. Mag.*, 16:235–248, 1933.

[28] K. E. Morgan, J. S. Allen, P. A. Dayton, J. E. Chomas, A. L. Klibanov, and K. W. Ferarra. Experimental and theoretical evaluation of microbubble behavior: Effect of transmitted phase and bubble size. *IEEE Trans. Ultrason., Ferroelectr., Freq. Contr.*, 47(6):1494–1509, 2000.

[29] K. E. Morgan, M. Averkiou, and K. Ferarra. The effect of the phase of transmission on contrast agent echoes. *IEEE Trans. Ultrason., Ferroelectr., Freq. Contr.*, 45(4):872–875, 1998.

[30] Allan D. Pierce. *Acoustics - An Introduction to Its Physical Principles and Applications.* Acoustical Society of America, New York, 1991.

[31] M. Plesset. The dynamics of cavitation bubbles. *Journal of Appl. Mech.*, 16:277–282, 1949.

[32] J. Proakis and D. G. Manolakis. *Digital Signal Processing. Principles, Algorithms, and Applications.* Prentice-Hall, New Jersey, 1996.

[33] Lord Rayleigh. On the pressure developed in a liquid during collapse of a spherical cavity. *Phil. Mag.*, 34:94–98, 1917.

[34] W. T. Shi, F. Forsberg, A. L. Hall, R. Y. Chiao, J. B. Liu, S. Miller, K. E. Thomenius, M. A. Wheatley, and B. Goldberg. Subharmonic imaging with microbubble contrast agents: Initial results. *Ultrasonic Imaging*, 21:79–84, 1999.

[35] K. Shung. Ultrasonic contrast agents and harmonic imaging. *J. Acoust. Soc. Am.*, 100:2645, 1996.

[36] D. H. Simpson, C. T. Chin, and P. N. Burns. Pulse inversion doppler: A new method for detecting nonlinear echoes from microbubble contrast agents. *IEEE Trans. Ultrason., Ferroelectr., Freq. Contr.*, 46(2):372–382, 1999.

[37] P. Sontum, Ostensen J., K. Dyrstad, and L. Hoff. Acoustic properties of nc100100 (sonazoid) and their relationship with the microbubble size distribution. In *1999 IEEE Ultrasonics Symposium*, volume 2, pages 1743–1748. IEEE, 1999.

[38] K. Spencer, J. Bednarz, P. G. Rafter, C. Korcarz, and R. M. Lang. Use of harmonic imaging without echocardoigraphic contrast to improve two-dimensional image quality. *Am. J. Cardiol.*, 82(6):794–799, 1998.

[39] Einar Stranden. Personal discussion. Aker Hospital, Oslo.

[40] C. Therrien. *Discrete Random Signals and Statistical Signal Processing*. Prentice-Hall, New Jersey, 1992.

[41] T. Varslot, Taraldsen G., T. F. Johansen, and B. A. J. Angelsen. Computer simulation of forward wave propagation in nonlinear, heterogeneous, absorbing tissue. In *2001 IEEE Ultrasonics Symposium Proceedings*, volume 2, pages 1193–1196. IEEE, 2001.

[42] F. M. White. *Viscous Fluid Flow*. McGraw-Hill, Singapore, 1991.

Peter: fund. nonlinearity only due to energy loss to higher harm. (??)